RESEARCH TRIANGLE INSTITUTE

N66 29342 (ACCESSION NUMBER)
(THRU)
232 (PAGES)
1 (CODE)
CR-60415 (NASA CR OR TMX OR AD NUMBER)
07 (CATEGORY)
FACILITY FORM 602

Interim Report, RTI Program RU-170

ANALYTICAL STUDY TO DEFINE AN EXPERIMENTAL PROGRAM FOR THE EVALUATION AND OPTIMIZATION OF MULTI-ELEMENT LARGE APERTURE ARRAYS

GPO PRICE $ ______
CFSTI PRICE(S) $ ______
Hard copy (HC) $6.00
Microfiche (MF) 1.25
ff 653 July 65

Contract NAS1-3780

Submitted to

Instruments Research Division
Langley Research Center
National Aeronautics and Space Administration
Hampton, Virginia

June, 1964

FOREWARD

This report was prepared by the Radiation Systems Laboratory of the Research Triangle Institute, Durham, North Carolina, on NASA contract NAS1-3780. The work has been administrated under the direction of the Communications Research Section, Instrument Research Division, Langley Research Center. Mr. C. P. Hearn is the Langley Technical Representative for the contract.

The program studies began on March 1, 1964, and will continue until August 31, 1964, with the final report due on September 30, 1964.

[redacted]

TABLE OF CONTENTS

TABLE OF CONTENTS (Continued)

TABLE OF CONTENTS (Continued)

LIST OF ILLUSTRATIONS

LIST OF ILLUSTRATIONS (Continued)

LIST OF ILLUSTRATIONS (Continued)

I. SUMMARY

This interim report covering the first three months of a six month contract contains analyses of several major problems associated with arrays of large-aperture antennas. Pre-contract studies, which were reported in RTI proposals and a report,[1, 2, 3, 4] serve as the basis for the present study program. Emphasis is placed on evaluating the basic limitations and characteristics of operational arrays with the purpose of planning an experimental program. This program will provide necessary data leading to optimum design of operational arrays and will permit thorough evaluation of the capabilities and limitations of these arrays.

Analytical studies have been devoted to the major parameters and characteristics of arrays and include:

(1) antenna characteristics -- diameter, polarization, spacing, and type of feed-reflector combination;

(2) sources of phase instabilities -- atmospheric phasefront distortion, equipment variations, and doppler uncertainties;

(3) intra-array phase compensation -- a method for removing pathlength variations in the data-links; extension of method to produce pathlength equalization of several receiving channels;

(4) angle acquisition and tracking methods, individual tracking capabilities and combinations of antennas;

(5) signal summation, effects of signal phase and amplitude variations; and

(6) phase acquisition and tracking, with particular emphasis on the long-range acquisition problem.

The major work on these analytical studies has been completed; the remaining work will be completed during the second half of the program.

The initial work has been completed on the experimental program planning. The optimum program is believed to include two phases:

(1) a two-antenna system with variable spacing, to be used for performing extensive tests on propagation effects, equipment phase variations, and data-link stabilization; and

(2) a prototype system which evolves from phase 1 into a multiple-antenna system; to be used for performing extensive tests on acquisition and tracking methods applicable to operational arrays; for studying other problems peculiar to arrays of large-aperture antennas; and for supplementing the information obtained with the two-antenna system.

The major emphasis will be placed on this program planning during the remainder of the program.

II. INTRODUCTION

This interim report covers activities for the first three months of Contract NAS1-3780, a six month contract beginning February 28, 1964. The major objectives of the contract are as follows:

(1) To identify and evaluate the limitations and major problems associated with operational arrays of large antennas;

(2) To design and recommend an optimum experimental program for obtaining the necessary data for evaluating the major operational problems; and

(3) To recommend parameters of a prototype system to the degree permitted by available data.

Pre-contract studies at RTI indicated that analytical studies and experimental measurements should be conducted in order to obtain data for evaluating the performance capabilities and limitations of arrays of large antennas and for determing optimum parameters of these arrays.[1, 2, 3, 4] Reference [4] provides essential background information to this project; it defines the major problems associated with arrays of large antennas and attempts to evaluate these problems and suggest solutions. Fundamental limitations are believed to consist primarily of unpredictable propagation effects. Practical limitations are imposed by data-link instabilities and by equipment limitations such as phase instabilities of receiver components, antenna performance degradation under various loading conditions, and instabilities of narrowband phase-locked loops. Because of the inability to evaluate the problems and limitations of antenna arrays solely on an analytical basis, RTI has emphasized the need for combined analytical and experimental studies. Thus, the main purpose of the current analytical study is to define a near-optimum experimental program which will provide the necessary data for the design of operational systems. Basically, the experimental program is envisioned as having two phases:

(1) a two-antenna system which is used as a research tool for obtaining data on the characteristics of propagation effects and on some of the basic components of operational arrays; and

(2) a prototype system which supplements data taken with the two-antenna system and provides important performance information which can be extrapolated to the performance of operational systems.

It may be inferred from the above paragraph that RTI believes a rather extensive experimental program should precede design and construction of operational systems. This belief is based primarily on technical considerations and has been arrived at after extensive attempts to evaluate array performance by analytical methods using available data.[4] An additional argument for supporting this approach is that the high costs of building operational arrays does not permit serious design errors resulting from sketchy or erroneous background information. Considerable experience has been obtained in this country on programs which are directed immediately toward operational systems, while basic technical questions remain unanswered. This experience shows that the preferred path toward expensive operational systems is a step-by-step series approach of the type outlined above, when the time schedule will permit such an approach. The time scale for the requirement of large operational arrays appears to permit such an experimental program; however, it is important that such a program begin at an early date if operational systems are contemplated for the 1970-1975 period. The study efforts during the first three months of this program have been concentrated in the areas which have a major influence on the general nature of the experimental program. Trips have been made to solicit criticism of the planned experimental program and to obtain data and opinions which verify or refute the previous computational results.[4] No major changes in experimental program requirements are believed to be in order as a result of these studies and discussions.

The remaining part of the program will concentrate heavily on the definition of experiments to be performed and on descriptions of equipment necessary for this purpose.

III. MAJOR CONSIDERATIONS FOR OPERATIONAL ARRAYS

Operational requirements for antenna systems to be employed for deep-space communications in the 1970 decade have not been well defined. This arises from the fact that space mission planning for this period has not reached an advanced stage. Present planning for new antenna installations at NASA deep-space tracking sites include 210 feet diameter antennas, which will be operational during the latter part of the present decade. In order to provide the desirable information flow for manned space flights to the neighboring planets, NASA personnel estimate that antennas with effective diameters of 500 feet will be required. This requirement is in addition to the other anticipated developments which will increase communications capabilities: greater spacecraft transmitter power (the order of 100 watts, CW); directive spacecraft antennas (e.g., 20 db gain); and the best low-noise receiving systems (approximately $50^{o}K$). It is assumed that mission requirements will expand to include explorations well beyond the nearest planets. Thus, the interest in large-area antenna systems is not for expanded bandwidth capability alone, but includes operation at extended ranges where the bandwidth capability may be only a few cycles per second.

The theoretical capabilities of arrays in terms of bit-rate performance versus operating range are discussed in reference [4]. It is shown that an upper limit of range performance is established by phase-front distortion caused by atmospheric "blobs," which refer to fine-grained refractivity variations in the troposphere and ionosphere. This upper limit can be achieved only if precise doppler compensation can be provided in order to restrict sufficiently the frequency band of signal uncertainty; it is expected that doppler prediction errors will also present a rather serious limitation to maximum range performance.

Operational systems are assumed to be of the form shown by the block diagram in Fig. III-1. A transmitting system provides a command-and-control link to the spacecraft, as well as a coherent reference which is used as a carrier for the spacecraft-to-earth communications channel. The exciter oscillator for this transmitter is a high-quality frequency standard, which is designed for good short-term stability (i.e., phase instabilities in the bandwidth above 0.001 cps). During the acquisition mode of operation, the spacecraft receiver phase-locks an internal oscillator to the ground-transmitter signal; a frequency off-set is imposed on the tracking oscillator by means of an on-board stable oscillator; spacecraft information is modulated onto this off-set carrier; and the resultant amplified signal is transmitted to the ground station. It is expected that this first step in signal acquisition imposes no serious limitations to array performance because relatively high power can be used in the ground transmitter and the space-probe receivers will be of fairly high quality (but obviously not as good as the ground receivers). The frequency off-set between the spacecraft transmitter and receiver reduces transmitter-receiver interference to an acceptable level; and if necessary, further interference reduction can be achieved by time-sharing the spacecraft transmitter and receiver, because continuous reception of the ground transmitter signal is not required.

The primary advantage in the "turn-around" technique described above (i.e., having the spacecraft acquire the ground transmitter signal and use it for a coherent carrier) is that the phase acquisition and tracking problems at the ground array are minimized. During acquisition, the frequency uncertainty of the received signal is essentially reduced to errors in doppler prediction and compensation, while the bandwidth of the signal carrier is determined by short-term oscillator instabilities and by propagation effects.

The minimum requirements for data exchange between the central station and the individual antenna sites are shown by the signal links in Fig. III-1. There are many configurations by which the individual antennas can be connected to a central location or to a reference antenna. The advantages of performing the signal-processing and control functions to the greatest possible extent at a central location are obvious. However, as a minimum, each antenna site must provide low-noise pre-amplification of the received signal, provision for putting this signal on the signal link to the central station, and the power units for driving the antenna to the correct angular position for space-probe acquisition and tracking. In general, each receive antenna has two output signals corresponding to orthogonal polarization components of the received signal (in order to maximize the effective antenna area in the absence of precise control or knowledge of the received-signal polarization vector.* In this case, the bandwidth of the signal links must be at least twice the information bandwidth of the space-probe transmitter. Notice that the basic data links shown in Fig. III-1 include the distribution of a coherent reference signal to each antenna site. This reference signal permits selection of carrier frequencies for the signal links in a manner which minimizes their phase instabilities and the mutual interference between the transmitters and

*A choice of polarization characteristics of the spacecraft transmitting antenna and earth station receiving antennas is suggested in Section IV.B.2 which should remove this dual-polarization requirement.

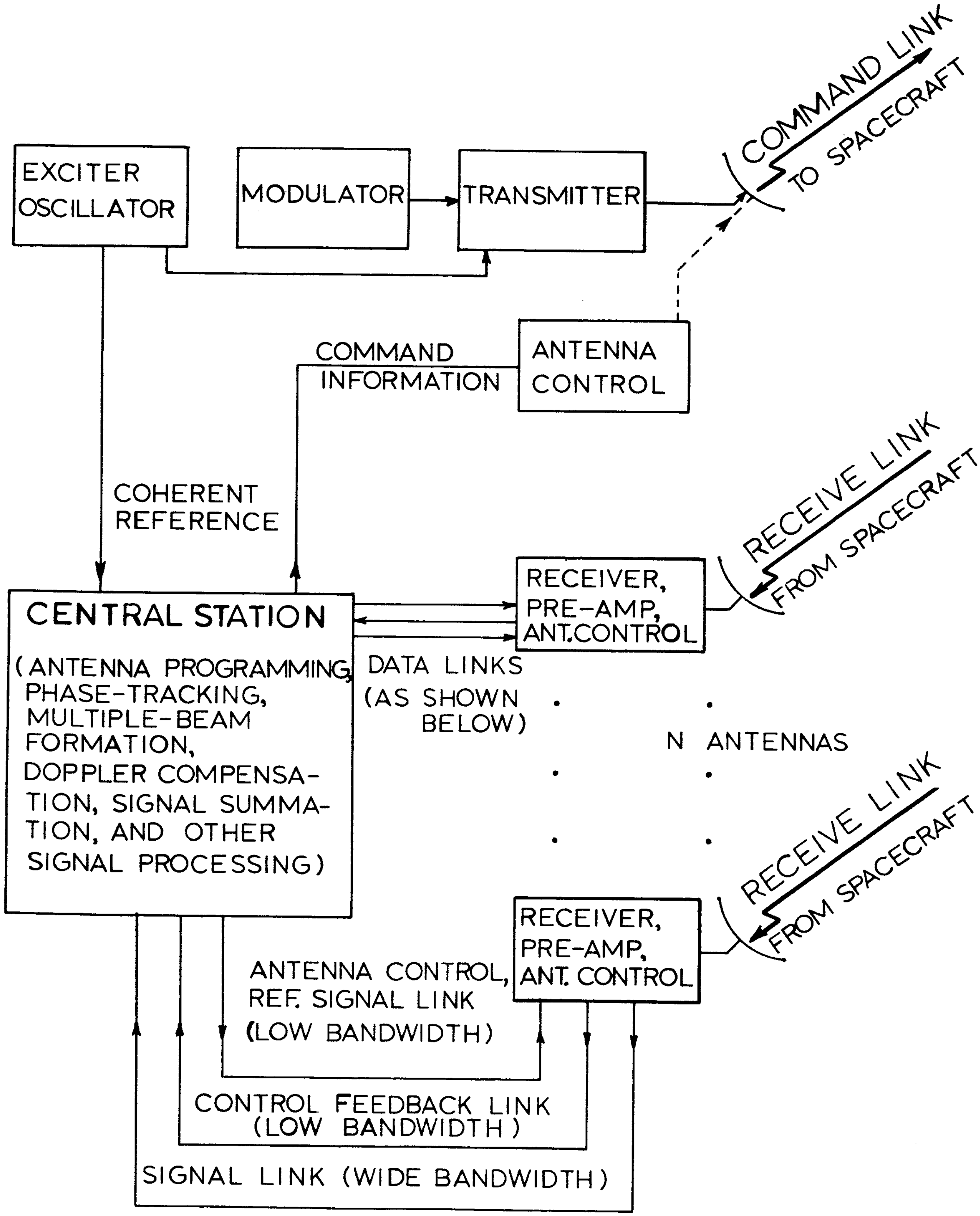

Fig. III-1. Communications system utilizing a receiving array of large-aperture antennas.

receivers of the array. It appears that coaxial cables operating at relatively low carrier frequencies (e.g., 100 Mc) will be suitable for this purpose.

The major parameters and considerations of an array of large-aperture antennas are: antenna diameter; array configuration; system noise temperature; phase tracker type; data-link stabilization method; angle and phase acquisition and tracking; and other signal processing. In addition to its primary function for deep-space communication, an array should also be capable of providing information on spacecraft range, range-rate, and angular position. Not only is this information required to support the communication function, but the array is ideally suited to these tasks by virtue of high receiver sensitivity and wide baseline coverage.

As a matter of interest, design objectives for operational arrays are listed in Table I and have been extracted from the RTI contract description.

TABLE I

Design Objectives, Operational Arrays

(1) Effective antenna diameter: Equivalent to a 500 foot paraboloid;

(2) Frequency range: 1-10 Gc, with primary interest at 2.2 and 8.4 Gc;

(3) Information bandwidth: 5 Mc maximum (operation with bandwidths up to 10 Mc will be considered), decreasing as necessary as the range of operation increases and finally approaches the maximum range of acquisition and tracking capabilities;

(4) Noise temperature: System equivalent noise temperature at zenith under clear weather conditions of less than 50 degrees Kelvin (consideration to be given to techniques for reducing the system temperature to 25 degrees Kelvin);

(5) Angular operation: from zenith to 4° above horizon in ecliptic plane and to 10° in other planes.

(6) Acquisition: Capability of acquiring in less than 15 minutes an unmodulated carrier from a spacecraft whose position is known to within ± 0.1 degree, utilizing the total system aperture and an input signal power of -170 dbm to each antenna;

(7) Reliability: Total aperture to be available 95 per cent of the time;

(8) Environment: That experienced at present NASA Deep Space Instrumentation Facility sites;

(9) Transmitter-Receiver Compatibility: The array will be used in the receiving mode only, but should be compatible with separate on-site transmitting antennas which provide an up-link to "turn-around" transponders in the spacecraft; these transponder outputs may then be used as carriers for the communications channel from the spacecraft to the ground array in order to permit coherent detection at the array.

There are several unanswered questions relating to the capabilities of arrays made up of large-aperture antennas. Some of these questions are of a fundamental nature involving environmental factors which are beyond the control of the design engineer. The most important of these questions concerns the nature of the phasefront distortion in the vicinity of the array. This distortion is one of the limiting factors in determining the maximum practical size of single antennas and has been a factor leading to the concept of independently-phased antennas.[5, 6] It was shown in reference [4] how this distortion also limits the capabilities of antenna arrays, but in a somewhat different manner from the single antenna. Other questions of a practical nature concern the performance of functions which are conceptually sound but which are difficult and expensive to implement. Major array parameters and the questions mentioned above are discussed further in Section IV.

IV. ANALYTICAL STUDIES

A. Introductory Discussion

The analytical studies described in this section reflect the fact that the program is directed toward the determination of array characteristics which affect the nature of an experimental program. All of the major array parameters affect this program to some degree; however, in many cases the effect is sufficiently small to permit bracketing parameter values closely enough by simple approximation methods. In this manner, intensive investigations into the design of operational systems may be avoided until the appropriate time when adequate data become available to justify such effort. For example, the computer requirements for antenna programming and signal processing are very important to operational systems. However, the design of a computer system for doing this is straightforward and similar to that used in other antenna systems. Therefore, this function is relegated to the design of operational systems and will not be treated in this program. Similarly, detailed design of phase trackers is not discussed in this section, because idealized circuit transfer functions are adequate for the comparison of the tracker types of interest and because the design has been proven feasible.[6]

The major array parameters cannot always be optimized on the basis of simple criteria. In many cases the factors affecting parameter choice are interdependent in rather subtle ways. For example, the choice of individual antenna diameter involves many considerations, including the acquisition procedure. If acquisition is to be performed independently on each antenna, as has been generally assumed,[5, 6, 7] the antenna diameter should be as large as possible, perhaps even beyond the optimum band determined by cost considerations alone.[7] On the other hand, if part or all of the antennas can be pre-focused so that acquisition is performed on partial or complete array gain, several considerations would favor selection of antenna diameter near the low end of the optimum diameter band (reference [4] and Section IV.B.1). This example also illustrates the difficulty in defining optimum parameters; different criteria will cause optimum values to vary widely and the selection of criterion is often based on debatable opinions.

The experimental program (including the prototype system) will be influenced greatly by the methods of angle and phase acquisition which are considered useful for operational systems. This program should be sufficiently flexible to permit testing a variety of techniques, because alternate techniques will be desirable even for operational systems. Consequently, a great deal of attention is devoted to these problems in this section. Similarly, intra-array data-link phase stabilization and atmospheric propagation effects have an important bearing on the acquisition and tracking capabilities of antenna arrays; and these questions are considered rather thoroughly in this section.

B. Antenna Characteristics

1. Diameter

The major cost of an array of large-aperture antennas will be the antennas and their associated mounts and drive mechanisms. The performance (accuracy, reliability, acquisition capability, etc.) is also critically dependent upon the characteristics of the individual antennas. Because of these factors, the selection of individual antenna diameter is one of the most important considerations in the array design. The optimum antenna diameter is determined primarily by the following factors:[4]

(1) cost of single antenna versus diameter;

(2) cost of associated equipment in the array;

(3) propagation effects;

(4) sidelobe requirements;

(5) theoretical gain limitations for large diameter/wavelength ratios (D/λ);

(6) beam-pointing requirements; and

(7) acquisition procedure.

Although most studies in the past have assumed that factors (1) and (2) predominate over the other factors, it is believed that the other factors may modify the conclusions significantly.

Considering factors (1) and (2), RTI has not made an effort to generate a curve of array cost versus individual antenna diameter. Such a curve is reported in reference [7], and the conclusion is reached that a very broad minimum exists in the diameter range of 15-45 meters. This result includes the added cost of providing better beam-pointing accuracy as the antenna diameter increases, in order to permit positioning the antenna beam within some fractional beamwidth of an absolute angular position.

The pre-contract study of propagation effects (factor 3) are reviewed briefly in Part C below. The results in Figs. IV.C-1 and IV.C-2 of that part show that phasefront distortion may be expected to result in significant losses in overall aperture efficiency in the 8-10 Gc band for antenna diameters greater than 30 meters. However, the degradation is not expected to be particularly serious in the 1-3 Gc band for diameters up to 90 meters. Furthermore, it appears that the degradation will be serious at all frequencies for diameters in excess of 200 meters. Therefore, with regard to array design, propagation effects will define an upper limit to antenna diameter based on some loss criterion, as illustrated in Fig. 12 of reference [4]. The results in this reference indicate that propagation effects will play a significant role in the determination of optimum diameter only at frequencies above 7 Gc, where the loss factor is allowed to fall in the 0-1 db range.

The results described above illustrate the danger in attempting to achieve larger and larger antenna area by means of single reflector-feed arrangements. A single 500 foot diameter antenna, for example, would be expected to incur large losses in the high end of the frequency band. It should be remembered that this discussion applies to antennas which must acquire spacecraft at low elevation angles. Propagation effects are expected to rarely cause serious losses in aperture efficiency for elevation angles above 30°, regardless of antenna size, as long as the antenna tracks the average direction of signal arrival over its aperture.

Factors (4) and (5) are believed to be important in the determination of optimum antenna diameter. It is well known that the requirement for low sidelobe level results in a trade-off between aperture efficiency and sidelobe level. It is further shown by Hansen[8] that aperture efficiency decreases for large diameter-wavelength ratios, when the aperture illumination is selected to maintain specified sidelobe levels below the peak gain.

Considering first the sidelobe requirement to prevent significant noise temperature degradation, a simple calculation shows that the average backlobe and sidelobe gain, $\overline{G_s}$, should satisfy the inequality:

$$\overline{G_s} \leq \frac{\Delta T}{300} \qquad \text{(IV.B-1)}$$

where ΔT is the maximum temperature increment allowed for earth contribution to system sky noise. ΔT should be small relative to the minimum sky noise. For example, for a minimum sky noise of 25^{o}, a value of $\Delta T = 5^{o}$ appears to be a reasonable specification. This specification imposes a far-out sidelobe requirement of 17 db below isotropic, one that may be difficult to meet for the large antennas used in this application. For example, a 30 meter antenna would have a gain of the order of 57 db at 10 Gc, requiring that the average backlobes be of the order of 74 db below the peak lobe. In order to emphasize the importance of sidelobe considerations, consider the following example. Assume that 90% of the area under an antenna power-sensitivity curve falls under the mainbeam. For this case, the average sidelobe level is 10 db below isotropic. Thus, the 17 db requirement given above means that special effort must be taken to insure that near-in sidelobes are well above isotropic. This is a somewhat unusual design requirement, and no applicable information is available which shows the tradeoff between aperture efficiency and required far-out sidelobe level. As a preliminary estimate, it is believed that sidelobe level considerations may present serious problems for antennas with gain in excess of 50 db (i.e., D/λ ratios greater that 150).

Considering now the theoretical gain limitations for large antennas, Hansen[8] shows that significant reduction in aperture efficiency can occur for large D/λ; this reduction corresponds to a greater portion of the antenna power (from the transmit standpoint) appearing in the sidelobes. The actual degradation is dependent upon a number of factors, and a detailed discussion of the results is not justified at this time. However, for D/λ in excess of 600, cases may exist for which the aperture efficiency will be in the range of 0.5 - 1.0 db below its value for $D/\lambda = 100$. This factor alone would modify the cost versus diameter curve significantly, when account is taken of the additional number of antennas needed to offset this efficiency reduction.

Beam-pointing considerations impose a similar requirement to the two factors discussed above in that the important parameter is D/λ. In order to hold the loss in aperture sensitivity to a reasonable value (say 0.5 db), the pointing accuracy should be within ± 0.2 beamwidth. Initial studies indicate that atmospheric scintillation would impose a limitation of the order of $D/\lambda \leq 1000$ (i.e., beamwidths greater than 0.06°) in order to meet this requirement.

The appearance of acquisition procedure as a factor in optimum diameter determination may at first appear puzzling. However, if the signal acquisition procedure is limited to independent acquisition on each antenna, as has generally been assumed,[5, 6, 7] the use of antenna diameters as large as permitted by atmospheric limitations on pointing accuracy would be in order. This assumes that operation of the array at long range and low communication bandwidths is important, as described in Section III. This factor would somewhat offset factors (3)-(6), which favor small diameter antennas.

If methods are worked out for signal acquisition on multilobe array patterns, as described in Part G, the influence of acquisition procedure on optimum antenna diameter is practically removed. At this time it appears that such "pre-focusing" can be accomplished quite effectively, and the experimental program includes tests for evaluating this capability. Therefore, there is a good chance that acquisition procedure need have little influence on the optimum antenna diameter.

It is obvious from the above discussion that the question of optimum antenna diameter requires further study. This study will be restricted to factors (3)-(7), and cost considerations will be assumed to give the broad optimum band between 15-45 meters, as reported in reference [7].

2. Polarization Requirements

The primary purpose of forming arrays of large-aperture antennas is to increase the receiving area to spacecraft signals. Therefore, it is important that the sensitivity not be degraded in other ways--for example, by polarization losses resulting from polarization mismatch between the antenna and the received wave. It is also important that whatever measures are taken to minimize polarizations losses do not degrade appreciably the system noise temperature of each receiving antenna.

Consider the case where linear polarization is used in the spacecraft transmitter. In order to minimize polarization losses between spacecraft signals and the ground antennas, one of two measures must be taken: (1) the ground antenna must be adaptively polarized (i.e., capable of receiving two orthogonally-polarized components and optimally combining them for maximum SNR); or (2) the spacecraft antenna must be capable of orienting its polarization vector to match the receiving characteristic of the ground antenna. The latter measure appears to impose very severe and undesirable requirements on the spacecraft, in addition to those already imposed by the requirement that the spacecraft antenna track the earth. (It is assumed that the spacecraft antenna will be directive as one measure for increasing the deep-space communication capability). Thus, if the spacecraft transmits linear polarization, the first measure should be taken. This measure can be implemented by equipping each antenna with a dual-polarization feed followed by two parallel receivers. Optimum signal combination can then be made by treating the signals as coming from separate antennas and adding them coherently with amplitude weighting selected in accordance with Section F below.

If the choice of spacecraft polarization characteristics can be made to optimize the match between spacecraft antenna and ground antenna polarization vectors, it is believed that the spacecraft polarization should be circular with an aribtrary, but consistent, sense. The following discussion leads to this conclusion.

Assume that each ground antenna uses a single receiver which is fed by a circularly-polarized feed designed to match the spacecraft transmitter polarization. The important consideration is the amount of polarization loss incurred in this system. Three sources of losses exist:

(1) polarization ellipticity of the spacecraft antenna;

(2) polarization ellipticity of the ground antenna; and

(3) polarization distortion introducted by the earth's atmosphere and magnetic field, or by interplanetary plasmas.

In order to simplify the evaluation, the three sources will be assumed to be independent; antenna design experience would indicate that this is a reasonable assumption as long as the polarization losses from the three sources are small.

In evaluating the first source of polarization loss, assume that sources (2) and (3) do not exist. It is easily shown that the fractional loss of the total signal intercepted by the ground antenna is expressed by

$$L_{pl} = \left(\frac{e - 1}{e + 1}\right)^2 \qquad \text{(IV.B-2)}$$

where e = ellipticity ratio of the transmitted field.
Because of the similarity between sources (1) and (2), a similar expression applies to the polarization losses caused by ellipticity of the ground antenna. A reasonable specification on ellipticity ratios is $e \leq 1.13$ (i.e., an ellipticity ratio less than 1 db). The resulting loss for each source would be less than 0.4%. A 2 db ellipticity specification would result in less than 1.5% polarization loss from each source.

Considering loss source (3), for the frequency band of interest (1-10 Gc), the polarization ellipticity introduced by the earth's ionosphere and magnetic field is expected to be negligible. From reference [9], the polarization rotation of a linearly-polarized vector varies as $1/f^2$ and is estimated to be approximately 4^{o} at 1 Gc. If this is taken to be the differential rotation between the two orthogonal components of a circularly-polarized wave, the resulting ellipticity would be approximately 1.07. The loss contribution from this source would be about 0.1%, a negligible amount. Actually, this assumption is pessimistic; a circularly-polarized wave would be expected to suffer less distortion than given by these numbers.

Loss source (3) also includes the polarization ellipticity introduced by interplanetary plasmas. Although conclusive data are not available on interplanetary plasma densities and magnetic fields, reference [21] would indicate that this effect would also be negligible for the frequency band of interest.

The above discussion indicates that the polarization losses incurred by a circularly-polarized system can be made negligible. This is an attractive selection from the standpoint of simplifying the receiving antennas. Only one polarization component need be received and only a single-polarization channel receiver is required. This simplification is particularly attractive for those antennas equipped with angle-tracking capability. While a dual-polarization, multiple-frequency, monopulse system is believed to present formidable problems with regard to design, development, costs, and system noise-temperature degradation, a single polarization system is believed to be reasonable with regard to these considerations.

3. Antenna Spacing

a. General

In establishing the minimum separation between antennas in an array, it is important that the spacing be sufficient to provide coverage down to the minimum required elevation angle without appreciable interference between antennas. This interference takes two forms:

(1) shadowing, which results in gain reduction, boresight errors, and beam distortion; and

(2) noise reflection and radiation, which results in degradation of the noise temperature of one antenna by noise reflection and radiation from another.

It is not practical to make a conclusive analysis of these effects, because of the complexity of the problem and the lack of information on certain antenna and terrain constants. It is believed that the criteria described below are conservative and that no appreciable performance degradation will be incurred if either of them is satisfied; however, this belief can be verified conclusively only by experimental methods.

Two clearance criteria will be described. They are both based on the assumption that a given antenna will experience no serious performance degradation if all adjacent antennas fall outside the main beam of this antenna. The main beam is defined to fall within the diameter for which the power density is one-half that at the peak of the beam. Although considerable increase in sidelobe levels occurs in the Fresnel region, the half-power beam diameter always includes the major part of the total radiated power. The difference in the criteria is in the methods of defining beam diameter. In the first case a simple assumption is made that the beam diameter is equal to the antenna diameter from zero range to the far-field range ($2D^2/\lambda$), beyond which it is assumed to diverge at an angle equal to the beamwidth. This criterion is referred to as the line-of-sight method. The second criterion is based on a more exact solution to the field distributions existing at cross-sections of the beam within the Fresnel Zone. This criterion is called the radiation-pattern method.

b. Line-of-Sight Method

Assuming that the antennas are located on a local horizontal plane, Fig. IV.B-1 shows the pertinent geometry:

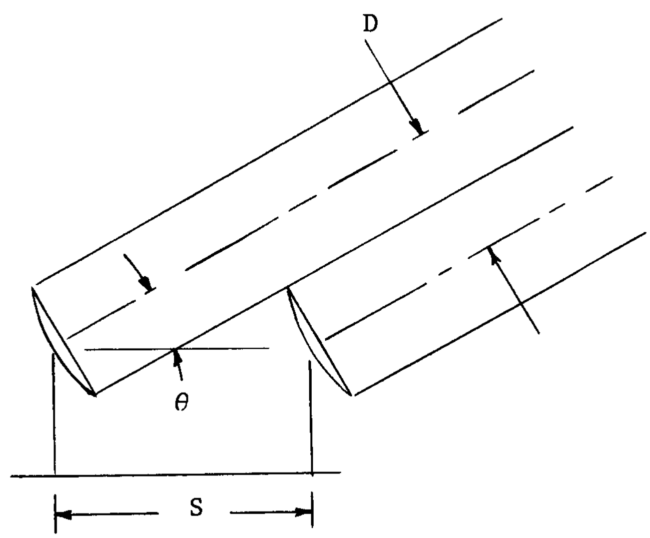

Fig. IV.B-1. Line-of-sight geometry.

From Fig. IV.B-1,

$$S = \frac{D}{\sin\theta} \qquad \text{(IV.B-3)}$$

where

S is minimum distance between antennas,

D is diameter of antennas, and

θ is minimum elevation angle.

For the lowest elevation angle specified for this study; 4^{o}, S is equal to 14.3 D.

c. Radiation Pattern Method

For circular aperture antennas whose illumination distributions are tapered to reduce sidelobes, the half-power beamwidth can be approximated as: $\theta = \beta \frac{\lambda}{D}$,

where θ is the half-power beamwidth,

β is a coefficient dependent on illumination taper,

λ is wavelength, and

D is antenna diameter.

This approximation applies for illumination distributions of the form $(1 - r^2)^P$. For P = 2, corresponding to reduction of the first sidelobe to 30 db below the main lobe, the value of β is 1.47.

For an antenna with a 30 db sidelobe requirement, the half-power beam diameter at the Fraunhofer, or far-field region boundary (assumed to be given by $2\,D^2/\lambda$), is implicitly expressed by

$$\tan 1.5\,\frac{\lambda/D}{2} = \frac{\frac{1}{2}\,D_B}{2\,D^2/\lambda}$$

or

$$D_B = 2\ (2\,D^2/\lambda \times \tan 1.5\,\frac{\lambda/D}{2}) \qquad \text{(IV.B-4)}$$

Assuming that $1.5\,\frac{\lambda/D}{2}$ is sufficiently small, $\tan \frac{1.5\,\lambda/D}{2} \approx 1.5\,\frac{\lambda/D}{2}$, and

$$D_B = 4\,D^2/\lambda \times 1.5\,\frac{\lambda/D}{2}$$

$$= 3\,D$$

In their paper on antenna power densities in the Fresnel region,[10] Hansen and Bailin plot beam-broadening factor, γ, as a function of multiples of $2\ D^2/\lambda$ for aperture illumination taper of $(1 - r^2)^P$ and circular apertures (see Fig. IV.B-2).

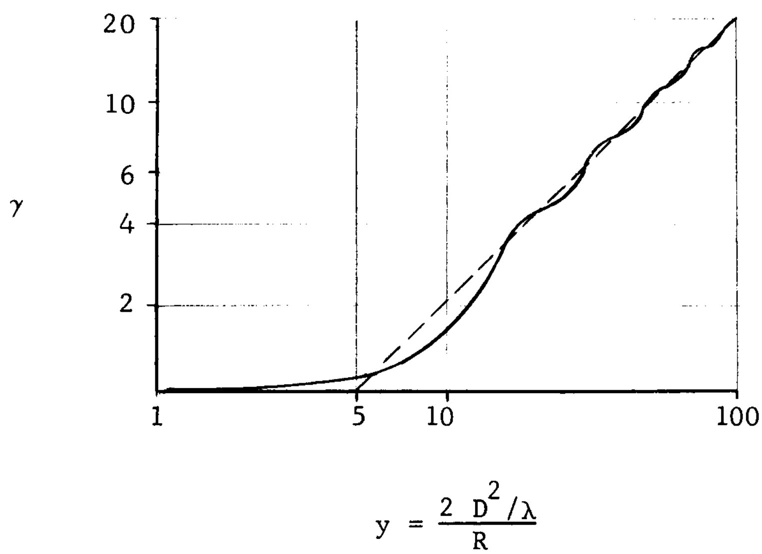

Fig. IV.B-2. Beam-broadening factor.

As can be seen from this plot, a good approximation to the curve in the region from y = 5 to y = 100 is the straight line shown. The slope of this line in the region shown is $\frac{1}{5}$, thus $y = 5\gamma$ and, beginning at y = 5 and going toward the aperture, the beam broadens approximately linearly from the far-field beamwidth to 20 times the far-field beamwidth at $y = \frac{2\ D^2/\lambda}{R} = 100$. An approximation for this variation is:

$$\frac{\theta}{\Theta} = \frac{y}{5} \Big|_{y\,=\,5}^{100} \qquad \text{(IV.B-5)}$$

where $$y = \frac{2\ D^2/\lambda}{R},$$

Thus, $$\theta = \frac{\Theta}{5} \left(\frac{2\ D^2/\lambda}{R}\right) \Big|_{R\,=\,0.01\ (2\ D^2/\lambda)}^{R\,=\,0.2\ (2\ D^2/\lambda)} \qquad \text{(IV.B-6)}$$

Using the expression for beam diameter,

$$D_B = 2\ R\ \tan\ \theta/2$$

and substituting equation IV.B-6 for θ,

$$D_B = 2\ R\ \tan\left[\frac{\theta}{10}\left(\frac{2\ D^2/\lambda}{R}\right)\right]\Bigg|_{R\,=\,0.01\ (2\ D^2/\lambda)}^{R\,=\,0.2\ (2\ D^2/\lambda)} \qquad \text{(IV.B-7)}$$

The variation in beam diameter, assuming beam broadening to be unity as shown in Fig. IV.B-2 in the range $R = .2\ (2\ D^2/\lambda)$ to ∞,

$$D_B = \frac{R}{(2\ D^2/\lambda)}\ (3\ D)\ \Bigg|_{R\,=\,0.2\ (2\ D^2/\lambda)}^{R\,=\,\infty} \qquad \text{(IV.B-8)}$$

Equations IV.B-7 and IV.B-8 completely describe beam diameter for all ranges greater than $.01\ (2\ D^2/\lambda)$. This beam diameter variation is plotted in Fig. IV.B-3. It can be seen from this plot that the cylindrical beam assumption is not a good one and that it is much too optimistic in the region from $0.33\ (2\ D^2/\lambda)$ to $2\ D^2/\lambda$. However, the assumption of a cylinder of 0.6 D appears to be good from 0.01 $(2\ D^2/\lambda)$ to $0.2\ (2\ D^2/\lambda)$.

Since we are concerned with large aperture antennas, it is pertinent to examine a practical situation to determine typical separation distances in terms of $2\ D^2/\lambda$ in order to estimate what portions of the plot in Fig. IV.B-3 apply. From previous considerations, the diameters most likely to be used lie in the range of 100λ to 1000λ. Using the first cylindrical assumption, the separation distance for 4° elevation was found to be of the order of 14D.

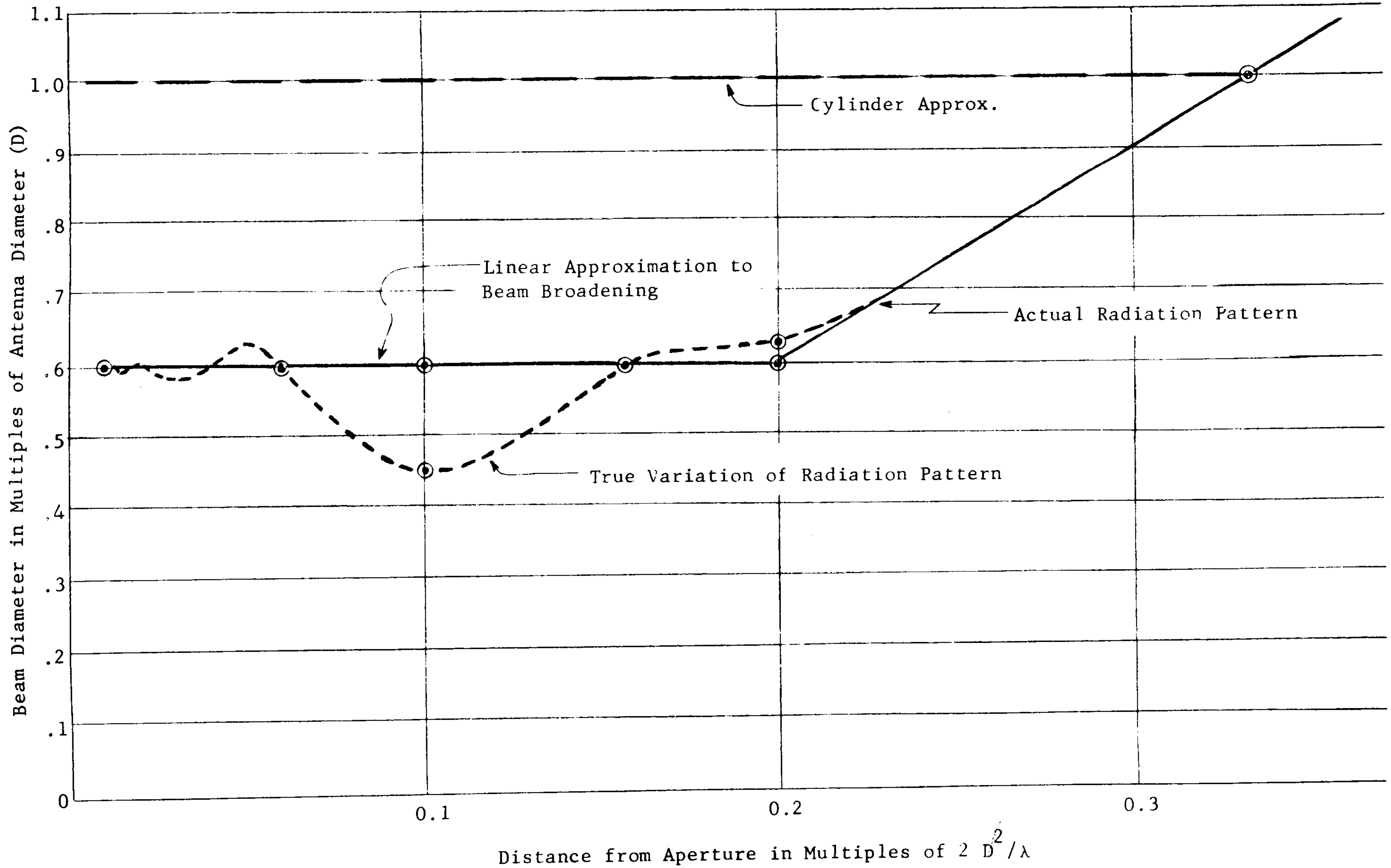

Fig. IV.B-3. Beam diameter variation.

The $2\,D^2/\lambda$ distance for a 100λ antenna is:

$$d = \frac{2\ (100\lambda)\ D}{\lambda} = 200\ D.$$

Thus, the separations proposed as minimum are in the order $\frac{14}{200} = .07(2\ D^2/\lambda)$; the cylindrical assumption actually is a good approximation for this order of separation distances, and it can be used for separations up to approximately 75 D without serious error.

The only azimuthal region in which unaffected coverage down to 4° elevation is specified is that required for viewing the ecliptic plane. At all other azimuths, the minimum elevation angle requirement is 10°. At these azimuths, the minimum separation must be:

$$S = \frac{D}{\sin 10^\circ} = 5.75\ D$$

The azimuth angle region in which the larger separation must be maintained is approximately $\pm 23.5^\circ$ about the East-West axis if the array is considered to be located at the equator, in order to obtain unobstructed view of the ecliptic. At other latitudes, this angular region becomes larger; at 36° latitude, the region is approximately $\pm\ 30^\circ$ about East-West. The required minimum spacing then, for an array located at latitudes near 36°, defines a region about a single antenna as shown in Fig. IV.B-4.

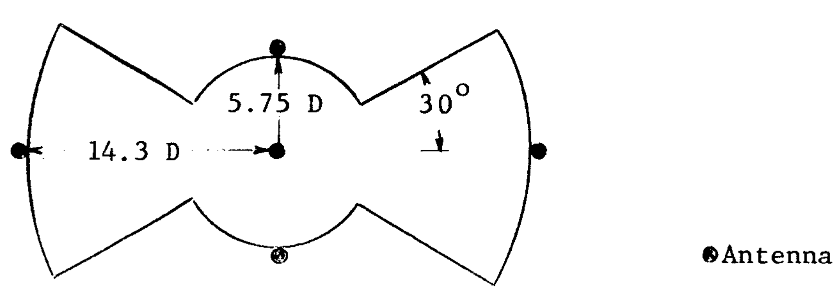

Fig. IV.B-4. Minimum spacing for array located at latitudes near 36°.

This configuration immediately suggests that a staggered configuration, as in Fig. IV.B-5, would be an optimum shape for realization of the largest number of antennas in a given area while still maintaining the required separation to prevent shadowing.

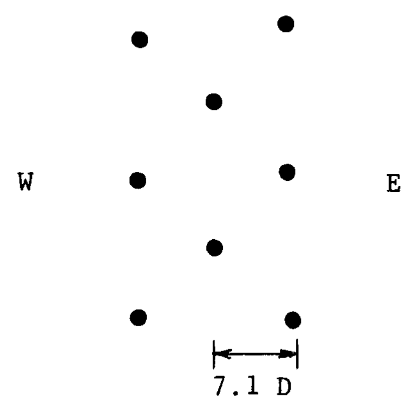

Fig. IV.B-5. Staggered configuration.

The required N-S separation is found, using the cylindrical approximation, as shown in Fig. IV.B-6.

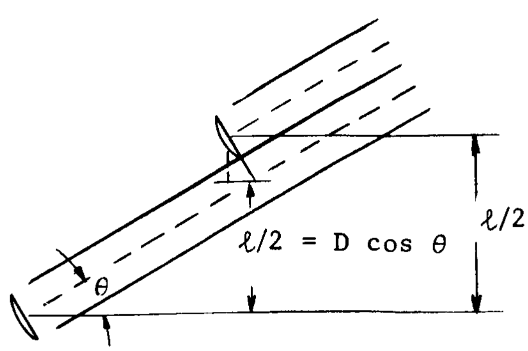

Fig. IV.B-6. Cylindrical approximation.

From Fig. IV.B-6

$$\tan 30^\circ = \frac{\ell/2 - D \cos 30^\circ}{7.1\ D}$$

$$\ell = 9.9\ D$$

Thus the minimum-spaced configuration is that shown below:

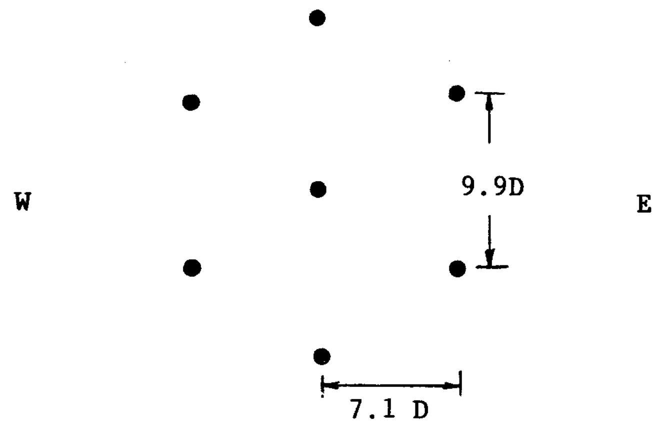

Fig. IV.B-7. Minimum spaced configuration.

The basic cell within this configuration is a triangular array with three antennas which require an area of approximately 35 D^2. Two of these basic cells form a rectangle of area 70 D^2. If the area of 70 D^2 is associated with each antenna, the approximate area occupied by an array of 500 foot equivalent aperture may be estimated. This area would allow a clearance space around the exterior of the array of a width roughly equal to 1/2 of the spacing between individual antennas, as shown in Fig. IV.B-8.

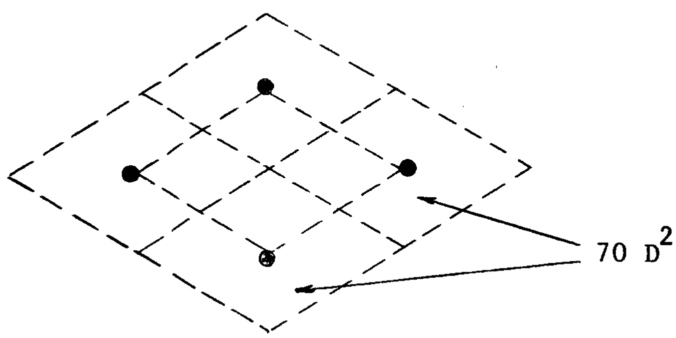

Fig. IV.B-8. Antenna clearance.

Then the area, including the clearance space around the exterior, of a 500 foot equivalent aperture array is:

$$A = nD^2 \ (70) = (500)^2 \ 70 = 175 \times 10^5 \ ft^2$$

If the array were roughly square, each side would be approximately 4200 feet long, including the clearance space about the exterior, and regardless of the number of antennas.

4. Antenna Type

After comparative study of the various types of antennas which could be used in the array, the Cassegranian two-reflector antenna appears to be the best choice for this application. The reflector-focal point feed antenna could be used, but the Cassegranian configuration offers the following advantages over the single reflector configuration:

(a) Sub-reflector support is much simpler than feed support since the sub-reflector is always located a shorter distance from the vertex than a focal-point feed would be.

(b) Since the feed can be placed at the parabolic vertex, long transmission lines leading to the feed are eliminated, placement and support of pre-amplifiers is not a problem, feed accessibility for replacement, etc., is no problem, and feed spillover does not provide coupling to the earth, thus providing improvement in noise performance relative to a single reflector antenna.

(c) Equivalent focal lengths much greater than actual physical lengths can be realized, thus making possible the use of deep dishes without small f/D ratios. This results in better off-axis feed performance, reduced cross-polarization losses, and better aperture illumination.

The single disadvantage of a Cassegranian antenna is the aperture blockage due to the sub-reflector. This can be minimized by reducing the diameter of the sub-reflector and decreasing the separation between feed and sub-reflector by moving the feed out along the axis from the vertex. An expression for the minimum sub-reflector diameter has been derived by Hannan[11]:

$$D_{b\ min} = \frac{2}{K} F_m \lambda, \qquad \text{(IV.B-9)}$$

where K = ratio of the effective feed aperture diameter to its blocking diameter,

F_m = focal length of the parabola, and

λ = wavelength.

In practice, sub-reflector blocking effects become negligible when D/λ is large. In any case, the blocking effect of the sub-reflector will not be a great deal larger than that of a feed and pre-amplifier for a single reflector antenna.

It also appears that the feed system will be monopulse rather than conical scan, even though a monopulse antenna requires more receiver channels than a conical scan system. The principal reasons for the choice of monopulse over con-scan are:

(1) amplitude modulation imposed on received signals by the con-scan system are undesirable;

(2) the offset scan angle in con-scan systems results in less gain for communication signals received

on axis, whereas the sum channel monopulse gain realizes full antenna gain;

(3) generally, conical scanning introduces mechanical or electrical problems which are eliminated with monopulse;

(4) beam scanning will worsen the noise problem or decrease efficiency since the sub-reflector is to be designed to give optimum aperture illumination for the fixed case.

Because monopulse feeds considerably increase the complexity of the array hardware, further consideration will be given this problem in the remainder of the program. Part 2 above discusses the possibility of using circular polarization for the spacecraft and ground antennas in order to permit the use of single-polarization antennas. If this is done, the monopulse configuration becomes quite attractive. Dual-polarization, multiple-frequency, monopulse systems are very complex and would probably impose significant degradation in system noise temperature.

C. Phase Instabilities

1. General Discussion

In order to make an array of antennas perform as a single antenna, with regard to effective receiving area, the received signals from all antennas must be summed coherently. This requirement imposes the need for compensating all differential phase variations between received signals prior to their summation. These variations are introduced by atmospheric phasefront distortions, by phase instabilities introduced in the signal paths between each antenna and the central summing point, and by differential doppler shifts introduced by the earth's rotation.

In addition to the differential phase variations, received signals will have phase and frequency uncertainties which are common to all antennas. Although it is not necessary to remove these common uncertainties from the signals in order to sum them coherently, it is desirable to minimize the frequency uncertainty and the bandwidth of phase fluctuations prior to the phase acquisition and tracking circuits. This minimization results in reduction of the acquisition and tracking thresholds, thus providing greater capability to operate at long ranges.[4]

The above paragraph indicates that the interest in minimizing phase fluctuations and frequency uncertainties arises from the desire to provide better acquisition and tracking performance at long ranges. The importance of this interest is dependent upon the anticipated applications of antenna arrays. If the sole interest were in providing large communication bandwidth capabilities at moderate ranges (say, bandwidths in excess of 1 kc), there would be little need for taking extreme measures to predict and compensate for frequency uncertainties and phase fluctuations (both common and differential). For these cases, the SNR will be sufficient in the signals at each antenna to permit independent phase acquisition and tracking on each signal.[4] However, since it is considered necessary for array capabilities to be pushed to extreme ranges where independent signal acquisition is difficult or impossible, minimization of frequency uncertainties and the bandwidth of phase fluctuations becomes very important in order to reduce threshold levels as much as possible. This subject was discussed in detail in reference [4] and will be considered further in Section IV.G below.

2. Atmospheric Phasefront Distortion

The subject of phasefront distortion of received spacecraft signals caused by refractivity variations in the atmosphere has been discussed rather thoroughly in an RTI report of pre-contract studies.[4] Atmospheric models were defined, based on all data which were readily available at that time. Because of the sparsity of data on fine-grained refractivity variations in the atmosphere, the assumed models were quite simple; a two layer troposphere and a three-layer ionosphere were selected, where each layer was assumed to possess statistical stationarity with respect to refractivity variance, scale size, and correlation time. Ranges of values of the significant parameters of these models were obtained from several sources. In spite of an extensive literature survey, the data available were insufficient to permit confidence intervals to be placed on the model parameters. However, these data were used to estimate ranges of "typical" model parameters under different seasonal, diurnal, and climatic conditions. Calculations of phasefront distortion of plane waves arriving from spacecraft and propagating through the entire atmosphere were made, based on the atmospheric models. The results of these calculations are shown in Figs. IV.C-1, and IV.C-2 and are included because of reference to them in other parts of this report.

At the start of this program, it had been hoped that data would become available for up-dating the atmospheric models as a result of visits to facilities conducting propagation studies, ionospheric research, and radio astronomy work. Unfortunately, this hope has not yet been borne out, although visits were made to Stanford University, California Institute of Technology, National Bureau of Standards, Cornell Aeronautical Laboratories, and two NASA Centers (Langley Research Center and Goddard Space Flight Center). These trips are reported in Appendix A. No serious disagreements were encountered in reviewing the results of previous calculations[4] with personnel from all of these organizations, and very little new data were uncovered. Questions were raised regarding the validity of extrapolating tropospheric characteristics from low altitudes to high altitudes; however, no alternate procedure was suggested. Actually, sufficient refractometer measurements have been made at several altitudes to indicate that the tropospheric models are at least typical, although no accurate confidence limits can be placed on them. Another question regarding the value of normalized electron density variance was raised. The assumed range was 2×10^{-5} to 4×10^{-4}; the opinion was expressed that values as high as 10^{-2} could be encountered for any system which operates through the auroral zone (a rather unlikely possibility). It was further pointed out that the assumption of ionospheric "blobs" elongated along the earth's magnetic lines may be realistic at times; however, there are theoretical reasons for expecting a "pancake" effect at other times (disturbed conditions), where the thickness along magnetic lines is less than that perpendicular to these lines.

Although interesting and useful, the discussions described above have not clarified the picture regarding atmospheric refractivity variations. The mechanisms determining the fine-grained structure of atmospheric refractivity appear to be poorly understood, especially with regard to the ionosphere. The inability to improve upon the atmospheric models by obtaining new data was not entirely unexpected.

The previous literature search was thorough enough to indicate that this might be the case. However, it was hoped that propagation data might have been obtained with some of the interferometer systems which are used for radio astronomy studies. Unfortunately, atmospheric propagation effects are of secondary interest to radio astronomers, being a nuisance which can be circumvented by appropriate measures (i.e., restricting measurements to high elevation angles, using long integration times, and using only the results obtained under quiet atmospheric conditions). The data recorded by radio astronomers appears to have been filtered to the extent that propagation effects have been removed.

The tentative conclusions to be drawn from the above discussion are:

(1) the phasefront distortion calculations reported in reference [4] are probably typical of those which will be encountered in practice; however, a great deal of uncertainty exists regarding the spread of values to be encountered, particularly with regard to ionospheric distortion;

(2) an extensive measurement program is desirable for determining the statistical parameters of propagation effects;

(3) although there are facilities which could be used for the measurement program, none of the facilities are being used for this purpose, and they probably cannot be diverted to an extensive propagation measurement program.

These conclusions support the belief expressed in references [1]-[4] that an experimental program should be conducted to permit thorough evaluation of atmospheric effects.

Because up-dating the results previously reported in reference [4] is not felt to be warranted, these results will be reviewed briefly. Fig. IV.C-1 shows the behavior of the fine-grained phase distortion with frequency and elevation angle. These curves correspond to the single-path standard deviation, as would be obtained by measuring the electrical pathlength of many parallel paths over an area having linear dimensions larger than the fine-grained correlation distance, but small relative to the gross scale discussed in reference [4]. Distributions of actual phase measurements (references [20] and [22] are superimposed on the curves (extrapolated to the longer paths by factors of about 2). Although this information does not serve as a check on the computed results (model parameters were influenced by these data), it is included to show that actual phase measurements are consistent with calculated results based on refractivity measurements. Unfortunately, the same degree of confidence cannot be placed in the left portions of the curves, because no single-path or differential-path phase measurements through the ionosphere are available for checking the computed results.

Fig. IV.C-2 shows the computed differential phase deviations as would be encountered over paths separated by the indicated distances. These distances are measured in a plane perpendicular to the line-of-sight. The E-W and N-S difference between the ionospheric portions of the curves results from the difference in assumed scale size (1 km E-W, 5 km N-S). The superimposed data (references [20] and [22] apply

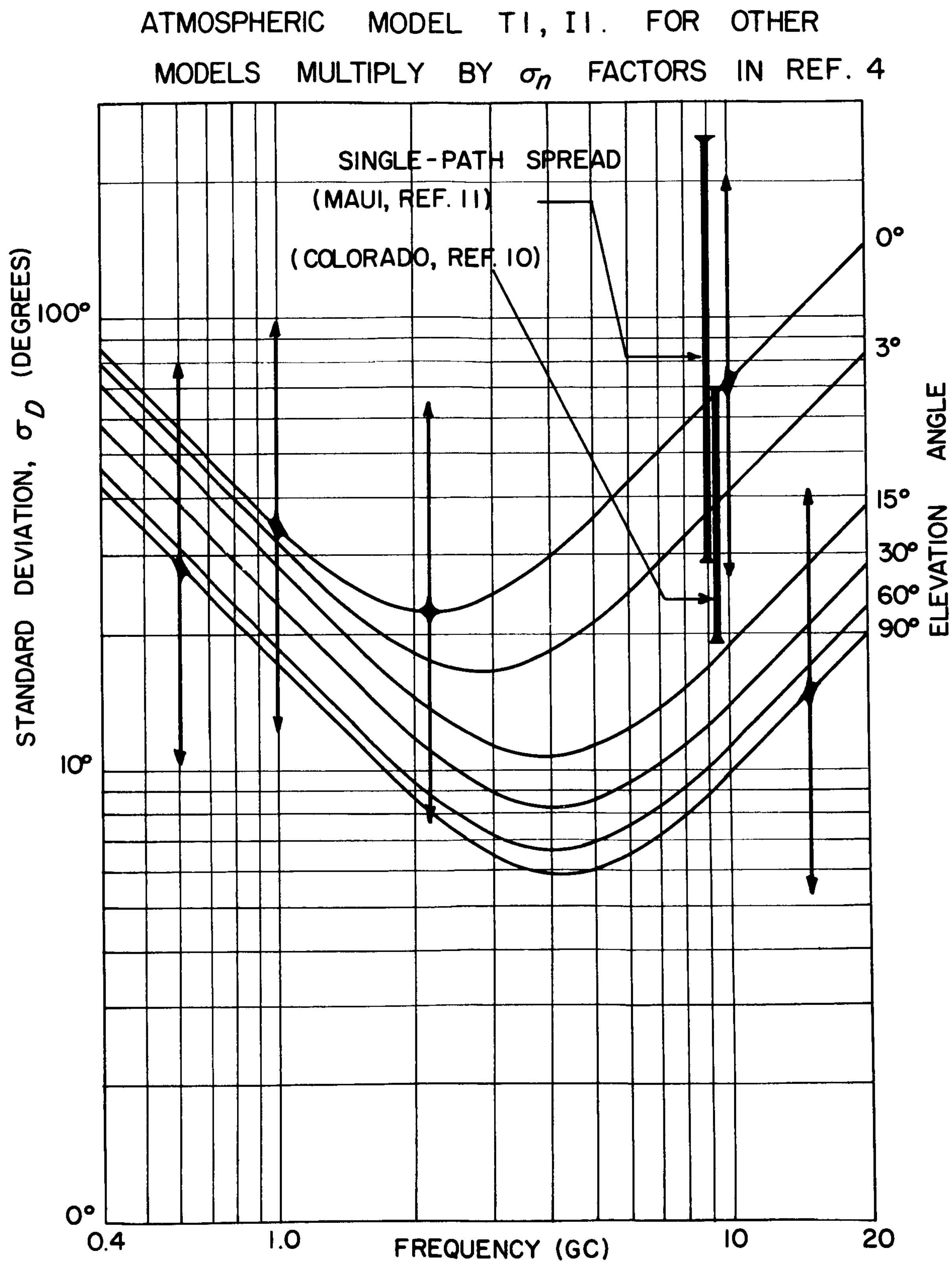

Fig. IV.C-1. Phasefront distortion versus frequency and elevation angle. Curves are average values, arrows show approximate spread. Model T1, I1 refers to a mid-latitude, clear atmosphere during high sunspot activity.

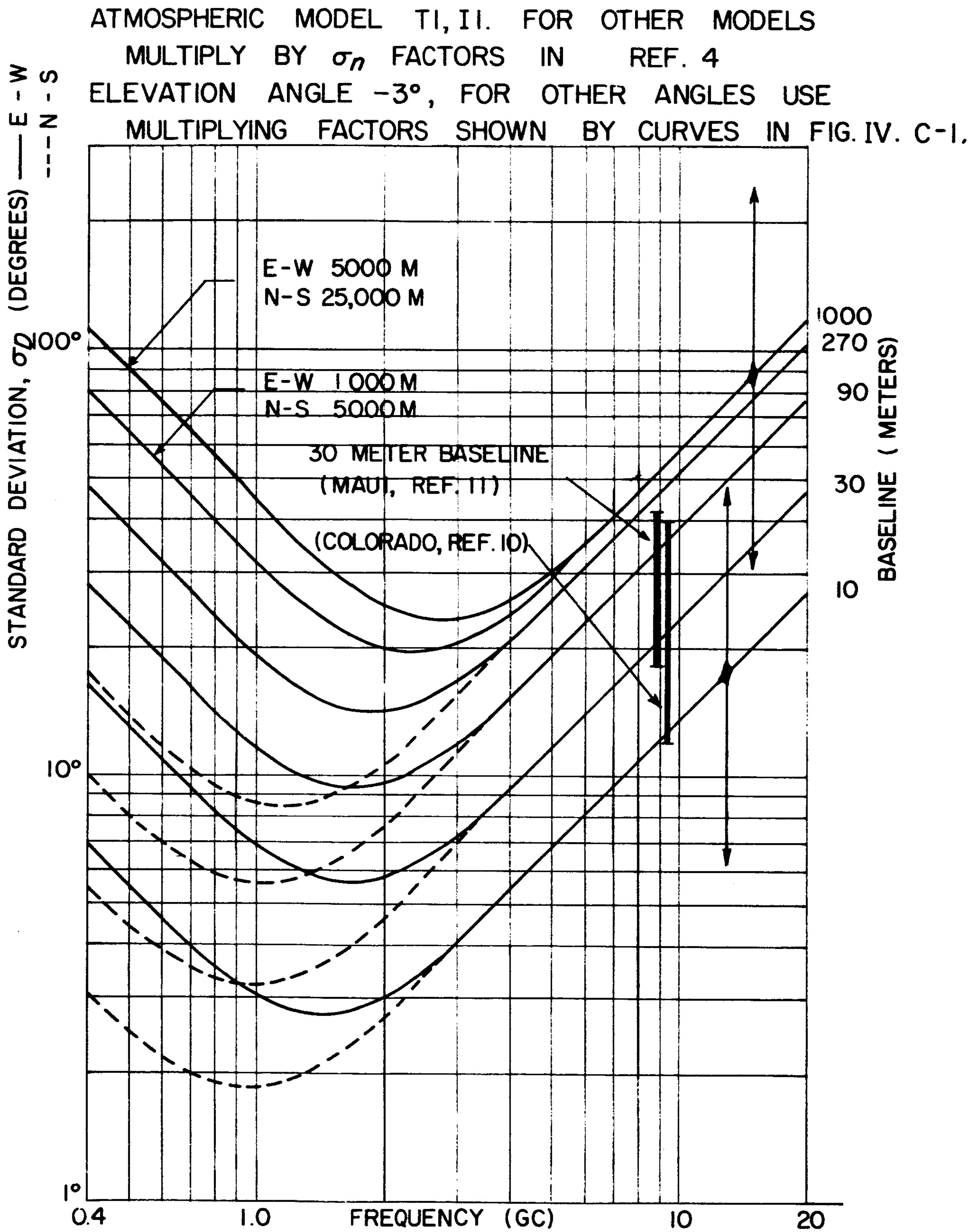

Fig. IV.C-2. Phasefront distortion versus frequency and baseline spacing. Curves are average values, arrows show approximate spread. Model Tl, Il refers to a mid-latitude, clear atmosphere during high sunspot activity.

to diverging paths from the transmitter rather than parallel paths for which the curves apply, but a useful comparison is permitted.

An optimum frequency range of 2-5 Gc is indicated for large-area antennas, (single or multiple apertures), operating from low to high elevation angles. Although a narrower band of optimum frequencies might be inferred from Figs. IV.C-1 and IV.C-2, it is felt that a more accurate designation of optimum frequency requires more accurate information on atmospheric parameters than is presently available.

The reduction in gain for large, single-aperture antennas caused by propagation effects is of considerable importance to antennas operating individually or in an array. Reference [4] estimates that the gain reduction from phasefront distortion for single-aperture antennas will be less than 1 db (95% confidence limits) for diameters less than 90 meters, frequencies in the 1-4 Gc range, and elevation angles above 3°. Similarly, an antenna with a diameter of 30 meters operating at 10 Gc and an elevation angle of 3° would suffer a gain reduction of 0-1 db. Further exploration of this subject would be desirable to obtain more specific results, but lack of complete data prevents this for the present. A tentative conclusion is that the optimum size for antennas in an array will be determined primarily by other factors than propagation effects (Section IV.B.1). However, aside from these other considerations, the approach of achieving very large antenna areas by the use of single apertures must be viewed with caution. Losses from propagation effects are expected to become excessive for antennas significantly larger than those in the examples given above.

If the correlation distance of phasefront distortion were large relative to the spacings between all antennas in an array, the differential phase variations between antennas would be significantly lower than the single path variations. This condition is not satisfied for either tropospheric or ionospheric effects; the results in Fig. IV.C-2 make it clear that continuous phase compensation (by differential phase trackers) must be applied to each received signal in an array. If this compensation were not provided, 1-4 db gain reductions would be encountered even in the optimum frequency range, 2-5 Gc. The required accuracy of the phase compensation is not particularly stringent; for example, rms errors of 0.5 radian result in gain reductions in the range of 0-0.3 db (95% confidence limits). Therefore, as long as the phase trackers are operational, gain reductions from tracking jitter will be small.

The correlation time of phasefront distortion is an important consideration to the design of phase acquisition and tracking circuits. As will be discussed in Section IV.G., the phase tracker performance is critically dependent upon the characteristics of the spectral density function of the phase noise on the input signals. The correlation function (with respect to time) and the power density spectrum have a Fourier Transform relationship. Therefore, the assumption of exponential covariance function of the single-path phasefront distortion,

$$\overline{\phi(t)\ \phi(t+\tau)} = \sigma_\phi^2\ e^{-|\tau|/\tau_o} \qquad \text{(IV.C-1)}$$

gives a power density spectrum

$$P(\omega) = \frac{2\sigma_\phi^2 \tau_o}{1 + \tau_o^2 \omega^2} \qquad \text{(IV.C-2)}$$

where $\phi(t)$ = phase distortion along a single path versus time,

σ_ϕ^2 = variance of $\phi(t)$,

τ_o = phase distortion correlation time, and

ω = radian frequency.

This relationship would give a spectrum bandwidth of $(2\pi\tau_o)^{-1}$, according to conventional definitions using half-power bandwidth.

The above results apply to single-path phase distortion. For the case of differential phase variations, the shape of the power density spectrum may differ appreciably from that given above. Differences may be expected particularly for ionospheric effects, where the antenna spacings will generally be smaller than the refractivity correlation distance. However, for tropospheric effects, the antenna spacings will generally be greater than the correlation distance. Consequently, in the latter case, the expression given above applies to differential as well as single-path phase variations, where σ_ϕ^2 is taken as the variance of the differential phase function. Because of the uncertainty in ionospheric scale size, the form of $P(\omega)$ given above will be used for both differential and single-path phase variations for all atmospheric propagation effects.

For the atmospheric models chosen in reference [4], the estimated correlation time of the phasefront distortion is in the range from 5-100 seconds. Because of this wide spread, the bandwidth of the phase trackers should be adaptable to the conditions existing at a given time, and the minimum bandwidth of the differential phase trackers (as limited by propagation effects) will probably be of the order of 0.005-0.05 cps. Although the pathlength changes common to all antennas in an array are larger than the differential pathlength changes, their bandwidth will be somewhat smaller because of the "high-pass" characteristic of spaced antennas on the phasefront distortion (spatial cut-off frequency inversely proportional to antenna spacing). Thus, propagation effects are also expected to limit the common phase-tracker bandwidth to the order of 0.005-0.05 cps.

The correlation time of phasefront distortion is determined by two factors: correlation time of refractivity deviations at fixed points relative to the earth's surface; and the rate of line-of-sight motion across the atmospheric "blobs." For cases where the spacecraft range is many earth radii, the angular line-of-sight rotation is equal to the earth's rotation rate. A simple geometric picture permits relating the correlation time to the antenna elevation angle and the refractivity scale size. Tropospheric "blobs" at an altitude of 5 km and scale size of 120 meters (isotropic) give the following sets of correlation times for the indicated elevation angles: 0° - 6 sec; 3° - 20 sec; 15° - 90 sec; and 90° - 330 sec. Similarly, ionospheric "blobs" at 300 km altitude give the results: 0° - 7 sec; 3° - 8 sec, 15° - 15 sec, and 90° - 48 sec. These results show that line-of-sight rotation is probably the predominate factor in determining correlation time for low elevation angles. In fact, the correlation time for ionospheric effects may be determined primarily by this factor for all elevation angles. This is evidently not the case for tropospheric effects, where refractivity correlation time is expected to be the predominate factor for high elevation angles.

Cloud effects were not considered explicitly in the calculations,[4] although one of the atmospheric models is based on Hawaii data taken during cloudy periods. Other Hawaii data have been used to estimate radar range errors with the following results: for 37% cloud cover (thickness unspecified), wind velocity 9 meters/sec, elevation angle 7°

and targets above the clouds, the estimated rms errors in range and range rate are 10 cm and 0.03 cm/sec, respectively. Assuming a scale size of 120 meters within the clouds, the estimated correlation time of the range-rate errors for this elevation angle would be 100 sec. Therefore, for the conditions listed above, rms phasefront distortion of the order of 1-3 cm could be expected from fine-grained refractivity "blobs" in the clouds. Fortunately, the bandwidth of this distortion would be quite narrow. For higher elevation angles, the rms distortion is less severe but the bandwidth is wider. Although this estimate is quite crude, it appears that heavy cloud cover could cause serious phasefront distortion which under some conditions would exceed that caused by other tropospheric effects. Similarly, heavy rainfall may cause serious phasefront distortion at frequencies above 3 Gc. The most effective cause for this distortion is believed to be refractive "blobs" rather than scattering, because the fraction of scattered power will generally be small relative to the feed-through power. More information on the refractivity distribution in clouds and rainfall is needed in order to permit conclusive evaluation of their propagation effects on the operation of arrays of large-aperture antennas.

There is some basis for the belief that interplanetary plasma (solar "blobs") may produce significant propagation effects on deep-space communication signals (reference [21]). Although the anticipated ionization densities are quite low and consequently would be expected to affect only the lower frequencies (say, less than 0.3 Gc), two important factors should be pointed out. First, at the frequencies of interest, phase changes produced by plasma-density deviations vary approximately as the reciprocal of the frequency. Thus, the improvement with increasing frequency is rather slow. Second, the extremely long communication ranges permit millions of km of intervening plasma "blobs." Because of the long ranges, multipath propagation between a spacecraft and a given point on the earth may occur and cause large and rapid changes in signal amplitude and phase.

Reference [4] summarizes the results of several references regarding the plasma density of ejected clouds of ionized gas shot out from the sun. Some deductions show that ionized gas flows outward from the sun at rates of 500-1500 km/sec and at one astronomical unit the density should be of the order of 500 electrons/cc. Another source has computed a density in excess of 10^3 ions/cc with velocities of 500-2000 km/sec as being necessary to explain observed geomagnetic storms. The plasma densities are naturally expected to be much greater near the sun than for distances comparable to one or more astronomical units. A sample calculation shows that in environments where the "blob" deviations are of the order of 25 electrons/cc, a wave at one Gc would be totally reflected for grazing angles less than $\sqrt{2}$ milliradians. Therefore, it is apparent that serious multipath effects could occur, even for frequencies of several Gc. Observations by Hewish indicate that multipath effects may have been responsible for observed broadening of the Crab Nebula when the ray paths passed within 60 solar radii of the sun. Although the measurements were made at low UHF and might not be representative of effects in the 0.5-10 Gc range, the fact that they were observed at all would indicate that the multipath effects must have been very severe.

Measurements of resonance absorption by interplanetary gases, comprised largely of single and combined hydrogen and oxygen atoms, have been made by observing the absorption dips of radiation from radio stars (H line at 1.42 Gc, OH lines at approximately 1.67 Gc).[4] The nature of the measurements required to detect the absorption lines show that they are quite weak. Consequently, the phasefront distortion introduced by these gases will probably be negligible over the frequency band of interest. However, it is possible that "blobs" of gases could cause rather rapid phase changes without amplitude absorption having been observed.

It must be concluded at this time that insufficient information is available on the characteristics of interplanetary plasmas and gases to permit evaluation of their propagation effects. The estimated dimensions and velocities of these "blobs" indicate that the bandwidth of phase fluctuations from these sources could be much larger than that of atmospheric-induced fluctuations.

Although it is emphasized above that phasefront distortion is the most serious atmospheric effect, amplitude modulation effects are also of interest. This is especially true for low-frequency modulation, which affects the choice of optimum signal combination (Section IV.F). As stated in reference [4], amplitude scintillation will be significant only at the low elevation angles. For these cases, ionospheric and tropospheric refractivity variations will often cause appreciable multipath interference, which results in amplitude modulation. The signal amplitude is expected to have an average component plus a random, Rayleigh-distributed component. Modulation depths of the order of 0-30% are expected for frequencies near 1 Gc (reference [36] where ionospheric effects predominate. Comparable modulation is expected from tropospheric effects at frequencies in the vicinity of 10 Gc. Therefore, although the amplitude modulation may degrade the effectiveness of signal summation, it is not expected to cause excessive reduction in sensitivity for any form of acquisition described in Section IV.G.

3. Equipment Phase Instabilities

Equipment phase instabilities fall into two classes: short-term variations caused by thermal noise effects and power-supply ripple; and long-term variations caused by slow drifts in temperature, power supply voltages, signal level, and circuit parameters.

The stable-oscillator circuit is the major cause of short-term phase instabilities; the phase fluctuations from this source will be common to all antennas and are expected to have a bandwidth of the order of 1 cps.[4] Long-term phase and frequency variations are not expected to present serious problems because of the "turn-around" technique described in Section III. If this technique is not operable, long-term drifts in the spacecraft oscillator may introduce frequency uncertainties of the order of tens or hundreds of cps, thus introducing a rather serious frequency-search problem at long ranges.

With the exception of fluctuations caused by noise for low SNR conditions, phase instabilities in other circuits can be reduced to small values by careful circuit design. The former fluctuations are fundamental and can be reduced only by improvement in SNR at the front end of the receiver channels. The necessary information for circuit design of operational systems is the behavior of each component's phase function to changes in environmental conditions, power supply voltages, and input signal characteristics. If this behavior is known, specifications can be set on all controllable factors to reduce the phase variations to acceptable values. For example, AM and PM produced on signals by power-supply ripple should be maintained at a low enough level to cause spurious sideband power to be negligible, relative to the power in the carrier and intentional sidebands. This requirement is not expected to impose serious design problems.

A more difficult problem regarding equipment phase instabilities is expected to be caused by slow drifts in phase shifts occurring at fractional cps rates. The equipment should be designed so that these rates are significantly smaller than the rates of phasefront variations discussed above. This requirement should present no serious design problems, once the necessary information regarding propagation effects has been obtained.

Phase and angle acquisition procedures may impose even more stringent specifications on equipment phase instabilities than the one just described. For one type of pre-focusing discussed in Section IV.G., it is necessary to maintain fixed phase relationships between the phase transfer functions of all receiver channels, from the antennas to the signal summing matrix in the central station. This requirement can only be achieved by an accurate phase compensation method (e.g., one type of which is discussed in Section IV.D.).

4. Doppler Uncertainties and Compensation

During the early phase of a deep-space flight, the velocity of the spacecraft will not be known accurately. Therefore, the necessary doppler correction will not be predictable with high accuracy. This presents no difficult problem during this phase because the signal-to-noise ratio of received signals will be quite high. As the spacecraft recedes from the earth, previous doppler measurements will permit more and more accurate doppler prediction. By the time signal acquisition becomes a problem, the only remaining doppler uncertainties should be caused by errors in information on gravitational forces and on velocity corrections which have been applied to the spacecraft. Thus far, very little information is available concerning the magnitudes of these errors, and data is needed to estimate bandwidth limitations on the phase acquisition circuits imposed by these uncertainties.

It is important at this time to point out that once the necessary doppler corrections have been determined, methods are available for applying them with almost unlimited accuracy (errors are determined solely by instabilities in the best available clocks). The compensation would probably be made in two steps: (1) the doppler component common to all antennas; and (2) the differential doppler components existing between signals received at the different antennas. The former component would fall in the kc to Mc range and would consequently require electronic correction; the latter component would fall in the cps range and could be corrected by electromechanical phase shifters. Both types of corrections can be made in a straightforward manner by the use of single sideband modulators operating on the received signals prior to signal summation. Pre-set digital counters can be used to monitor the doppler corrections, where the counter outputs are fed back into the offset oscillator (or rotating phase shifter) to produce the required counter output. These techniques have been implemented in other applications (e.g. doppler navigation readouts), and present no serious design problems.

D. Intra-Array Phase Compensation

1. Introductory Discussion

Before discussing the method of phase compensation which is the main subject of this part, another system previously described in the literature will be reviewed briefly. Fig. IV.D-1 illustrates a system which is designed for observation of phase variations along line-of-sight paths in the troposphere. The system is well suited to the task and may be adapted to compensation of data-link phase variations. Referring to Fig. IV.D-1, each end of the path contains a stable oscillator, offset from the other by an audio frequency, f_a. Each oscillator output is transmitted to the other end of the link, where it is mixed with the other oscillator output to produce an audio signal at frequency f_a. The two audio signals are brought together into a phase comparison circuit (over a link producing negligible phase shift to the audio envelope). Variations in the data-link propagation time, $\Delta\tau_1$, appear on the output of this circuit as phase variations, $-2\omega_1\Delta\tau_1$. This measurement of $\Delta\tau_1$ may be the main purpose of the system, or it could be used to provide compensation for variations in τ_1.

The phase-compensation method described below operates on a different principle from the one illustrated in Fig. IV.D-1. A single stable oscillator is used, and variations in data-link delay time are self-compensated. In many cases, data-link phase variations comprise the major problem in stabilizing the phase shift from a given antenna to the central comparison site. For these cases, the method to be described below in 2 is sufficient and provides self-compensation. Other systems may require additional stabilization of phase shifts through the receiver channels (preamplifiers, mixers, IF amplifiers, IF data-link, etc.). For these systems, the added compensation provided by the method described below in 3 may be employed.

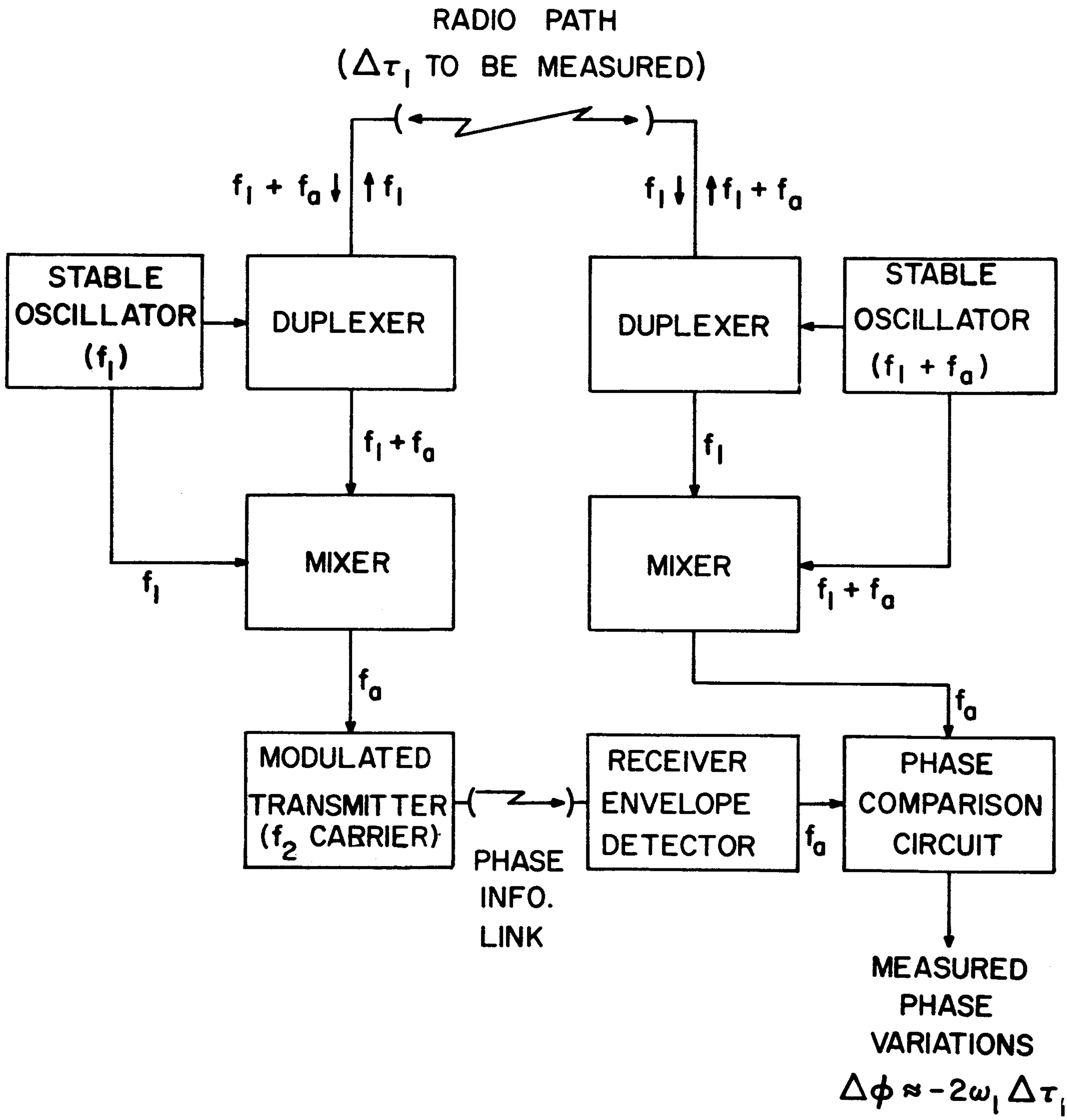

Fig. IV.D-1. System for measurement of line-of-sight phase variations.

The phase compensation method will be described in three steps: phase compensation for a coherent reference to be supplied at several separated sites, Figs. IV.D-2 and IV.D-4; measurement of phase shift through each receiver channel, Figs. IV.D-3 and IV.D-4; and equalization of the phase shifts through any number of channels, Fig. IV.D-5. The first step is not necessary in a strict sense, because the received signals could be transmitted from the antenna sites to a central summing point over RF links, in this manner avoiding frequency translation at the antenna sites. However, for practical reasons (e.g., interference and channel phase-stability considerations) it is generally desirable to perform a frequency translation at the antenna sites, either to another RF or to an IF. Translation to an IF has the advantage of reducing the signal phase variations caused by changes in propagation time of the signal link; in most cases signal-link phase variations can be reduced to a negligible degree by this technique.

All illustrations are simplified by showing only one of the N antenna sites; also, circuits which do not modify the signal form (i.e., amplifiers, phase-locked receivers, etc.) are omitted, although such circuits will be needed for implementation. The following symbol notation is used:

f_o	- basic oscillator frequency;
a, b, c, d, e	- rational number multipliers of f_o giving intermediate frequencies (these are integers or the ratio of integers);
m, n	- rational number multipliers of f_o giving RF carrier frequencies;

ϕ_{si} - phase of received signal at the i th antenna, with respect to the phase of a reference signal at the central station derived from the stable oscillator;

ϕ_{v1}, ϕ_{v2}, etc. - phase shifts through the receiver channel from the antenna phase center to the indicated point in the channel;

$\phi_{\ell 1}$, $\phi_{\ell 2}$, $\phi'_{\ell 2}$, etc. - phase shifts introduced by the bilateral part of the relay link, or stable modifications of these phases by multipliers;

ϕ_{a0}, ϕ_{a1}, ϕ'_{a1}, etc. - phase shifts introduced by stable, small-dimension circuits, or modifications of these phases by mixers or multipliers;

ϕ_b, ϕ_c, ϕ_d, series - same as ϕ_a series originating at different points;

ϕ_{ab} series - phase shifts resulting from a combination of the ϕ_a and ϕ_b series;

E_{si0}, E_{si1}, etc. - received signal at the indicated points in the i th signal channel;

E_{ti0}, E_{ti1}, etc. - test signal at the indicated points in the signal channel.

In order to simplify the notation, each time a phase modification is introduced by multiplication or addition in a circuit, the phase subscript is advanced by one integer. For example, in passing through the first mixer, the channel phase is advanced from ϕ_{v1} to ϕ_{v2}. In passing through a given circuit element, the phase modification is attributed to one term, although several terms may appear in the expression for input phase.

It is important to notice the nature of the phase terms. The ϕ_v series is sensitive to signal level, frequency, power supply voltages, and environmental conditions. The ϕ_ℓ series is sensitive primarily to environmental conditions. The ϕ_a, ϕ_b, ϕ_c, and ϕ_d series and combinations of these series result from compact circuits operating at constant signal level, constant frequency, and under controllable environmental conditions. Thus, although the ϕ_v and ϕ_ℓ series will show considerable variation with time (at rates in the order of minutes, hours, or days depending upon circuit design and local conditions), the ϕ_a through ϕ_d series can be made extremely stable over indefinite periods of time by careful design and occasional checking. Therefore, it may be assumed that these phase terms can be compensated during design and by maintenance-type adjustments. The problem considered here is the compensation of the ϕ_v and ϕ_ℓ phases, including their time variations. It will be assumed that these variations are negligible during the round-trip propagation time from the central station to each antenna site.

2. Compensation of Reference Signals Supplied to Separated Antennas

Referring to Fig. IV.D-2, the operation of the system is self-explanatory. The first form of E_{si4}, the output of the second mixer, is derived by tracing the received and reference signals through their respective paths. Simplification of this form is made by starting with reference signal E_{r1}, the input to the Multipliers block at the antenna site and observing:

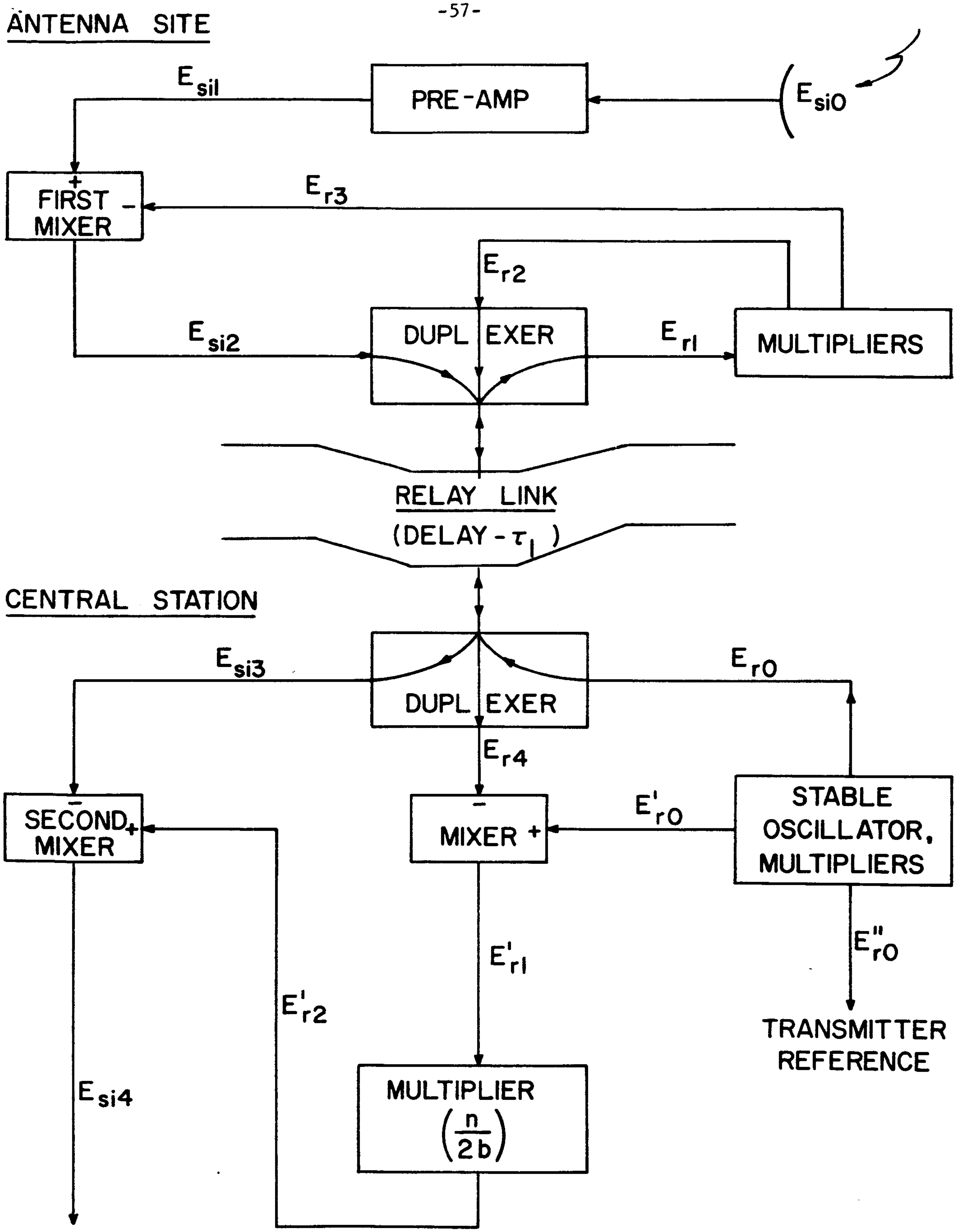

Fig. IV.D-2a. System for providing compensated reference signal at separated antenna sites.

Symbol	Frequency $\underline{/\text{Phase}}$
E_{r0}	$af_o \; \underline{/\phi_{a0}}$
E_{r1}	$af_o \; \underline{/\phi_{\ell 1} + \phi_{a1}}$
E_{r2}	$bf_o \; \underline{/\phi_{\ell 2} + \phi_{a2}}$
E_{r3}	$nf_o \; \underline{/\phi'_{\ell 2} + \phi'_{a2}}$
E_{r4}	$bf_o \; \underline{/\phi_{\ell 3} + \phi_{a3}}$
E'_{r0}	$cf_o \; \underline{/\phi_{c0}}$
E'_{r1}	$(c-b)f_o \; \underline{/-\phi_{\ell 3} + \phi_{ac0}}$
E'_{r2}	$\frac{n}{2b}\,(c-b)f_o \; \underline{/-\phi_{\ell 4} + \phi_{ac1}}$
E_{si0}	$mf_o \; \underline{/\phi_{si}}$
E_{si1}	$mf_o \; \underline{/\phi_{si} + \phi_{v1}}$
E_{si2}	$(m-n)f_o \; \underline{/\phi_{si} + \phi_{v2} - \phi'_{\ell 2} - \phi'_{a2}}$
E_{si3}	$(m-n)f_o \; \underline{/\phi_{si} + \phi_{v3} - \phi'_{\ell 2} - \phi'_{a2}}$
E_{si4}	$\left[\frac{n}{2}\,(1 + \frac{c}{b}) - m\right] f_o \; \underline{/-\phi_{si} + \phi_{v4} + \phi'_{\ell 2} - \phi_{\ell 4} + \phi_{ac2} + \phi'_{a2}}$
	$= \left[\frac{n}{2}\,(1 + \frac{c}{b}) - m\right] f_o \; \underline{/-\phi_{si} + \phi_{v4} + \phi_{aci}}$

Fig. IV.D-2b. Symbol definition for Fig. IV.D-2a.

Signal	Relay-link Phase	
E_{r1}	$\phi_{\ell 1} = -a\omega_o \tau_1$	
E_{r3}	$\phi'_{\ell 2} = -n\omega_o \tau_1$	
E'_{r1}	$\phi_{\ell 3} = -2b\omega_o \tau_1$	(IV.D-1)
E'_{r2}	$\phi_{\ell 4} = \phi'_{\ell 2}$	

Thus, phase variations introducted in distributing the reference signal (i.e., variations in τ_1) do not appear on the output signal E_{si4}. The phase of the input signal, ϕ_{si}, and phase shifts through the signal path, ϕ_{v4}, are retained in this output signal. A highly stable phase term, ϕ_{aci}, appears in the output and is caused by multipliers and passive, small-dimension circuits.

The method of compensation described above is obviously applicable to any number of widely-spaced sites. It is not dependent upon the type of relay link used (i.e., transmission line or radio), nor upon the length of the link (as long as the assumption of negligible variation of τ_1 during the round trip delay time is valid). Multipath effects should be compensated as long as this condition is met. Sufficient signal strength must obviously be maintained in transmission over the link, in order that receiver thresholds at the terminal ends are exceeded.

Although a common signal and reference relay link is shown in Fig. IV.D-2, this is not necessary. Phase compensation will still be achieved for separated links, as long as the same link is used for round-trip propagation of the reference signal. Phase variations introduced on the signal by the relay link between the antenna sites and the central station are added to ϕ_v rather than ϕ_ℓ, an aribtrary but convenient choice since the compensation method in Fig. IV.D-2 does not remove these variations. Actually, variations in τ_1 will have practically negligible effect on ϕ_v for cases where signals are transmitted over this link at an intermediate frequency. In fact, this insensitivity to variations in τ_1 represents an important advantage in distributing a coherent reference to each antenna site and transmitting signals over the relay link on an IF carrier. Transmission of the reference signal over the relay link at IF does not provide a similar advantage, because phase variations are multiplied up to the local oscillator carrier frequency, nf_o. In many applications, the self-compensation described above may be adequate; and the added compensation for signal-channel phase variations described below may not be necessary.

The method of reference signal compensation described above is based on a simple concept: delay time variations, $\Delta\tau_1$, on the up-link are introduced negatively on the signal in the first mixer as a phase term, $n\omega_o\Delta\tau_1$; variations on the round-trip link, $2\Delta\tau_1$, are introduced positively on the signal in the second mixer as a phase term, $\frac{n}{2}\omega_o 2\tau_1$. The technique is more generally applicable to other multiplication ratios (not just $\frac{1}{2}$), as will be shown below.

3. Signal Channel Phase Measurement

In many applications of widely-spaced antennas, it is desirable that signal phase shifts introduced between the phase center of an antenna and some central point of comparison (or addition) be closely equalized, or held at some fixed relationship. Although the method described above may be adequate for providing relatively-stable phase shifts through the signal channels, it does not maintain fixed and known phase relationships over long periods of time. A variation of the system previously described will be used to illustrate how the required equalization can be accomplished, where channel phase shift measurements are first made, Fig. IV.D-3. A switch at the antenna terminals permits introducing a test signal, E_{ti0}, into the system. Because this signal is derived from the same source as the reference signal to the first mixer, E_{r3}, variations in τ_1 on the up-link are partially cancelled in this mixer, giving

$$\begin{aligned} \phi'''_{\ell 2} &= \phi''_{\ell 2} - \phi'_{\ell 2} \\ &= (m-n)\omega_o \tau_1 \end{aligned} \qquad \text{(IV.D-2)}$$

Suitable methods of generating the reference signal for the second mixer, E'_{r3}, result in a relay-link phase term given by

$$\begin{aligned} \phi_{\ell 4} &= \frac{m-n}{2b} \phi_{\ell 3} = (m-n)\omega_o \tau_1 \\ &= \phi'''_{\ell 2} \end{aligned} \qquad \text{(IV.D-3)}$$

Thus, the relay link variations do not appear on the output signal, E_{ti4}. Phase shifts introduced in the signal path (i.e., the ϕ_v series) appear on E_{ti4} in an identical manner to their appearance on E_{si4}. The stable phase term, ϕ_{adi}, is different from that on E_{si4}.

Obviously, there are many alternate methods for accomplishing the results described above. The actual choice of multiplying factors and the circuit design (mixers, filters, duplexers, and multipliers) are quite flexible. Advantage should be taken of this flexibility to minimize circuit complexity and interference problems between the many

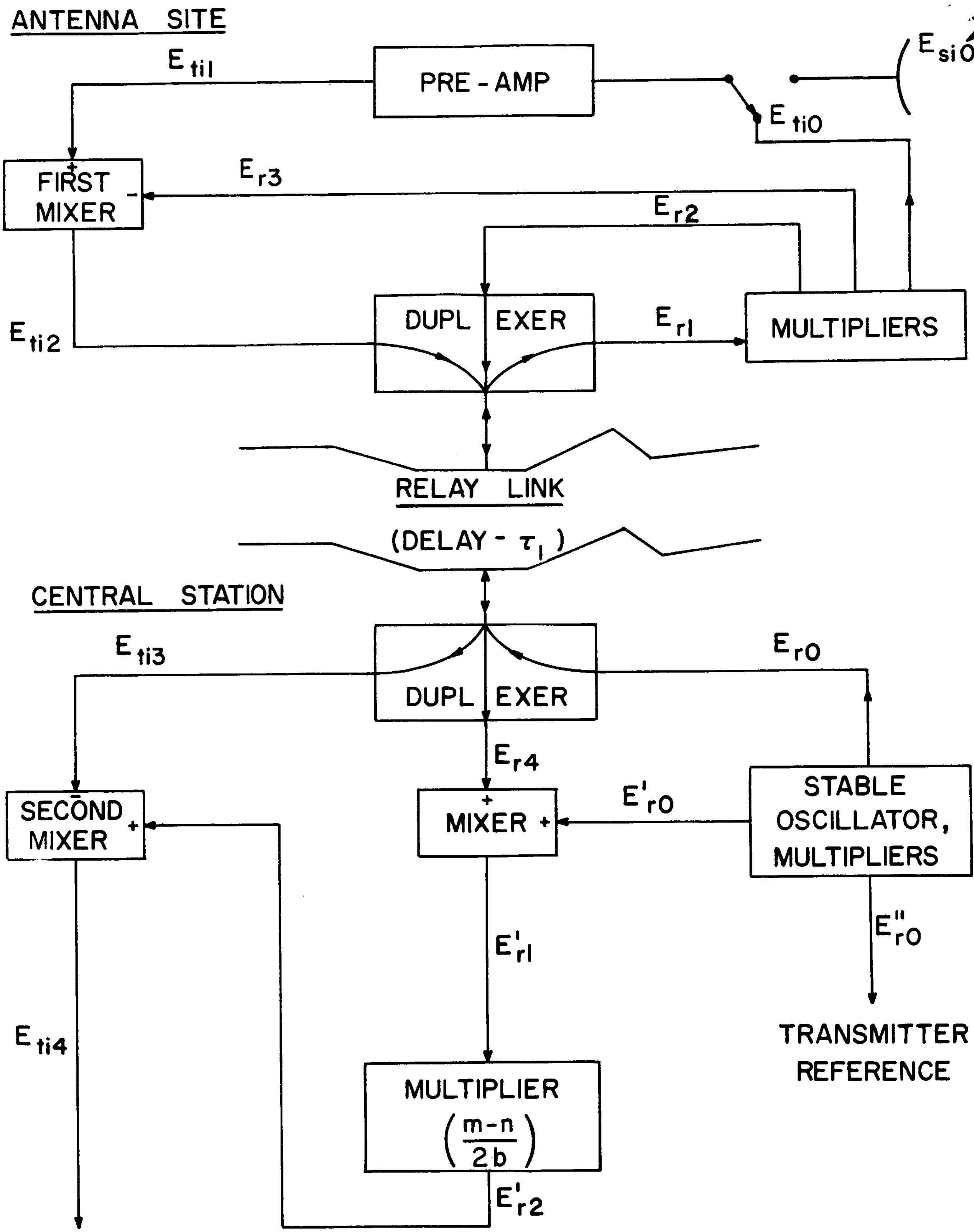

Fig. IV.D-3a. System for measurement of signal-channel phase shifts.

Symbol	Frequency $\angle$ Phase
E_{r0}	$af_o \ \angle \phi_{a0}$
E_{r1}	$af_o \ \angle \phi_{\ell 1} + \phi_{a1}$
E_{r2}	$bf_o \ \angle \phi_{\ell 2} + \phi_{a2}$
E_{r3}	$nf_o \ \angle \phi'_{\ell 2} + \phi'_{a2}$
E_{r4}	$bf_o \ \angle \phi_{\ell 3} + \phi_{a3}$
E'_{r0}	$\left[\frac{n}{m-n}(c-b)-b\right] f_o \ \angle \phi_{d0}$
E'_{r1}	$\frac{n}{m-n}(c-b)f_o \ \angle \phi_{\ell 3} + \phi_{ad0}$
E'_{r2}	$\frac{n}{2b}(c-b)f_o \ \angle \phi_{\ell 4} + \phi_{ad1}$
E_{ti0}	$mf_o \ \angle \phi''_{\ell 2} + \phi''_{a2}$
E_{ti1}	$mf_o \ \angle \phi_{v1} + \phi''_{\ell 2} + \phi''_{a2}$
E_{ti2}	$(m-n)f_o \ \angle \phi_{v2} + \phi'''_{\ell 2} + \phi'''_{a2}$
E_{ti3}	$(m-n)f_o \ \angle \phi_{v3} + \phi'''_{\ell 2} + \phi'''_{a2}$
E_{ti4}	$\left[\frac{n}{2}(1+\frac{c}{b})-m\right] f_o \ \angle \phi_{v4} - \phi'''_{\ell 2} + \phi_{\ell 4} - \phi'''_{a2} + \phi_{ad2}$
	$= \left[\frac{n}{2}(1+\frac{c}{b})-m\right] f_o \ \angle \phi_{v4} + \phi_{adi}$

Fig. IV.D-3b. Symbol definition for Fig. IV.D-3a.

signals in the system. Fig. IV.D-4 represents a possible choice of parameters for illustrative purposes, but these are not necessarily a good set for circuit implementation. In this figure, synchronous RF and IF switches are indicated. Consequently, E_{si4} and E_{ti4} appear on the output for switch positions 1 and 2, respectively. Alternately, both E_{si} and E_{ti} can be allowed to pass through the channel simultaneously, spacing them in frequency to allow filter separation. Another possibility is to impose some distinctive modulation on E_{ti0} and employ synchronous demodulation and narrow-band filtering to separate E_{si4} and E_{ti4}. In the latter case, the carrier frequencies of E_{ti} and E_{si} could be identical, however, it may be desirable to use suppressed carrier modulation on E_{ti} to avoid interference between the two signals.

4. Equalization of Multiple-Channel Phase Shifts in Antenna Arrays

The results shown in Figs. IV.D-3 and IV.D-4 for E_{si4} and E_{ti4} will be compared further in order to illustrate how they can be used to equalize multiple-channel phase shifts for a number of separated antennas connected to a central station, as in Fig. III-1c. The time-sharing system shown in Fig. IV.D-4 will be used to describe the equalization method. This system is a combination of Figs. IV.D-2 and IV.D-3, employing the second-mixer reference derived in Fig. IV.D-2 when the system is operating in the receive mode (switch position 1) and that derived in Fig. IV.D-3 for operation in the test mode (switch position 2). The system is also adaptable to the alternate methods of applying the test signal mentioned above (i.e., frequency separation of E_{si} and E_{ti}).

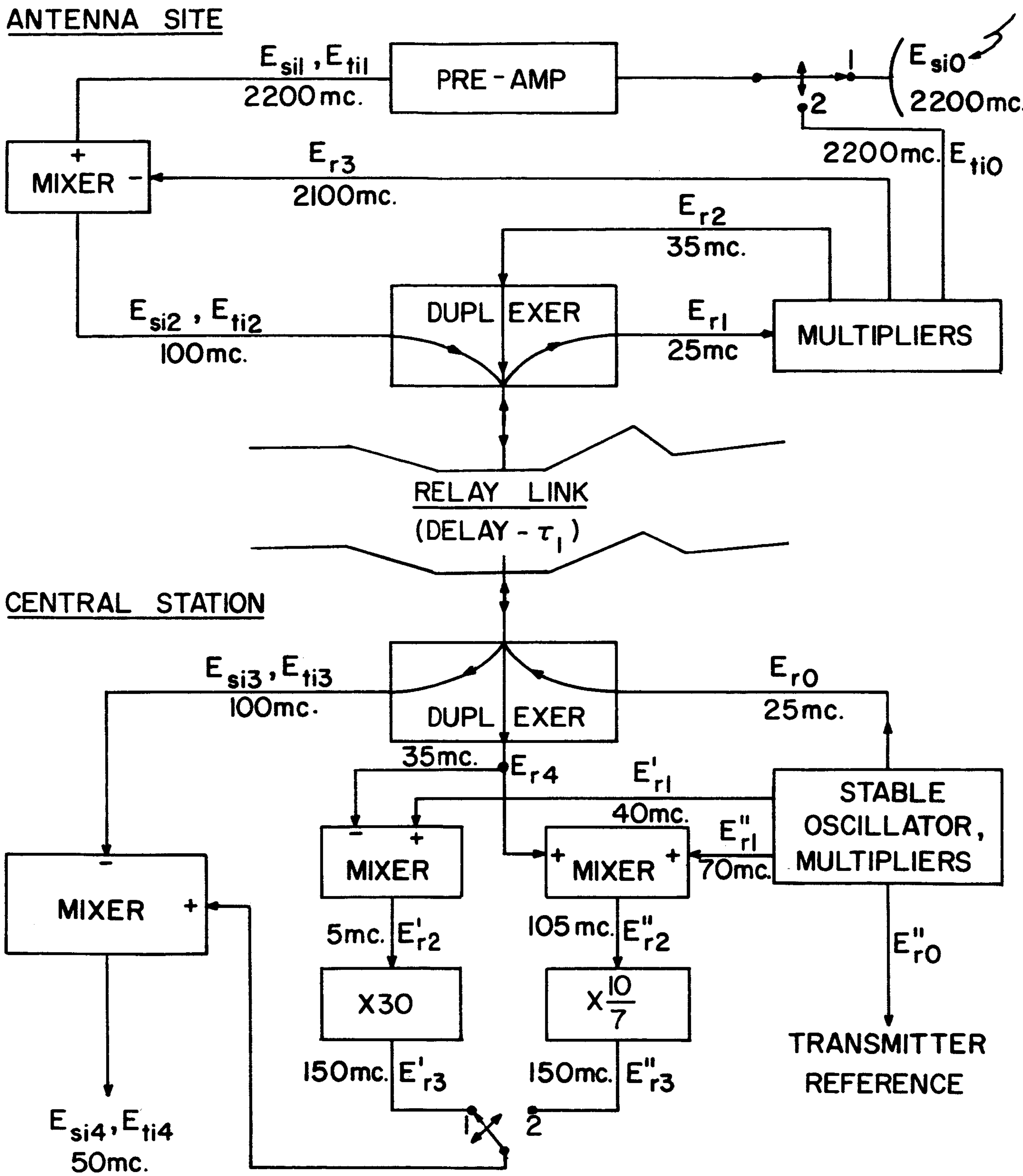

Fig. IV.D-4. Illustrative example of a system combining techniques shown in Figs. IV.D-2 and IV.D-3.

Referring to Fig. IV.D-5, the phase-control loops in the second mixers cause all output E_{ti4} signals to assume equal phases, because they are slaved to a common reference from the stable oscillator. In order to equalize the channel phase shifts, the terms, $\phi_{aci} - \phi_{adi}$, must be removed from the resulting signals. This is the difference phase term in a given channel between the receive and test modes. Therefore, when the system is operating in the receive mode (switch position 1, output E_{si4} signals), all channels have equal phase shifts within an integer number of periods, between the antenna phase centers and the beam-forming matrix. This condition may or may not form a focused beam in space, depending upon the geometry of the antenna phase centers and upon phasefront distortion introduced by refractivity variations of the atmosphere. Assuming negligible atmospheric effects, the required beam-forming matrix can be derived from the geometry of the antenna phase centers. For example, it is possible to establish a number of overlapping beams (each having the array gain and the corresponding SNR) in order to provide high-gain coverage throughout the beam of each antenna.

It will be noticed in Fig. IV.D-5 that all signal channels have variable delay lines within the phase-control loops. These delay lines may be continuously variable or adjustable in steps and are necessary to provide approximate envelope synchronization of wideband signals from all antennas. The required delay values are a function of antenna pointing angle. Because these delay lines are in the phase control loops, phase compensation can be provided for all sets of delay lines.

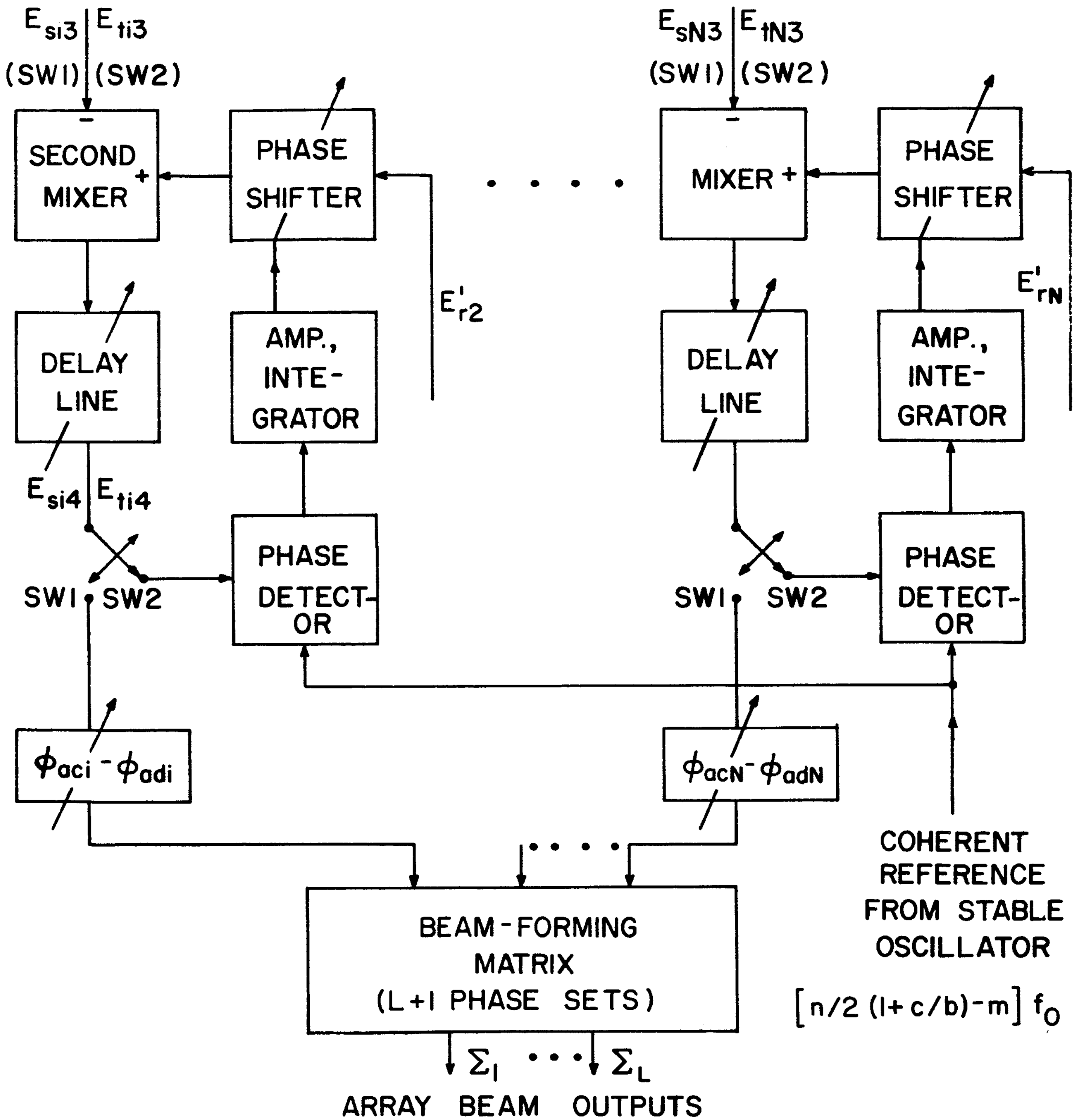

Fig. IV.D-5. System for equalizing multiple-channel phase shifts.

For communication with deep-space probes, the use of an array for reception of spacecraft signals (i.e., the down-link) is of principal interest. Single-aperture antennas appear to be adequate for transmission on the up-link.[4] During extremely long-range operation, where down-link data rates are limited by SNR considerations to a few bits per second, angle and phase acquisition of the spacecraft signal becomes a serious problem. Although phasefront distortion caused by atmospheric refractivity variations is a serious consideration to these arrays, the technique illustrated in Fig. IV.D-5 can be useful for pre-focusing the array in many cases. Calculations in reference [4](discussed in Section IV.C.2.) show that phasefront distortion will be serious enough to degrade the pre-focused array lobes; however, there appear to be few cases where the lobes would be essentially destroyed. Thus, the beam-forming technique can be useful to varying degrees during angle and phase acquisition; the system would then become self-focusing after phase tracking starts.

Arrays of large-aperture antennas are more easily adapted to the reception of signals than to transmission, because of the self-focusing capability provided by phase-tracking received signals at each antenna.[5, 6] However, the phase-compensation method described above can be adapted to phase-equalization for diverging paths from a central point to many widely-spaced antennas. A coherent carrier can be distributed from a stable oscillator through a beam-forming matrix (both located at a central station) to power amplifiers located at the antenna sites. The transmit beam formed in this manner would be based on "open-loop" computation of the required phases to focus the beam, determined strictly by the geometrical arrangement of the antenna phase centers. Thus, de-focusing caused by refractivity variations in the troposphere and ionosphere would degrade such a beam; as pointed out above, the degradation may be small enough to be acceptable in many cases. For applications which permit acquiring a signal in the receive mode prior to array transmission, a transmitter beam-forming matrix can be made adaptable so that phase corrections applied to the receiving array can also be applied to the transmitting array.

5. Conclusions

A method for providing reference signals to the antennas through stabilized relay links has been described. By using these reference signals to heterodyne the received RF signals down to an IF carrier, signal transmission can be made over the data link with no appreciable phase variations being introduced by time delay variations of this link. If long-term equalization of several signal channels from separated antenna sites to a central station is desired, the method may be extended to accomplish this purpose.

The phase compensation method is applicable to stations which are separated by radio links as well as transmission-line links, providing sufficient signal strength is present at the terminal receivers and that the propagation delay between stations does not change appreciably during the round-trip propagation time.

Phase compensation can be applied usefully to arrays of large-aperture receiving antennas and appears to be particularly appropriate to the long-range acquisition problem. It may also be applied to transmitting arrays, although the number of applications for such arrays appears to be more limited than that of receiving arrays. Propagation effects may be expected to degrade the array patterns and gain for beams formed in this manner, however, many cases are expected to exist for which the degradation will be small enough to be acceptable.

E. Angle Acquisition and Tracking

1. Introduction

Prior to the utilization of an antenna array for purposes of communicating with a spacecraft, it is necessary to locate the position of the craft and establish continuous tracking of the beacon in position, frequency and phase. It is the purpose of this section to: (1) outline certain limitations relating to the problem of directing an antenna array to locate the spacecraft beacon (angle acquisition) and, once located, continue to follow the relative motion of the craft (angle tracking); (2) define signal detection probability as related to the acquisition problem; and (3) compare monopulse and conical scan tracking techniques for use with a single antenna of the array.

The inclusion of tracking techniques applied to a single antenna is made since it is deemed necessary to provide individual tracking capability for one or more antennas within the array in order to accomplish accurate boresighting, provide single antenna acquisition capability, and increase the overall versatility of the system by including the capability of using different portions of the array for separate functions. Tracking techniques applicable to combinations of antennas will not be discussed; however, because of the importance of these techniques, they will be considered in detail during the second part of the program.

The problem of angle acquisition of the spacecraft can be broken into two parts which relate to the distance of the craft from the earth.

During the initial phase of the mission, the errors in predicted position and doppler are likely to be large due to the lack of sufficient data to make accurate predictions. During this phase the received beacon power will be relatively high such that acquisition can be accomplished by utilizing the beamwidth of a single antenna and by widening the bandwidth of the receiver in order to encompass the wide variations in beacon frequency. Thus, angle acquisition will present no particular problems during the initial phase of the mission. However, it is during this portion of the mission that accurate position and doppler information must be obtained in order to allow a refinement of predicted position and doppler elements for the second phase of the mission when the received signal strength is low enough to require minimization of all coordinate uncertainties (i.e., angle, frequency, and phase). It is anticipated that during the initial phase, angle acquisition will be accomplished by each separate antenna. After each individual antenna acquires the beacon signal, the phase tracking required for coherent summation of the received signals permits using the capabilities of the entire array for angle tracking. In this manner the systematic tracking errors such as those incurred due to tracking system biases, real-time resolution capability, oscillator drifts, etc., can be refined to within the accuracy and resolution capability of the narrow array beam and the phase trackers. Thus, the accuracy of the recovered tracking data will be limited only by the capability of the entire array and the random errors which are caused by unpredictable sources such as atmospheric effects, changes in antenna phase centers, and instabilities of equipment phase shifts.

2. Limitations of Measurement

The maximum errors incurred during the initial phase of data recovery and processing will impose the final limitations on the angle acquisition capability at the extreme ranges of the mission. In view of this fact, it will be of interest to briefly review the current state-of-the-art capability in the applicable areas of measurements.

Position encoding[13] -- commercial digital position encoders are currently available with a resolution capability of 1 part in 2^{20} (approximately 1.24 seconds of arc). It must be noted, however, that this is the resolution of the 20 bit digital word as generated and does not include errors in data gears. It is believed that overall angular position encoding resolution for a large antenna structure can be more realistically set at approximately 5 seconds of arc.

Frequency standard[14] - primary frequency standards utilizing cesium beams currently exhibit an accuracy of 2 parts in 10^{12}. It is not anticipated that this degree of precision would be required for predicting position elements. Quartz crystal oscillators are currently available which exhibit long term stability of 5 parts in 10^{10} per day and short term stability of 1 part in 10^{10} averaged over one second intervals. This is probably approaching the limit for a secondary frequency standard in view of the fact that recently instituted VLF broadcasts by the National Bureau of Standards allows a precision of approximately 1 part in 10^{10} as received at a distant station when averaged over a 24 hour period.

Antenna boresighting - beam pointing errors will be caused by variations in antenna boresight alignment due to structural sags as a function of pointing angle in the individual antennas. These variations can be determined experimentally, within the resolution allowed by propagation effects and the position encoder, by utilizing the antennas as a radio telescope to observe discrete celestial radio sources whose positions are accurately known. Once the functional form of the boresight shifts are known, the variations can be programmed out of the beam-pointing angle for purposes of angle acquisition.

Phasefront distortion effects -- the effects of phasefront distortion on angle acquisition capability is of a fundamental nature. Present indications are that tropospheric effects will limit the angle prediction capability to a few seconds of arc at the minimum elevation of 4^{o}; the errors will diminish rapidly with increasing angle and should be negligible, relative to the other factors, for elevation angles above 10^{o}.

Thus, the major sources of errors in positioning the antennas for angle acquisition is expected to be caused by the position encoders, antenna boresight errors, and phasefront distortion caused by atmospheric irregularities; time measurements are not expected to cause serious errors.

3. Acquisition-Signal Detection Probability

The problem of acquiring the spacecraft beacon during the second phase of the mission, i.e., when the range approaches the limit of the acquisition capability of a single antenna, will involve a three-dimensional search in azimuth, elevation, and frequency. By utilizing refined tracking information obtained from the initial phase of the mission, the required range of search in each dimension can be minimized. For a given range of uncertainty in position and frequency, a trade can be made between channel bandwidth, averaging time, SNR, and signal detection probability. It is the purpose of this section to define these interrelationships which will then form the basis for additional investigation of the problem of acquisition, utilizing the capabilities of the entire array.

With regard to the search through the range of frequency uncertainty, this search must be made during the time the antenna moves one beamwidth. The time required for searching through each beamwidth is given by $\frac{\Delta F \tau}{n B}$/beamwidth, where

ΔF = range of frequency search,

n = number of parallel detection channels,

B = channel predetection bandwidth, and

τ = signal averaging time for a given probability of detection.

For a conical beam of width, Θ, and conical angle of uncertainty, $\Delta\theta$, the number of angle positions to be searched is approximately $[\Delta\theta/\Theta]^2$, where Θ and $\Delta\theta$ are assumed to be small relative to one radian. Thus, the total search time is given by

$$T \approx \frac{\Delta F \tau}{n B} \left[\frac{\Delta\theta}{\Theta}\right]^2 \text{ seconds} \qquad \text{(IV.E-1)}$$

The channel bandwidth, B, and averaging time, τ, are related and, as shown in the next paragraph, depend on the SNR and detection probabilities.

In order to detect a signal in the presence of noise, it is necessary to take an average of independent samples of the composite signal plus noise and compare it with a known long-term average noise level. If the average of M such independent samples exceeds the long-term average noise level N by an amount KN, then there results a probability of valid detection p, and of false detection q. E. L. Kaplan,[15] has published curves which relate the detection probabilities to SNR, M, and K. Two of these curves are reproduced in Figs. IV.E-1 and IV.E-2.

For a given SNR and threshold, M may be selected to give the desired valid detection probability, p. The probability of valid detection can be increased, for a given averaging time, by decreasing the predetection bandwidth, B (of course, B must be kept compatible with the signal bandwidth). A decrease in B has a much greater effect on p than does a corresponding increase in M. To increase p from 50% to 90% requires an increase in M by a factor of about 25. To accomplish this same result would require a decrease in B by a factor of about 6.

For a given M, the false detection probability, q, may be controlled by the proper choice of threshold level, (Fig. IV.E-2). For a system of n channels, the average time between false detection, T_F, is:

$$T_F = \frac{M}{nBq} \text{ sec} \qquad \text{(IV.E-2)}$$

As pointed out by the Sampling Theorem, it is possible to obtain independent samples from a flat spectrum of B cps at intervals of 1/B sec, so that for large M the averaging time, τ, is:

$$\tau = \frac{M}{B} \text{ sec} \qquad \text{(IV.E-3)}$$

It is common practice to utilize continuous averaging by passing the detector output through a low-pass filter, rather than averaging discrete independent samples. In this case M asymtotically approaches

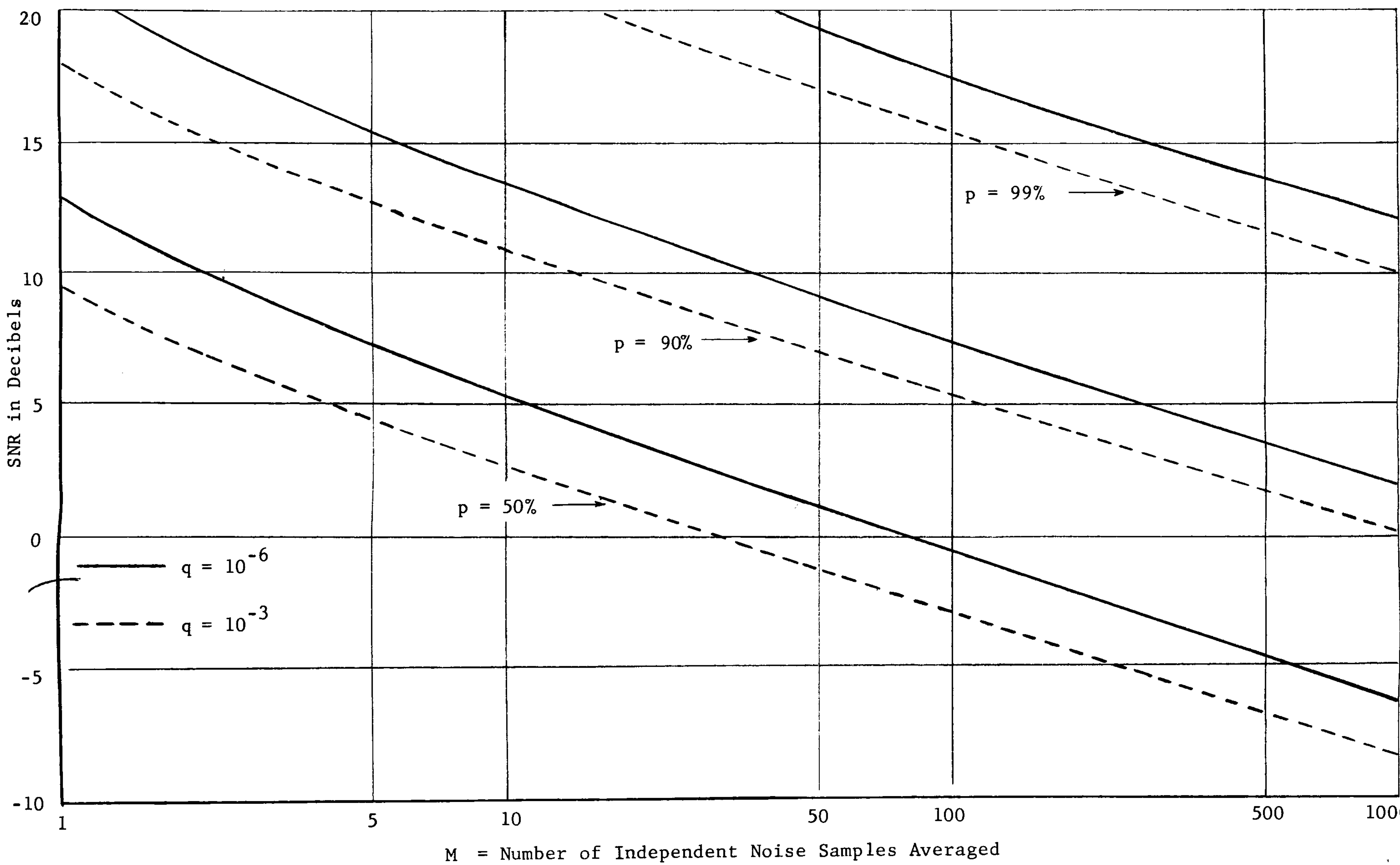

Fig. IV.E-1. SNR required for the detection of a fading sinusoidal signal.

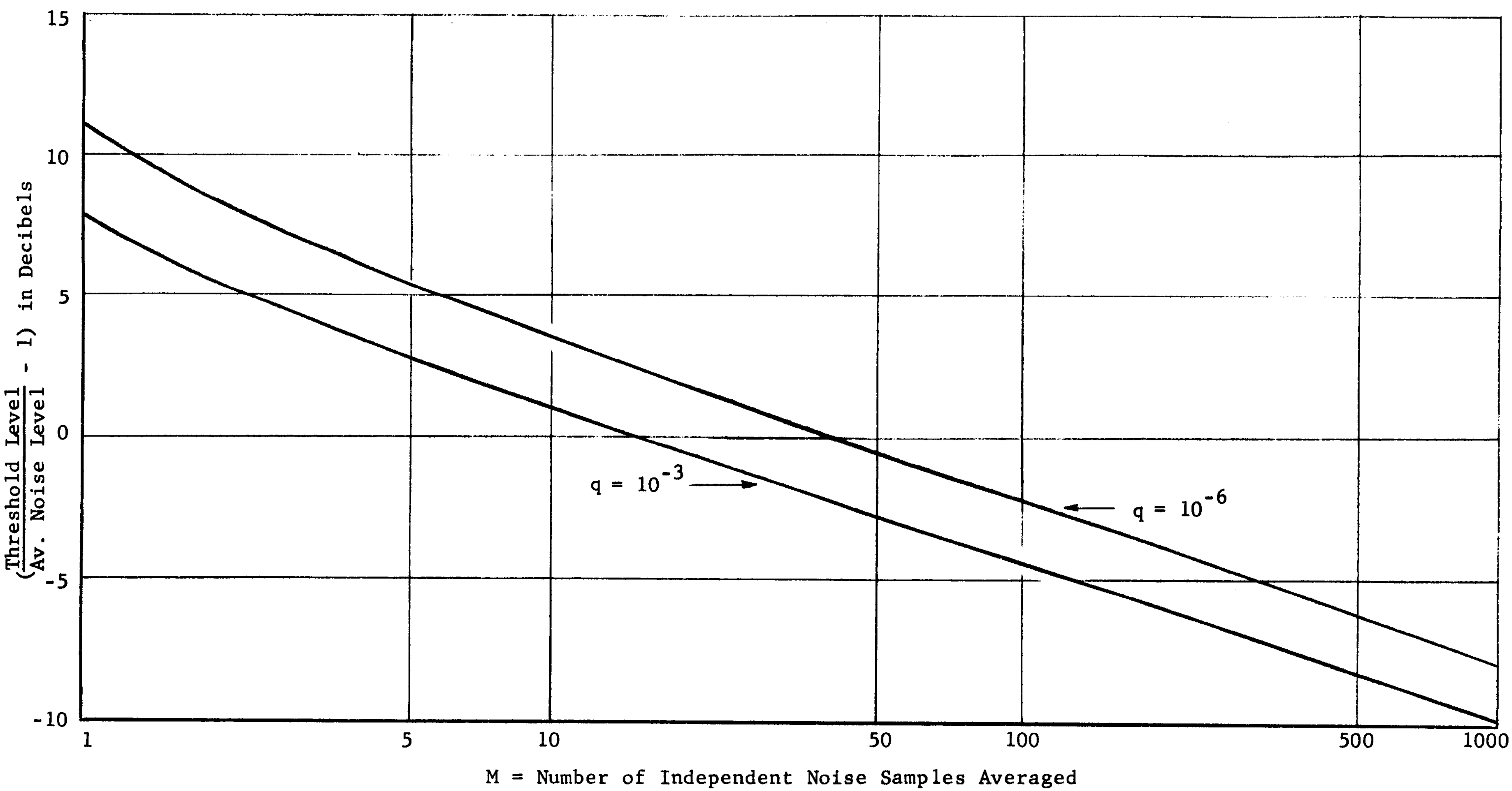

Fig. IV.E-2. Required threshold as a function of M for two different false alarm rates.

the product of predetection bandwidth and averaging time, as the product increases.

With these interrelations defined, the fundamental limitations on array acquisition capability can be specified for a given range of uncertainty in position and frequency. As the limit of the acquisition capability of the array is approached, it will be possible to effect an active trade between these parameters in order to increase the maximum range at which acquisition can be accomplished. Insufficient information on bandwidth limitations and doppler uncertainties is available at this time for making numerical computations.

4. Angle Tracking - Single Antenna

The fundamental problem involved in tracking a spacecraft is to determine the direction from which the RF energy from the spacecraft beacon is being received and to derive a servo control error signal which is proportional to the magnitude and sense of the difference between the direction of the beacon and a fixed reference axis. Two fundamental tracking techniques, monopulse or simultaneous lobing and conical scan or sequential lobing, will be compared with regard to tracking accuracy under the effects of interfering signals and noise. In addition, the two general types of monopulse system, amplitude sensing and phase sensing, are compared on the basis of their use in a single antenna structure.

The evaluation as here presented compares simplified and idealized monopulse and conical scan systems. The inclusion of sophisticated signal processing techniques utilizing phase lock loops to improve threshold characteristics has been avoided in order to simplify the analysis, and because their application to any of the systems described would provide essentially comparable improvement to each.

The major portion of this evaluation is based on the results of an analysis conducted by Messrs. R. J. Massa and R. W. Chittenden:[16] "Technical Note on Satellite Tracking Techniques and an Evaluation of Interference Phenomena," ASTIA publication AD-244264. These results are reproduced in Appendix B, which also includes an analysis of the effect of an extraneous interfering low frequency amplitude modulation of the spacecraft beacon.

The monopulse systems shown in Figs. IV.E-3 and IV.E-4 and the conical scan system shown in Fig. IV.E-5 are discussed in Appendix B. In addition to the results reproduced from reference [16], an evaluation of the effects of an extraneous interfering low frequency amplitude modulation is evaluated. Massa and Chittenden, by assuming SNR = 1, have had curves of static rms angle-tracking error vs received beacon power plotted by a computer; these results are reproduced in Fig. IV.E-6. It is to be noted that the curve which applies to the conical scan system does not include the effects of amplitude modulation on the received beacon.

A comparison between the SNR of amplitude sensing monopulse and conical scan (unmodulated source), equations (B-3) and (B-7) in Appendix B indicates that the monopulse system provides superior performance on the basis of equal received beacon power. This can be explained by the fact that the error signal power output of the conical scan system is derived from the product of the sideband power, P_{SB}, and the unmodulated carrier power P_R. The power in the sidebands is:

$$P_{SB} = \frac{a_1^2}{4} \tag{IV.E-4}$$

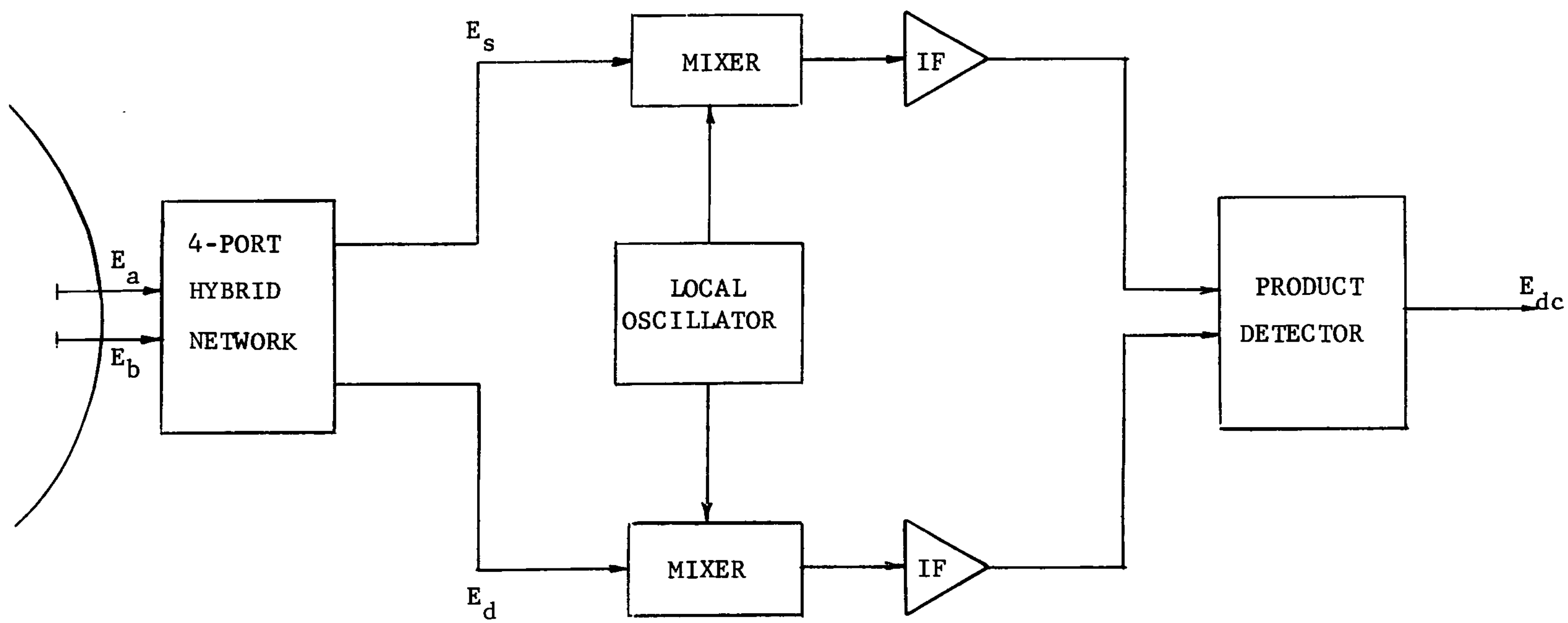

$$E_s = \frac{1}{\sqrt{2}} (E_a + E_b)$$

$$E_d = \frac{1}{\sqrt{2}} (E_a - E_b)$$

Fig. IV.E-3. Monopulse amplitude sensing.

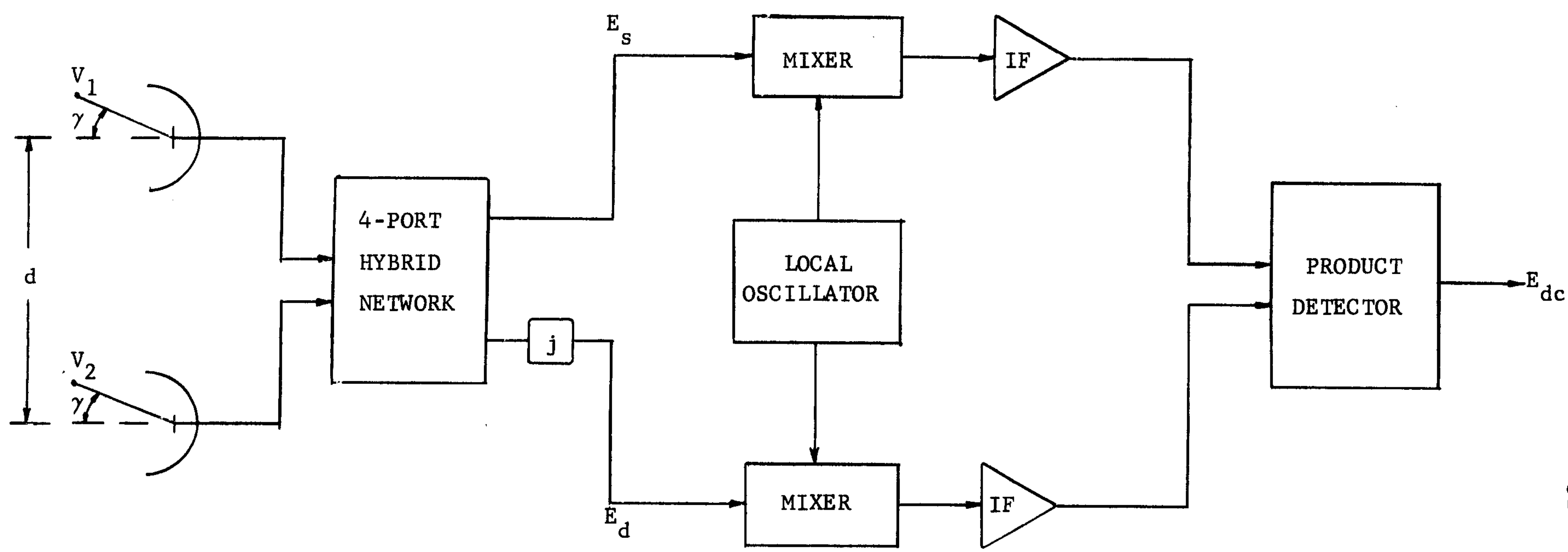

$$E_s = \sqrt{2}\ V \cos \frac{\beta}{2}$$

$$E_d = j\sqrt{2}\ V \sin \frac{\beta}{2}$$

$$\beta = \frac{2\pi}{\lambda} d \sin \gamma$$

$$|V| = |V_1| = |V_2|$$

Fig. IV.E-4. Monopulse phase sensing in a single plane-block diagram.

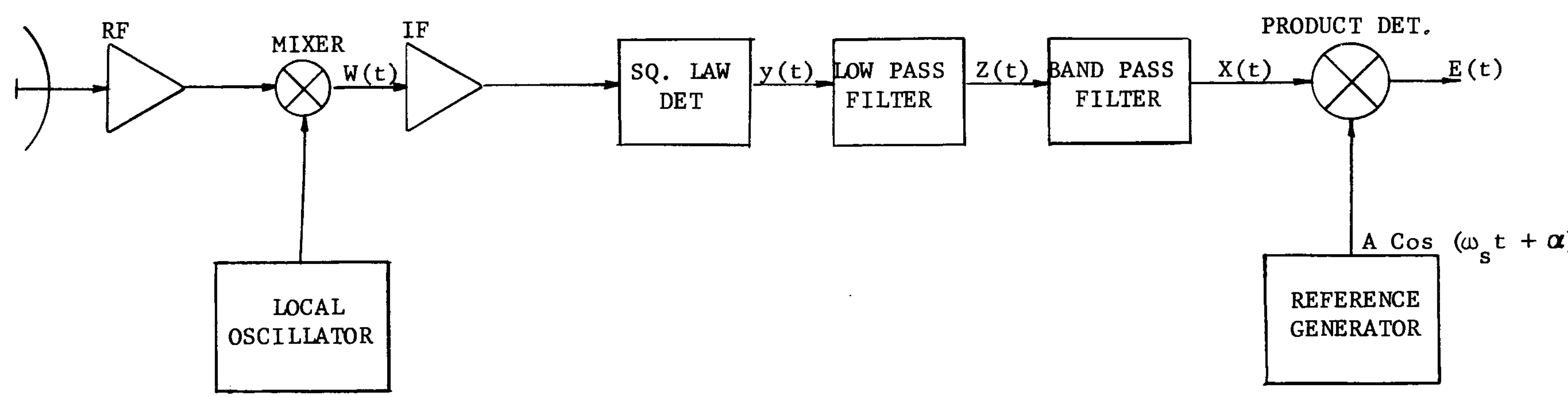

Fig. IV.E-5. Signal processing schematic conical scan system.

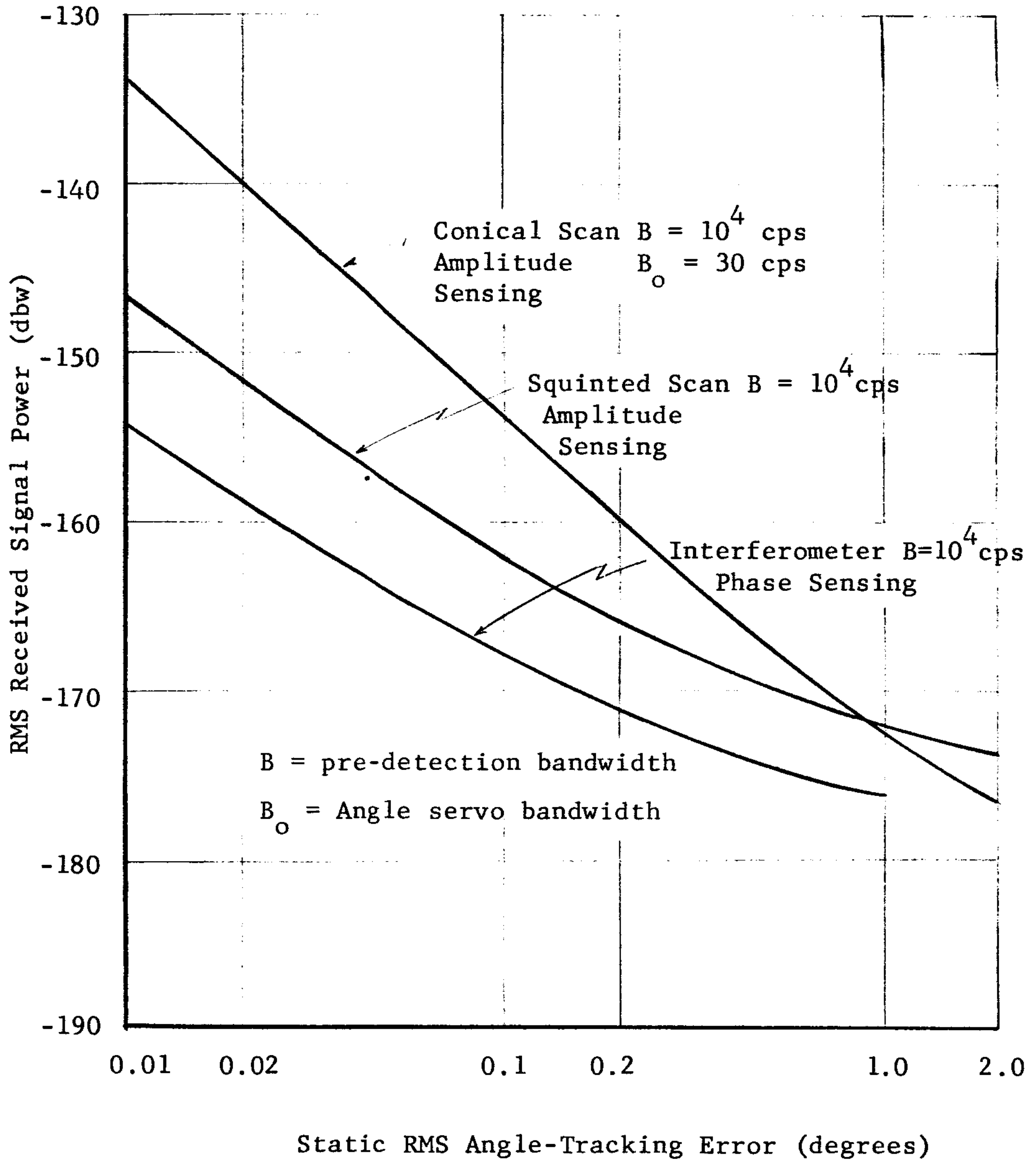

Fig. IV.E-6. Comparison of the Three Angle-Tracking Systems for Equal Baseline/Aperture-to-Wavelength Ratio ($\frac{D}{\lambda}$ = 15).

From Appendix B, equation (B-7)

$$a_1 = \frac{(\sqrt{K_1} - \sqrt{K_2})}{\sqrt{2}} (V)$$

$$\text{and} \qquad P_R = V^2$$

where:

a_1 = amplitude of the conical scan modulation,

$\sqrt{K_1}$, $\sqrt{K_2}$ are normalized field directivity patterns, defined in Appendix B, equation (B-3), and

V = amplitude of the unmodulated carrier.

Thus

$$P_{SB} = \frac{(\sqrt{K_1} - \sqrt{K_2})^2}{8} P_R \qquad \text{(IV.E-5)}$$

Since the sideband power for 100% amplitude modulation equals one-half the power in the unmodulated cases, the product (P_{SB}) (P_R) in the numerator of equation (B-7) will be less than the product (P_R) (P_R) over the range of interest.

A consideration of the effect of an interfering modulation, $a_2 \cos(\omega_e t + \theta)$, on the beacon shows the SNR ratio of the conical scan system to be further degraded. Two cases of interference are considered in this evaluation. For Case I, $B_o > \omega_e$, the line spectral component of the interfering sideband is not rejected by the output low-pass filter. An examination of the denominator of equation (B-19) in Appendix B indicates that both a line spectral component at the interfering frequency and a continuous spectral component $(\frac{a_2^2}{2} RB_o)$

around dc, which is produced by the beat between the interfering sideband and noise, appear in the output. The resultant error signal voltage has the form:

$$E(t) = bA\left[\frac{a_1 v}{2}\cos(\Psi-\alpha) + \frac{a_1 a_2}{2}\cos(\Psi-\alpha)\cos(\omega_e t+\theta) + \text{NOISE}\right] \quad \text{(IV.E-6)}$$

The desired error signal is:

$$bA\,\frac{a_1 v}{2}\cos(\Psi-\alpha) \quad \text{(IV.E-7)}$$

However, if a_2 becomes large the system can track:

$$bA\,\frac{a_1 a_2}{2}\cos(\Psi-\alpha) \quad \text{(IV.E-8)}$$

during the time that $\cos(\omega_e t + \theta) \approx 1$. In fact, there exists the definite possibility that the system can alternate between the desired component and the false component since the desired error signal approaches zero on boresight. This will result in a tendency for the antenna to oscillate about the true target position.

For Case II, $B_o < \omega_e$, the line component of the interfering modulation is removed. In this case, the degradation in SNR is due to the additional noise term, $(\frac{a_2^2}{2} RB_o)$, incurred due to the interfering modulation. Though this case does not produce antenna oscillation, it must be noted that it is based on an unrealistic assumption. Because the interfering modulation is assumed to be extraneous in nature, it would be impossible to specify a low pass filter which would remove the line component in the output.

An examination of Fig. IV.E-6 indicates that in order to obtain equal angle-tracking error performance the conical scan system must operate at a significantly higher SNR than the monopulse system. The results of the analysis above indicate that the conical scan system provides an inherently poorer SNR characteristic, thus further degrading tracking performance; therefore, it is concluded that monopulse tracking techniques are to be preferred over a conical scan system for the individual antenna tracking requirements.

Within the general framework of monopulse tracking, there are two basic configurations: (1) amplitude-sensing and (2) phase-sensing. A comparison of the two systems as applied to a single antenna cannot be based directly on the results obtained from reference [16] since those results are obtained from a variable baseline system in which the baseline (phase center separation) to wavelength ratio of the phase-sensing system is made equal to the aperture-to-wavelength ratio of the amplitude-sensing system. The error sensitivity of phase-sensing systems is determined by the phase-center separation. When the two phase centers are incorporated within a single reflector, the separation is also an important factor in determining the level of close-in sidelobes. Generally, a compromise in spacing is used which causes the error sensitivity of phase-sensing to be comparable to that of amplitude sensing for a given antenna size.

In both systems a hybrid combining network is used to produce outputs which are the sum and difference of two input signals for each tracking axis. For the amplitude-sensing system, the two input signals are obtained from squinted beams which have essentially coincident phase centers; for the phase-sensing system, these signals are obtained from identical beams which have separated phase centers. Phase variations prior to the combining network produce tracking errors, while post-network variations reduce the pointing-error sensitivity. For single-reflector systems, or those which are closely spaced (say, in a phase-sensing system), it is not necessary or desirable to incorporate amplifiers in front of the hybrid network. Because of the greater feed separation of phase-sensing systems, the noise temperature will generally be higher than that of amplitude-sensing systems. Also, the former systems generally have higher sidelobes than the latter, further degrading the noise temperature.

The requirement of squinted beams in an amplitude system tends to slightly reduce the effective main lobe antenna gain.[18] However, this disadvantage is generally offset by the required compromise between error sensitivity and sensitivity of the sum channel receiver, as mentioned above. This fact coupled with the difficulty of designing a phase-sensing single reflector antenna which has both high difference-pattern sensitivity and low-noise characteristics tends to rule out the use of phase-sensing monopulse for the individual antenna tracking.

5. Conclusions

For purposes of discussing angle acquisition, the spacecraft mission is divided into two parts: (1) the spacecraft is near the earth; received signal power is high, but errors in predicted position and doppler are large; (2) the range of the spacecraft approaches the limit of the acquisition capability of a single antenna.

During the first part of the mission, angle acquisition will present no serious problems since the received signal power will be sufficient for acquisition utilizing the beamwidth of a single antenna and a wide band receiver.

During the second part of the mission, it will be desirable to use the capabilities of the entire array for acquisition. In order to accomplish this, it will be necessary to use all available a-priori information to narrow the range of search. In order that this information have the necessary accuracy for future acquisition, angle tracking which utilizes the capabilities of the entire array should be used during the first part of the mission. In this manner systematic tracking errors can be refined to within the accuracy and resolution capability of the narrow array beam and the phase trackers.

A review of the state of the art in measurement devices and calibration techniques indicate that the limitations on positioning accuracy for angle acquisition will be imposed by the accuracy and resolution capability of the position encoders, antenna boresight errors, and phasefront distortion caused by atmospheric irregularities; time measurements are not expected to cause serious errors.

An investigation into the interrelationships between valid detection probability, false detection probability, threshold level, SNR, channel bandwidth, and averaging time indicate that the fundamental limitations on array acquisition capability can be specified for a given range of uncertainty in position and frequency. An active trade between these parameters will allow an increase in the maximum range at which acquisition can be accomplished.

A comparison of tracking techniques as applied to a single antenna within the array indicates that on the basis of tracking accuracy and susceptibility to interference, monopulse tracking is to be preferred over conical scan. The conical scan system is inherently simpler; however, the monopulse system provides more accurate angle tracking in the presence of noise and has the particular advantage of being insensitive to the time dependence of the amplitude of the received signal. It is believed that susceptibility of the conical scan system to low frequency amplitude modulation, as might be present due to continual realignment of a spacecraft directive antenna, is sufficient reason to remove it from serious contention as a deep space probe tracking system.

The amplitude-sensing monopulse system is chosen over phase-sensing for use with a single antenna since the compromise phase center spacing required in a single reflector antenna to obtain reasonable difference pattern sensitivity while maintaining low sidelobe characteristics results in degraded system performance in both error sensitivity and noise characteristics.

The tracking techniques investigated in this analysis have been limited to those used with a single antenna; however, the use of wide baseline separation of the antennas making up an array provides an excellent opportunity for supplementing the individual antenna tracking with tracking methods which utilize multiple antennas. Further study of these methods will be made during the remainder of the program.

F. Signal Summation

To provide a useful signal from the array that has a SNR equal to the sum of the SNR's of the individual channels of the array, the voltages in the individual channels must be summed in the proper manner. The requirements that must be met for optimum predetection* summation

*The advantages of predetection summation over postdetection summation are discussed in detail in references [23] and [24].

of voltages consisting of a useful signal and additive noise have been discussed elsewhere,[23, 24, 25, 27] and are summarized below:

1. The several signals to be summed must be in phase with slowly varying envelopes.

2. The additive noise voltage must be uncorrelated from channel to channel with zero mean value.

3. The gain of each channel must be proportional to the rms signal and inversely proportional to the mean square noise in the channel with the same proportionality constant for each channel.

The first condition is met by providing active phase compensation in each channel of the array, as will be discussed in Section IV.G.

The second condition is an assumption that should hold true for any well designed system with independent preamplifiers in each channel. Any correlated noise voltages will arise from external interfering sources, and these sources were not considered in the analysis that led to the foregoing results.

The third condition requires that the useful signal amplitude and the average channel noise power be measured continuously and the gain of each channel compensated accordingly.

Systems for implementing the third condition above are relatively complex, and with low channel SNR, it may be difficult to measure the signal amplitudes accurately. Therefore, it seems useful to gain an insight into the benefits of the optimum system by comparison of the optimum with schemes that, while not optimum, are simpler to realize. Consider, for example, a situation in which:

1. Noise power is the same in each channel, with value N.

2. The n signal envelopes have some arbitrary channel-to-channel distribution with an average rms value A_m and a standard deviation of the rms values of σ_A. (These averages are taken over a time much longer than a period of the signal, but may change slowly with time, without affecting the results).

For a system using the optimum method of summation of in-phase signals, the expected value of the output SNR is found as:

$$E\left[S_o/N_o\right]_{OPT.} = E\left[\sum_{i=1}^{n} \frac{S_i}{N_i}\right] = \frac{1}{N} E\left[\sum_{i=1}^{n} A_i^2\right] = \frac{n(\sigma_A^2 + A_m^2)}{N} \qquad \text{(IV.F-1)}$$

where:

S_i is the signal power in i th channel,

N_i is the noise power in i th channel,

n is the number of channels,

A_i is the rms amplitude of the i th signal, and

E is the expectation operator.

For a system with no gain compensation, the expected value of the output SNR is:

$$E\left[S_o/N_o\right] = E\left[\frac{\left(\sum_{i=1}^{n} \sqrt{S_i}\right)^2}{\sum_{i=1}^{n} N_i}\right] = \frac{1}{nN} E\left[\left(\sum_{i=1}^{n} A_i\right)^2\right]$$

$$= \frac{1}{nN}\left[n(\sigma_A^2 + A_m^2) + n(n-1) A_m^2\right] \qquad \text{(IV.F-2)}$$

$$= \frac{\sigma_A^2 + nA_m^2}{N}$$

This latter system, because of the assumption of equal noise power in each channel, is somewhat similar to an "equal gain" diversity system, in which the gains of each channel are adjusted to be equal. The two systems may be compared by examining the ratio of the average output SNR's:

$$\frac{E(S_o/N_o)}{E(S_o/N_o)_{OPT.}} \approx \frac{\sigma_A^{\ 2}}{n(\sigma_A^{\ 2} + A_m^{\ 2})} + \frac{A_m^{\ 2}}{\sigma_A^{\ 2} + A_m^{\ 2}} < 1 \qquad \text{(IV.F-3)}$$

With a fairly large number of channels, the first term in the above expression becomes insignificant, so that:

$$\frac{E(S_o/N_o)}{E(S_o/N_o)_{OPT.}} \approx \frac{1}{1 + \left(\frac{\sigma_A}{A_m}\right)^2} \qquad \text{(IV.F-4)}$$

Thus, for example, if the signal has a ratio of standard deviation to mean of 0.1, the average array degradation (referenced to the optimum summation) of SNR for the system without gain compensation is 0.043 db.

It therefore appears that the benefits obtained by optimum weighting may be small in certain cases and that other methods may do almost as well; but before any decisions can be reached, data must be obtained on the statistics of the channel-to-channel variations in signal and noise rms amplitudes. A lower bound on the uncompensated channel-to-channel variations may be calculated from the antenna pointing accuracy specifications, but the upper bound is uncertain at the present time. As discussed previously in Section C, the possibility of encountering fading should not be overlooked. Data from an experimental system are needed to provide sufficient information on the statistics of fading, in the 1-10 Gc range, as well as the expected channel-to-channel amplitude variations due to equipment vagaries.

G. Phase Tracking and Acquisition

1. General Discussion

The necessity for active phase tracking of individual signals arriving at widely spaced antennas in a multi-element array is recognized by all who have investigated the problem.[4, 5, 6, 27] As has been pointed out previously, it is convenient to group the phase modulation into two categories, that modulation which is common to all received signals, and that which is not common. The distinction between the two is not clear-cut for random phase fluctuations caused by the atmosphere, and a statistical description is required in terms of correlation functions. The amount of atmospheric modulation that is common depends upon which specific pair of antennas is being examined and the atmospheric conditions existing at a particular time. To statistically describe the situation for n antennas, an n x n correlation matrix is required.

For non-atmospheric effects, it is easier to distinguish the common and differential phase variations. Intentional signal modulation, doppler shifts due to radial motion of the probe, and phase fluctuations due to transmitter instabilities should be common to all antennas of the array, while doppler shifts due to angular rotation of the line of sight to the transmitter and phase shifts caused by the equipment in the different receiving channels will not in general cause the same phase variations in each channel of the array. It is the differential phase shifts that must be compensated for before signal summation takes place. This is the function of the <u>phase trackers</u> in an array.

The general problems involved in performing phase acquisition are discussed in some detail in reference [4]. In this report, four methods of performing phase acquisition are discussed:

(1) independent phase acquisition with each antenna.

(2) acquisition on the spacecraft signal using cross-correlation phase trackers.

(3) probabilistic acquisition.

(4) aided acquisition - pre-focusing on radio stars or beacons.

To the above, another technique may be added, which may be designated as (5) "open loop acquisition." These five techniques are briefly described below.

The first method is self-explanatory and is applicable at relatively short ranges where the individual channel SNR is high at the bandwidths required to acquire and track the common phase fluctuations.

The second method is suggested as a means of permitting acquisition at longer ranges than those that could be achieved by the first method. The cross-correlation tracker tracks the differential phase variations only; and therefore, it is expected that the tracker bandwidth requirements may be considerably less than those bandwidths required to acquire and track the common phase fluctuations.

The third method above, "probabilistic acquisition," is a technique whereby signals of improved SNR over that obtained in the receiver of a single antenna may be obtained without the necessity of active continuous phase tracking. A discrete switching between several signal-phase combinations replaces the function of the continuous phase trackers. When used in conjunction with cross-correlation phase trackers, this technique will provide a reference signal with improved SNR, thereby further extending the acquisition range of method (2). When used alone, the technique provides for partial use of the full potential array gain.

The acquisition method designated as "aided acquisition" involves pre-focusing the array on a known source, such as a radio star. Once the array has been focused on this source, a precomputed set of phase relationships may be used to form a fence of high gain lobes within the beamwidth of a single antenna. Acquisition using the full array gain may then be accomplished as the spacecraft enters one of the high gain lobes. As an alternative technique, a single high gain lobe may be programmed to search within the beamwidth of a single antenna. It may be possible to steer the individual antenna beams through some angle after pre-focusing. The angle through which the antennas may be steered before experiencing serious degradation of the high gain lobes is uncertain, and awaits experimental evaluation.

The last acquisition method mentioned above is "open loop acquisition." This technique involves precise compensation of all phase shifts experienced in the ground equipment by a technique such as described in Section IV.D. This technique essentially pre-focuses the array on a simulated source by providing reference signals at each antenna that are identical, or have precalculated phase relationships. The phase fluctuations caused by the atmosphere are <u>not</u> compensated by this technique, so that the usefulness as an acquisition method is limited to those occasions and operating conditions when atmospheric degradation of the high gain lobes is not extreme. It is felt, however, that the compensation of the phase differences occurring in the receiving equipment will be a first step in any of the acquisition schemes mentioned.

In this section, the feasibility of several of the above acquisition techniques will be examined in more detail, insofar as the available data permits. In Part 2, various simplified phase tracker configurations that may be used to acquire and track the spacecraft signal are discussed. No attempt has been made to delve into the detailed design of the configurations and block diagrams are used throughout.

Part 3 contains an analysis of the effect of phase errors on the array gain, both random and steady-state. The results of the analysis of random errors are not limited to small phase errors and provide a useful tool to evaluate the feasibility of such acquisition methods as "open loop acquisition" and "probabilistic acquisition."

Part 4 is an analysis of the performance of the cross-correlation phase tracker. This section also contains a brief summary of some of the characteristics of phase-lock loops and results in the determination of approximate thresholds of the cross-correlation phase tracker.

In Part 5, the benefits and complexity of probabilistic acquisition are discussed with numerical examples provided.

Part 6 provides a comparison between the techniques of independent phase acquisition in each channel, acquisition using cross-correlation trackers, open loop acquisition methods, and pre-focusing techniques.

Part 7 sums up the results of these preliminary analyses and points out the data necessary and experiments that should be conducted to confirm or deny the theoretical analyses.

2. Phase Tracker Configurations

a. Individual Loops

A phase tracking loop consists of a phase comparison circuit and a phase correction circuit as shown below in Fig. IV.G-1.

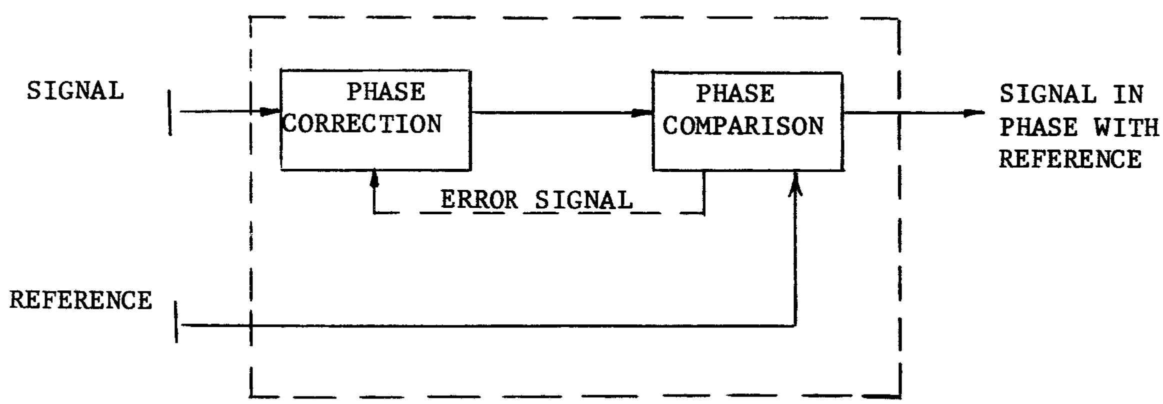

Fig. IV.G-1. Phase tracking loop.

Several means are available for performing the phase comparison operation; however, the simplest technique, as well as one of the most accurate, consists of quadrature multiplication of the signal and reference to obtain an output voltage with a low frequency component that indicates the magnitude and direction of the phase error. Because of the simplicity and universal acceptance of this technique, other techniques have not been considered.

The phase correction operation may be performed by a voltage controlled oscillator, by motor driven phase shifters, or electronic phase shifters of the "phase modulator" types. These latter circuits are generally limited in range to phase shifts of less than $\pm \frac{\pi}{2}$ radians and hence cannot track a continuous difference in frequency.

Motor driven phase shifters and VCO's have both been used in phase tracking loops, and each have advantages. Motor driven phase shifters look attractive for differential phase compensation, where the frequency differences in the various channels will be only a few cycles per second. If it becomes necessary to compensate for differential doppler, programming a small phase rate should be easier with motor driven phase shifters than with VCO's. On the other hand, the large doppler corrections common to all antennas cannot be made with motor-driven phase shifters and require the use of a VCO or some form of electronic offset oscillator.

Three phase tracking configurations are shown in Fig. IV.G-2, each differing in the method of performing the phase correction operation.

b. Configurations in the Array

The numerous signals available at the array provide a wide choice in the phase tracking configurations to be used in an array of several antennas. The individual channel phase tracker reference signal may be derived from a stable oscillator, from the transmitted signal, from another channel of the array, or from a sum of several channels of the array. Some of the choices available for differential phase tracking and compensation are shown in Fig. IV.G-3, using a 4-channel array as an example. These configurations may be classified as to the method of performing acquisition, using the categories defined previously. Figs. IV.G-3a and IV.G-3b represent configurations in which initial acquisition must be performed independently on the total phase fluctuations in each channel, or in one channel. In Fig. IV.G-3c initial acquisition must be accomplished on the common phase fluctuations, but use is made of the enhanced SNR obtainable in a sum signal if the

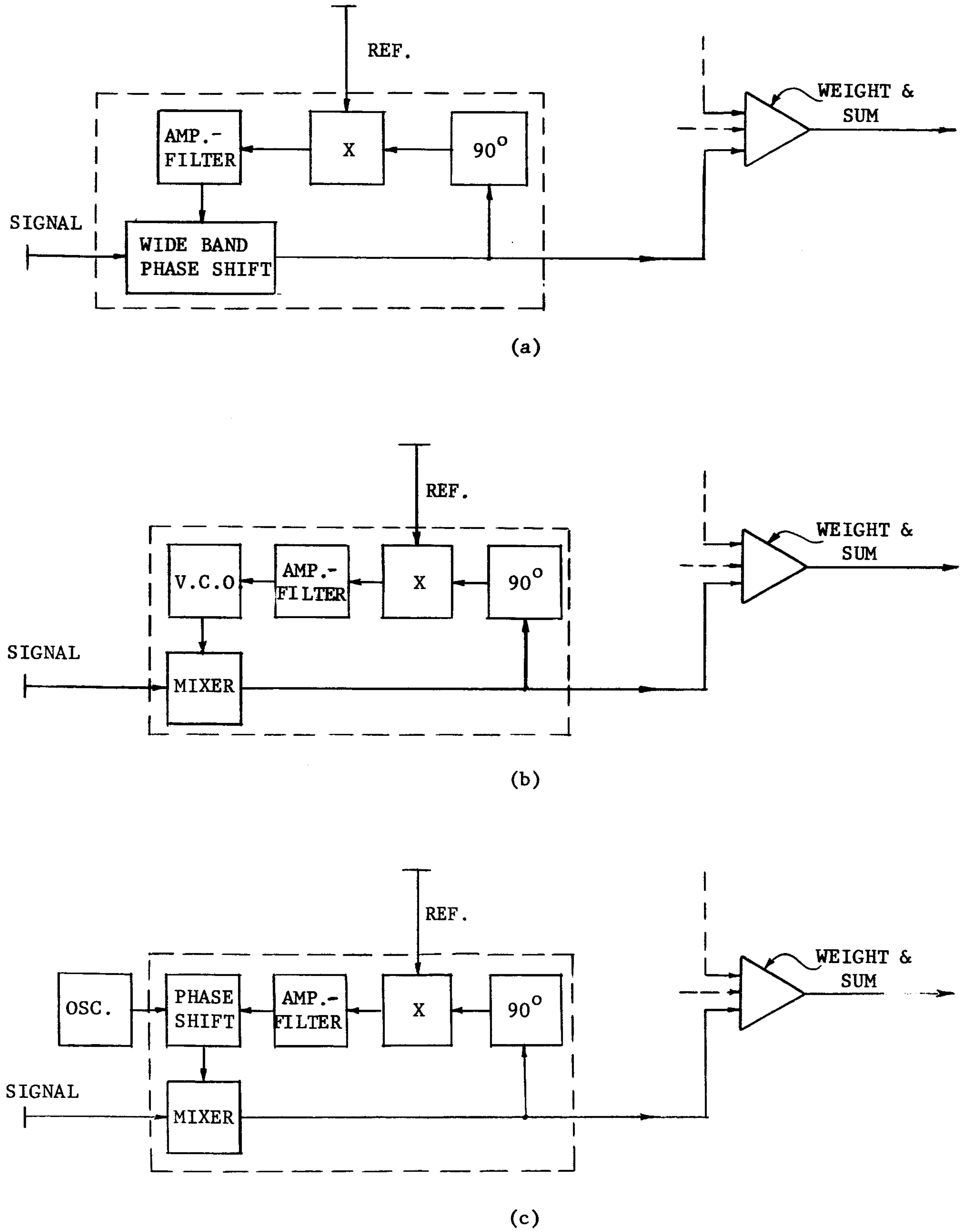

Fig. IV.G-2. Simplified phase tracker configurations - individual loops.

[A] Common Reference

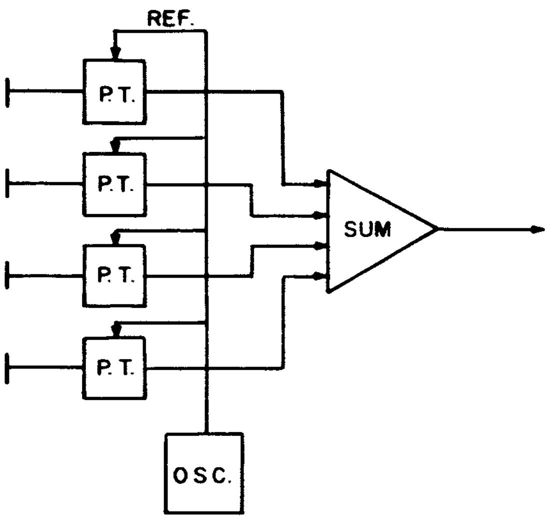

[B] Aided Common Reference, Single Channel Feedback

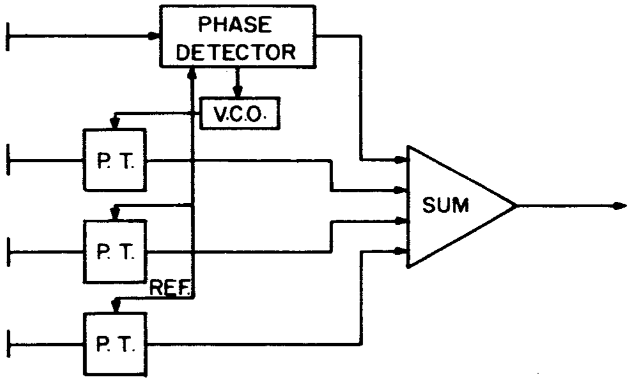

[E] Cross-Correlation Tracker - Adjacent Channel Reference

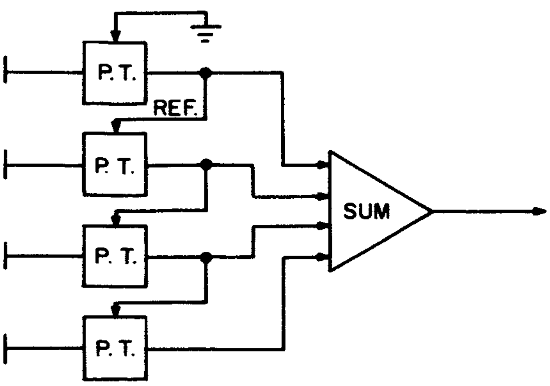

[F] Cross-Correlation Tracker - Single Channel Reference

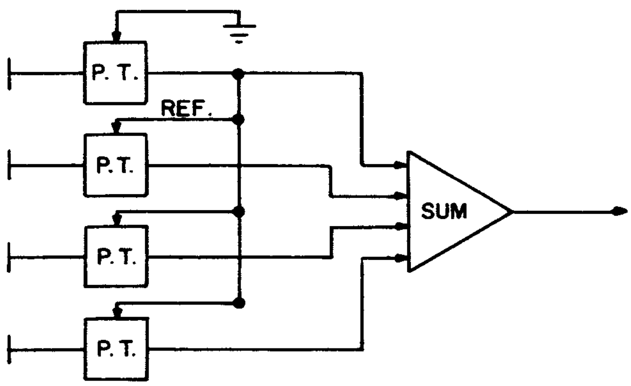

[C] Aided Common Reference, Sum Channel feedback

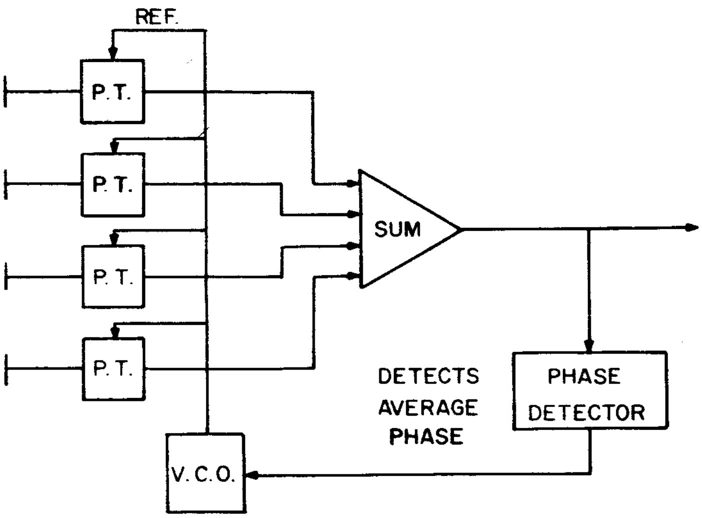

[D] Cross-Correlation Tracker - Sum Channel Reference

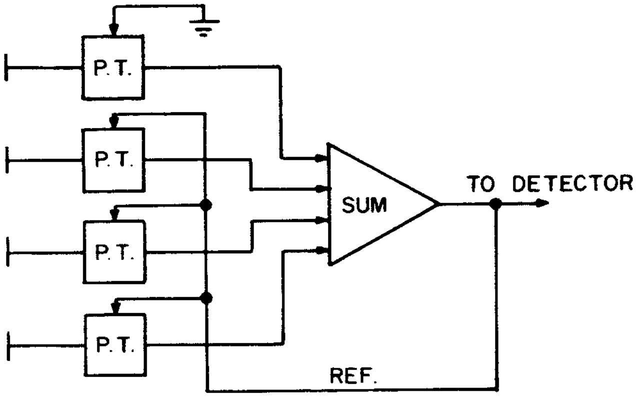

[G] Series - 2 x 2 Correlation

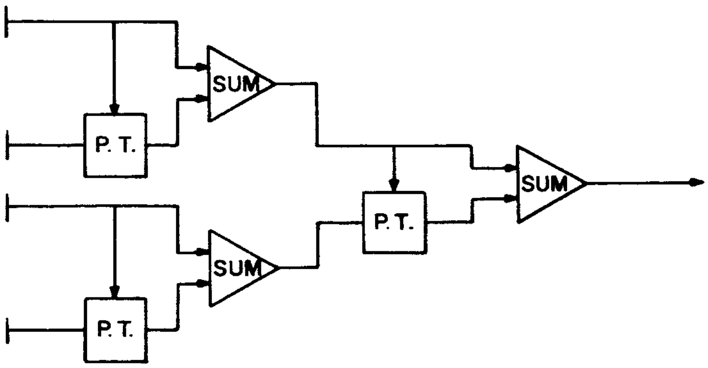

[H] Combinations-Sequenced Circuits, For Example:

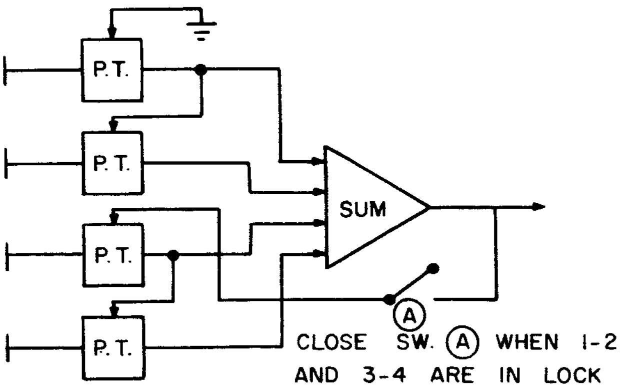

Fig. IV.G-3. Differential phase tracking configurations in a 4 channel array with predetection summation. P.T. = Phase tracker as in Fig. IV.G-2.

individual channel phases are not completely random. The remaining configurations are all classified as cross-correlation phase trackers, differences in the configurations primarily being the source of the tracker reference signal.

The configuration that will give the best performance considering threshold, accuracy, reliability, and acquisition capability is not obvious; and the following considerations are intended to assist in the proper design choices and to point out the data gaps existing at the present time.

3. The Effect of Phase Errors on the Array Gain

Errors in tracking the differential phase fluctuations will cause a decrease of the array gain in comparison to the gain that would be achieved with proper summation of exactly in-phase signals. The phase errors may be random in nature or may be fairly constant. This latter type of error will arise if a first order tracking loop is used to track a constant frequency difference, for example.

a. Random Errors

The effect of random tracking errors on the array gain may be determined as follows: Consider n signals of equal amplitude and slowly varying random phase:

$$e_1 = A \sin (\omega_o t + \phi_1)$$

$$e_2 = A \sin (\omega_o t + \phi_2) \qquad \text{(IV.G-1)}$$

$$e_n = A \sin (\omega_o t + \phi_n)$$

These signals are summed to obtain a composite signal:

$$E(t) = A \left[\sum_{i=1}^{n} \cos \Phi_i \sin \omega_o t + \sum_{i=1}^{n} \sin \Phi_i \cos \omega_o t \right] \qquad \text{(IV.G-2)}$$

The power of the sum signal is proportional to the voltage squared, averaged over the period $T = 2\pi/\omega_o$

$$S = \frac{1}{T} \int_0^T |E(t)|^2 dt = \frac{A^2}{2} \left[\left(\sum_{i=1}^{n} \cos \Phi_i \right)^2 + \left(\sum_{i=1}^{n} \sin \Phi_i \right)^2 \right] \qquad \text{(IV.G-3)}$$

For simplicity in notation, define:

$$X = \sin \Phi$$

$$Y = \cos \Phi$$

$$U = \sum_{i=1}^{n} \cos \Phi_i = \sum_{i=1}^{n} Y_i \qquad \text{(IV.G-4)}$$

$$V = \sum_{i=1}^{n} \sin \Phi_i = \sum_{i=1}^{n} X_i$$

Then the sum signal power is:

$$S = \frac{A^2}{2} [U^2 + V^2] \qquad \text{(IV.G-5)}$$

And the expected value of this power is:

$$E\{S\} = \frac{A^2}{2} [E\{U^2\} + E\{V^2\}] \qquad \text{(IV.G-6)}$$

Evaluating the terms in the brackets gives:

$$E\{U^2\} = \sum_{i=n}^{n} E\{Y_i^{\,2}\} + \sum_{i=1}^{n}\sum_{j=1}^{n} E\{Y_iY_j\} \qquad i \neq j$$

$$E\{V^2\} = \sum_{i=1}^{n} E\{X_i^{\,2}\} + \sum_{i=1}^{n}\sum_{j=1}^{n} E\{X_iX_j\} \qquad i \neq j$$

$$\sum_{i=1}^{n} E\{Y_i^{\,2}\} = n(\sigma_y^{\,2} + m_y^{\,2})$$

$$\sum_{i=1}^{n} E\{X_i^{\,2}\} = n(\sigma_x^{\,2} + m_x^{\,2}) \qquad \text{(IV.G-7)}$$

$$\sum_{i=1}^{n}\sum_{j=1}^{n} E\{X_iX_j\} = n(n-1)\, m_x^{\,2} \qquad i \neq j$$

$$\sum_{i=1}^{n}\sum_{j=1}^{n} E\{Y_iY_j\} = n(n-1)\, m_y^{\,2} \qquad i \neq j$$

where:

m_x is the mean value of the X_i and

$\sigma_x^{\,2}$ is the variance of the X_i.

All that remains is the evaluation of these means and variances from the probability density of the phase random variable, $P(\phi)$.

$$m_x = \int_{-\infty}^{\infty} \sin\phi\, P(\phi)d\phi$$

$$m_y = \int_{-\infty}^{\infty} \cos\phi\, P(\phi)d\phi$$

$$\sigma_x^{\,2} = \int_{-\infty}^{\infty} \sin^2\phi\, P(\phi)d\phi - m_x^{\,2} \qquad \text{(IV.G-8)}$$

$$\sigma_y^{\,2} = \int_{-\infty}^{\infty} \cos^2\phi\, P(\phi)d\phi - m_y^{\,2}$$

For a <u>normal</u> phase density function:

$$P_n(\phi) = \frac{1}{\sqrt{2\pi}\sigma_\phi} e^{-\phi^2/2\sigma_\phi^2} \qquad \text{(IV.G-9)}$$

Evaluation of the integrals gives for the sum signal power:

$$E\{S\} = \frac{nA^2}{2} [1 + (n - 1) e^{-\sigma_\phi^2}] \qquad \text{(IV.G-10)}$$

(Normal)

For a <u>uniform</u> phase density function:

$$P_u(\phi) = \frac{1}{2B} \qquad -B < \phi < B \qquad \text{(IV.G-11)}$$
$$= 0 \qquad \text{Elsewhere}$$

$$E\{S\} = \frac{nA^2}{2} [1 + (n - 1) \frac{\sin^2 B}{B^2}] \qquad \text{(IV.G-12)}$$

(Uniform)

These expressions can be written in terms of the array SNR and single channel SNR by assuming that the sum channel noise power is n times the individual channel noise power. Then,

$$SNR_{SUM} = SNR_1 [1 + (n - 1) e^{-\sigma_\phi^2}] \quad \text{(Normal)} \qquad \text{(IV.G-13)}$$

$$SNR_{SUM} = SNR_1 [1 + (n - 1) \frac{\sin^2 B}{B^2}] \quad \text{(Uniform)} \qquad \text{(IV.G-14)}$$

These results are plotted in Figs. IV.G-4 and IV.G-5.

It is also possible to obtain the variance of the signal power; however, the expressions are complex and no numerical calculations

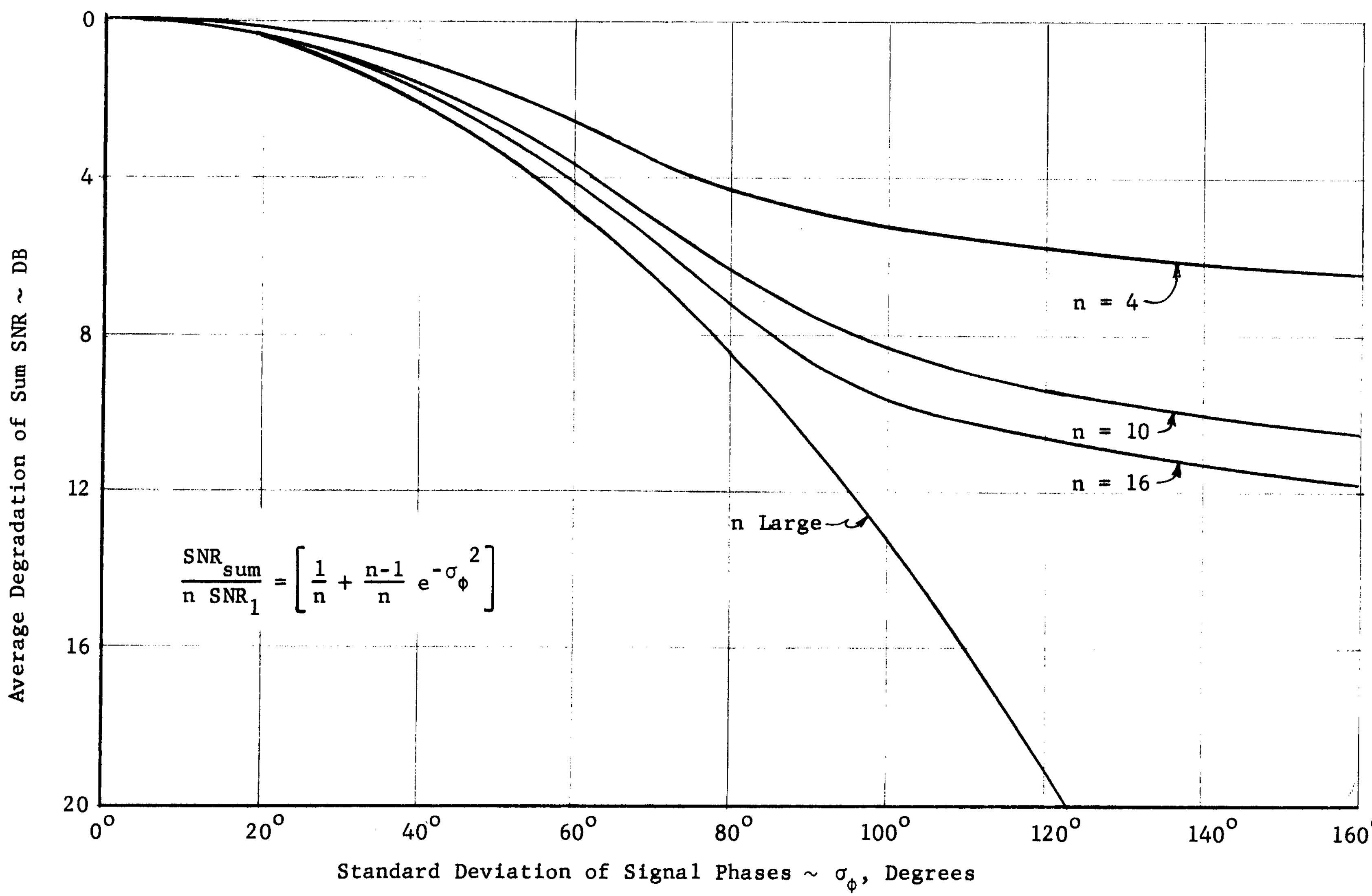

Fig. IV.G-4. Average degradation of sum SNR due to random phases of n equal amplitude sinusoidal signals -- phases normally distributed.

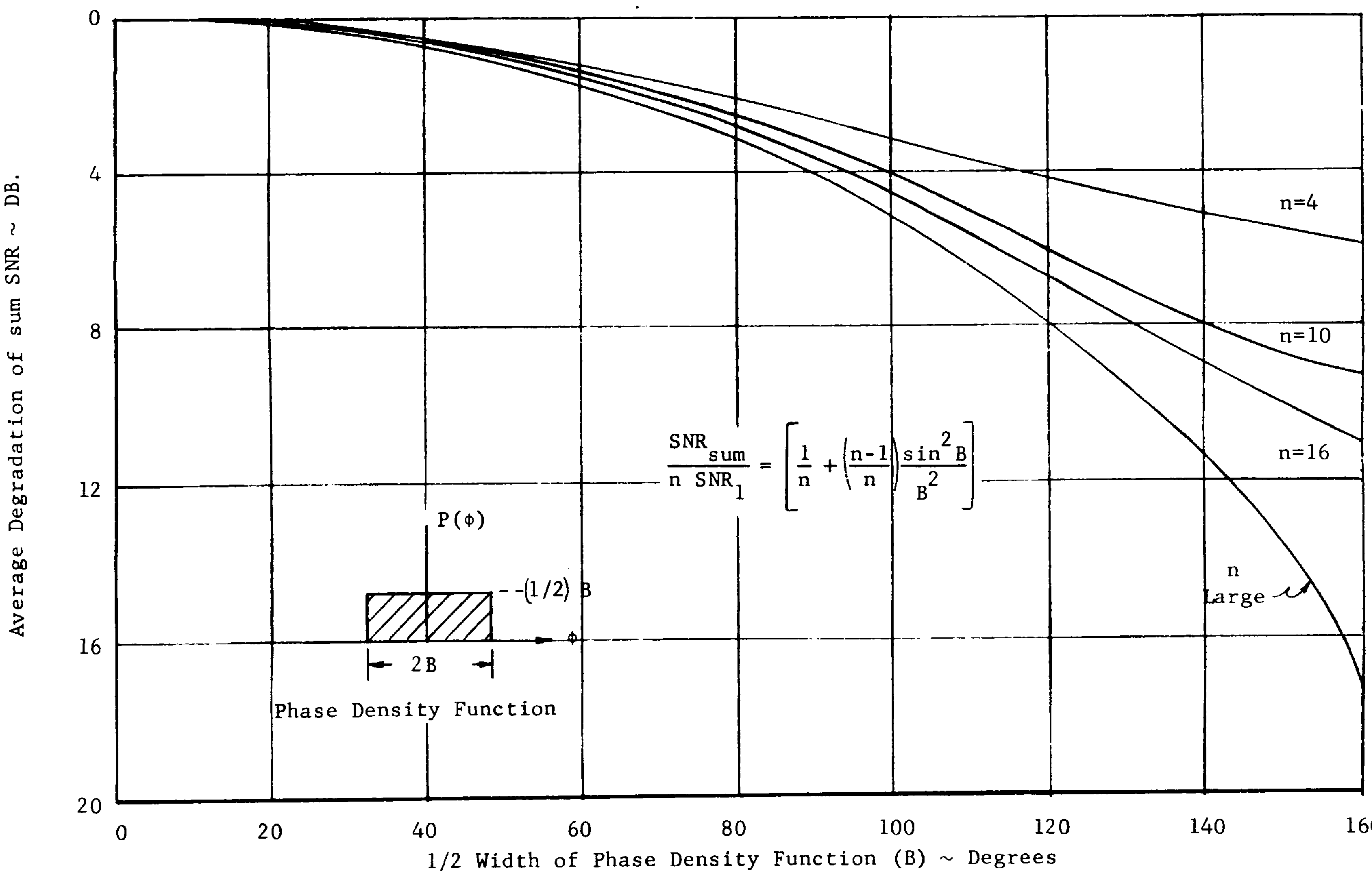

Fig. IV.G-5. Average degradation of sum SNR due to random phases of n equal amplitude sinusoidal signals--phases uniformly distributed.

have been made as yet. Note that in the above analysis, no assumption of small phase error is required.

b. Steady-State Errors

The purpose of this analysis is to investigate the effect of steady-state phase tracking errors on an operational array. These phase errors will occur if a first order loop is tracking a frequency difference, if a second order loop is tracking a rate of change of frequency, etc. The case to be considered is that of a first order loop used as a differential phase tracker, as this mechanization has been advocated and is the simplest configuration that can be used. This is also one of the few cases where steady-state errors may seriously degrade the performance of the array.

With a first order loop, a frequency difference between two antennas of the array will cause a steady-state phase error given by:

$$\Delta\phi = \sin^{-1} \frac{\Delta\omega}{4B_n}$$

where:

$\Delta\phi$ is the steady-state phase error (rad),

$\Delta\omega$ is the frequency difference (rad/sec), and

B_n is the loop equivalent noise bandwidth (rad/sec).

Frequency differences between antennas in the array will arise because of rotation of the line of sight to the transmitter, as shown in Fig. IV.G-6.

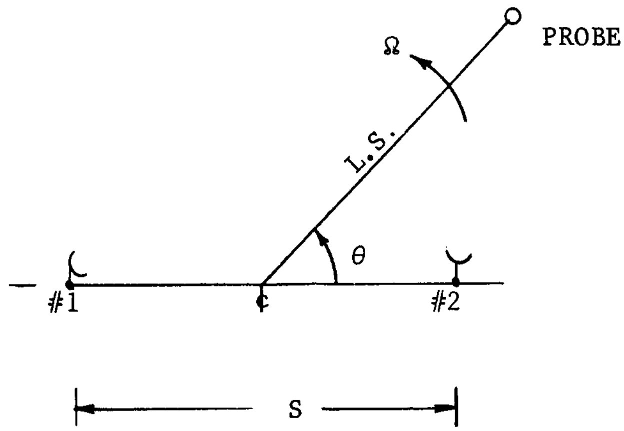

Fig. IV.G-6. Two-antenna geometry.

The frequency difference between ant. #1 and ant. #2 is given by:

$$\Delta\omega \approx \frac{2\pi S\Omega}{\lambda} \sin\theta \quad \text{rad/sec} \qquad \text{(IV.G-15)}$$

where:

Ω is angular rotation of the line of sight,

S is the spacing between antennas,

λ is the wavelength transmitted, and

θ is the elevation angle.

This frequency difference is small at long ranges; for example, with antennas spaced 5,000 feet apart, at 10 Gc, and viewing a probe fixed in inertial space, the calculation at zenith gives:

$$\Delta\omega \approx 23 \quad \text{rad/sec}$$

Thus the inidvidual phase errors will be small until the loop bandwidth is on the order of cycles or fractions of cycles per second.

Now consider a line of equally spaced antennas in the plane of the motion of the line of sight as shown below:

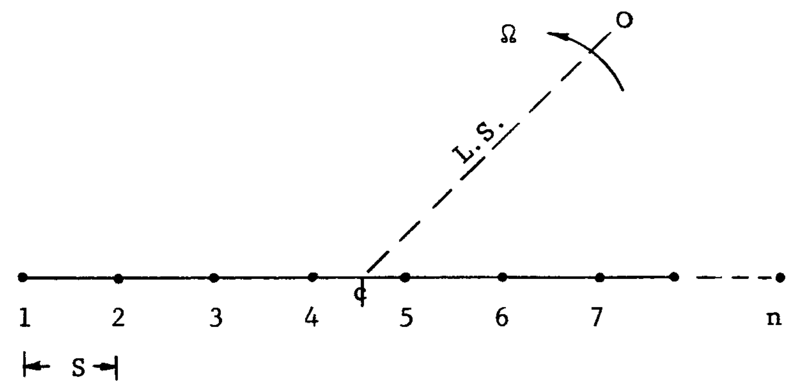

Fig. IV.G-7. Equally spaced geometry.

Using ant. #1 as a reference, the frequency difference between #1 and #2 can be designated as $\Delta\omega$. Then the frequency difference between #1 and #3 will be $2\Delta\omega$, etc. These frequency differences cause phase errors $\Delta\phi$, $2\Delta\phi$, $3\Delta\phi$, ..., $n\Delta\phi$, and the summed signal of all n antennas may be written as: (for equal amplitude sinusoidal signals)

$$e_{SUM} = \sum_{k=0}^{n-1} A \sin (\omega_o t + k\Delta\phi)$$

or, equivalently:

$$e_{SUM} = \sum_{K=1}^{n} A \sin (\omega_o t + k\Delta\phi) \qquad \text{(IV.G-16)}$$

The sum signal power is then $\overline{e_s^2}$ and is equal to:

$$S_o = \frac{A^2}{2} \left[\left(\sum_{k=1}^{n} \cos k\Delta\phi \right)^2 + \left(\sum_{k=1}^{n} \sin k\Delta\phi \right)^2 \right]$$

The squared terms sum to n, and for the cross product terms:

$$\sum_{k=1}^{n} \sum_{j=1}^{n} \cos k\Delta\phi \cos j\Delta\phi + \sum_{k=1}^{n} \sum_{j=1}^{n} \sin k\Delta\phi \sin j\Delta\phi$$

$k \neq j$

$$= \sum_{k=1}^{n} \sum_{j=1}^{n} \cos (k - j) \Delta\phi \qquad j \neq k$$

Thus the output power is written as:

$$S_o = \frac{A^2}{2} \left[n + \sum_{j=1}^{n} \sum_{k=1}^{n} \cos (k - j) \Delta\phi \right] \qquad \text{(IV.G-17)}$$

To further reduce the expression, a small angle assumption is made.

Let: $\cos (k - j) \Delta\phi \approx 1 - \dfrac{(k - j)^2 \Delta\phi^2}{2}$

Then after expanding this expression and summing, there is obtained:

$$S_o \approx S_1 \left[n^2 - (\Delta\phi)^2 \frac{n^2 (n^2 - 1)}{12} \right] \qquad \text{(IV.G-18)}$$

where:

$S_1 = A^2/2$

This expression gives the in-line array power in terms of the individual signal power and the number of antennas in line, with a given phase tracking error between two adjacent antennas. For the first order loop:

$$\Delta\phi = \sin^{-1} \frac{\Delta\omega}{4B_n} \approx \frac{\Delta\omega}{4B_n} \approx \frac{\pi S\Omega \sin\theta}{2\lambda B_n} \qquad \text{(IV.G-19)}$$

The in-line array signal-to-noise ratio is then:

$$SNR_o = SNR_1\, n \left[1 - \left(\frac{\pi S \Omega \sin\theta}{2\lambda B_n}\right)^2 \left(\frac{n^2 - 1}{12}\right) \right] \qquad \text{(IV.G-20)}$$

where:

SNR_1 is the signal-to-noise ratio in a single channel.

To obtain a numerical estimate of the degradation of an array due to steady-state phase tracking errors of the type discussed, the configuration and antenna spacings must be specified. As an example of the calculation, consider the following special case:

1. A square configuration of $q = n^2$ antennas, aligned with one side parallel to the plane of motion of the line of sight and with an individual antenna spacing of $\frac{3500}{\sqrt{q}}$ feet.
2. Assume values for the other parameters in the expression of:

λ = .0984 ft. (10 Gc)

$\Omega = 7 \times 10^{-5}$ rps (earth's rate)

$\theta = \pi/2$ (zenith)

For this special case, each column in the array will degrade as given by (IV.G-20); and since there are n columns, for the square array with $\frac{3500}{\sqrt{q}}$ spacing, we have:

$$SNR_o = SNR_1\, q \left[1 - \left(\frac{\pi(3500)\Omega \sin\theta}{2\lambda B_n}\right)^2 \left(\frac{q - 1}{12q}\right) \right] \qquad \text{(IV.G-21)}$$

Substituting the other numerical values gives, for the degradation of the array in db (for large q):

$$\text{db loss} = 10 \log \left(\frac{q\mathrm{SNR}_1}{\mathrm{SNR}_o}\right) \approx 10 \log \left[\frac{B_n^{\,2}}{B_n^{\,2} - 1.28} \right] \qquad \text{(IV.G-22)}$$

Bandwidths of 1.2 cps and .4 cps give .1 db and 1 db array losses, respectively, for this case.

From the above calculations, we conclude that the steady-state phase errors in an array using <u>first order loops</u> for differential phase tracking will become a problem for those ranges requiring loop equivalent noise bandwidths on the order of 1 cycle. If bandwidths of this order are anticipated, a second order differential phase tracker will be required, or the differential doppler shift may be compensated for by computation of the expected frequency differences, and insertion of a phase rate in each tracker to bring the signals to the same frequency.

4. The Performance of Phase Trackers with a Noisy Reference

a. Effect of Noise

In the "cross-correlation" phase tracker, the reference is a signal that is similar to the signal to be tracked in phase, such as the signal in an adjacent channel or the sum channel of an array. The mathematical operations performed by the cross-correlation loop are represented in block diagram form below in Fig. IV.G-8:

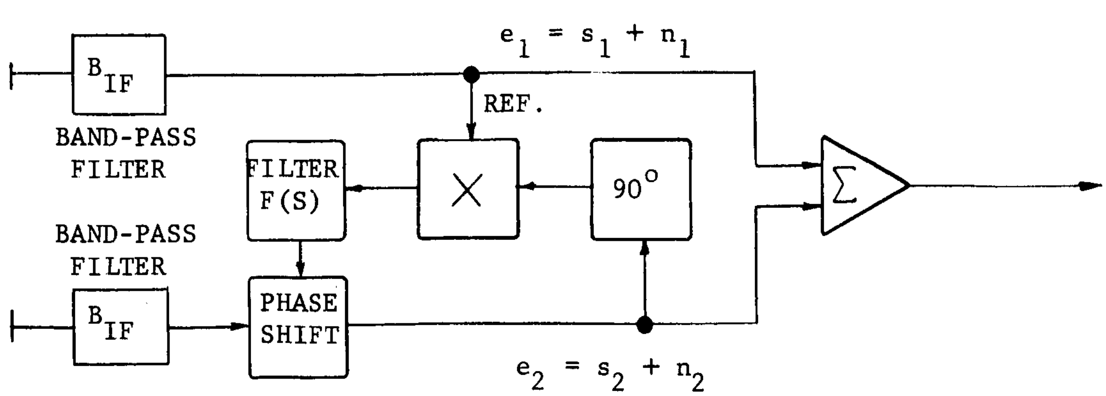

Fig. IV.G-8. Cross-correlation phase tracker.

In the following analysis, each input signal will be considered to consist of constant amplitude sinusoidal voltages with additive gaussian noise:

$$e_1 = \sqrt{2}\, A \sin \omega_o t + n_1(t)$$

$$e_2 = \sqrt{2}\, B \sin \left[\omega_o t + \epsilon(t)\right] + n_2(t) \tag{IV.G-23}$$

where:

$\epsilon(t) = \phi_d(t) - \phi_c(t)$,

$\phi_d(t)$ = differential phase shift referenced to e_1, and

$\phi_c(t)$ = phase correction introduced by the phase shifter.

Here, signal e_1 is considered to be the reference signal.

Following conventional procedure, each noise term is resolved into in-phase and quadrature components:

$$n_1(t) = n_{11}(t) \sin \omega_o t + n_{12}(t) \cos \omega_o t$$

$$n_2(t) = n_{21}(t) \sin \left[\omega_o t + \epsilon(t)\right] + n_{22}(t) \cos \left[\omega_o t + \epsilon(t)\right] \tag{IV.G-24}$$

Then the voltage at the output of the low-pass filter is found to be:

$$-V = AB \sin \epsilon(t) + \frac{A}{\sqrt{2}} \left[n_{21} + \frac{B}{A} n_{11} + \frac{n_{11}n_{21}}{\sqrt{2}\; A} - \frac{n_{11}n_{22}}{\sqrt{2}\; A} \right] \sin \epsilon(t)$$

$$- \frac{A}{\sqrt{2}} \left[n_{22} + \frac{B}{A} n_{21} + \frac{n_{12}n_{21}}{\sqrt{2}\; A} + \frac{n_{22}n_{11}}{\sqrt{2}\; A} \right] \cos \epsilon(t) \tag{IV.G-25}$$

Now let:

$$n_3(t) = \left[n_{21} + (B/A)\, n_{11} + \frac{n_{11}n_{21}}{\sqrt{2}\ A} - \frac{n_{12}n_{22}}{\sqrt{2}\ A} \right] \sin \epsilon(t)$$

$$- \left[n_{22} + (B/A)\, n_{21} + \frac{n_{12}n_{21}}{\sqrt{2}\ A} - \frac{n_{22}n_{11}}{\sqrt{2}\ A} \right] \cos \epsilon(t) \qquad \text{(IV.G-26)}$$

If the phase shifter provides a phase shift ϕ_c that is directly proportional to $-V$, the system equation may be written (in operational notation) as:

$$\phi_c(t) = \frac{A}{\sqrt{2}} F(s) \left[\sqrt{2}\ B \sin \epsilon(t) + n_3(t) \right] \qquad \text{(IV.G-27)}$$

And in block diagram form, the system is represented as:

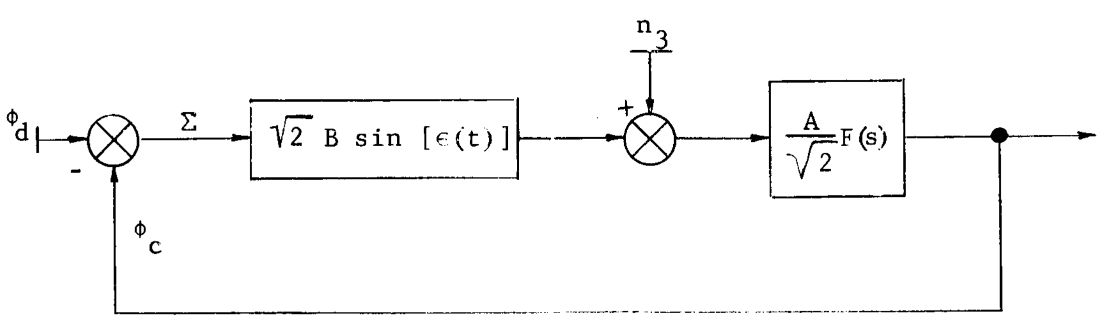

Fig. IV.G-9. System block diagram.

This is the same representation as usually used for a "phase-lock loop" except that an inherent integration is not present, and the loop gain here depends upon the amplitude of two signals rather than on one signal and a fixed amplitude reference. The noise process is of course different, also. If the original noises may be considered as gaussian processes, then the equivalent noise $n_3(t)$ will not be gaussian because of the product terms in the expression. However, as the SNR increases, the product terms contribute less to the total; and the voltage should approach a gaussian process at high SNR.

The "power" of the process, $n_3(t)$, may be related to the power of the original noise voltages $n_1(t)$ and $n_2(t)$ by calculating the average value of $n_3^2(t)$:

$$E\{n_3^2(t)\} = N_3 = N_2 + \frac{S_2}{S_1} N_1 + \frac{N_1 N_2}{S_1} \tag{IV.G-28}$$

where:

N_1 = power of n_1 process,

N_2 = power of n_2 process,

$S_1 = A^2$; signal #1 power, and

$S_2 = B^2$; signal #2 power.

And it has been assumed that $\overline{\cos \epsilon(t) \sin \epsilon(t)} = 0$.

This result may also be obtained by considering the normalized spectral density of the processes e_1 and e_2:

$$\begin{aligned} \Phi_{e_1}(\omega) &= \delta(\omega - \omega_o) + \Phi_{n_1}(\omega) \\ \Phi_{e_2}(\omega) &= \Phi_{s_2}(\omega) + \Phi_{n_2}(\omega) \end{aligned} \tag{IV.G-29}$$

Then the spectral density of the process n_3 may be found from:

$$\begin{aligned} \Phi_{n_3}(\omega) = \frac{1}{S_1}\Big[& \delta(\omega - \omega_o) * \Phi_{n_2}(\omega) + \Phi_{s_2}(\omega) * \Phi_{n_1}(\omega) \\ & + \Phi_{n_1}(\omega) * \Phi_{n_2}(\omega) \Big] \end{aligned} \tag{IV.G-30}$$

where:

$*$ indicates the convolution operation and

$\delta(\omega - \omega_o)$ represents an impulse at ω_o

For the special case when the input noise spectral densities are constant over bandwidths B_{IF}, and the signal modulation $\epsilon(t)$ is small, the spectral density of the noise n_3 will appear as shown in Fig. IV.G-10.

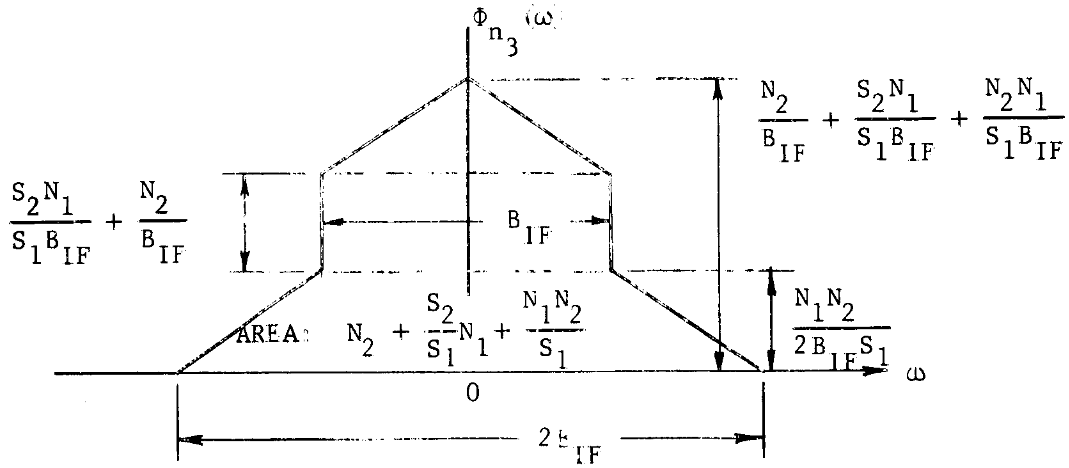

Fig. IV G-10. Spectral density of the noise n_3.

For the case when the signal modulation causes the signal s_2 to occupy a bandwidth B_s, the noise spectral density will spread out as shown in Fig. IV.G-11.

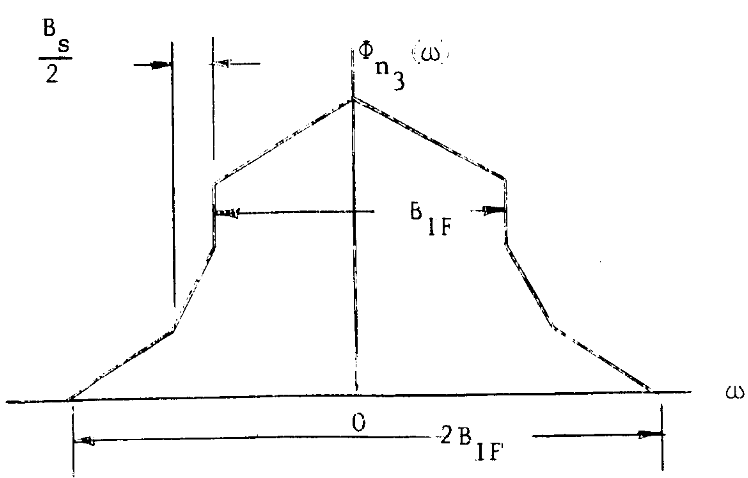

Fig. IV.G-11. Spectral density with signal modulation.

Note that the shape of the spectrum near zero frequency is not changed by the finite bandwidth occupancy of s_2.

Using this idealized spectral density, and under the assumption that the loop acts as an idealized low-pass filter, it is possible to obtain an expression for the noise power in the loop. Let the IF noise density be Φ_n (constant) over the pass band of the IF, B_{IF}. Then the noise power in the loop may be written as:

$$N_L = B_L \left[\Phi_n + \Phi_{n_1} \left(\frac{S_2}{S_1}\right) + \frac{\Phi_{n_1} \Phi_{n_2}}{S_1} B_{IF} \left(1 - \frac{B_L}{2B_{IF}} \right) \right] \qquad B_L < B_{IF}$$

or as: (IV.G-31)

$$N_L = \frac{B_L}{B_{IF}} \left[N_2 + N_1 \frac{S_2}{S_1} + \frac{N_1 N_2}{S_1} \left(1 - \frac{B_L}{2B_{IF}}\right) \right] \qquad B_L < B_{IF}$$

For certain special cases, the above expression may be simplified considerably:

a) Case for $N_1 = 0$ (no noise on reference)

$$N_L = B_L \Phi_{n_2} \quad \text{or} \quad (SNR)_{LOOP} = \frac{B_{IF}}{B_L} (SNR)_{IF} \tag{IV.G-32}$$

b) Case for $N_1 = N_2 = N$; $S_1 = S_2 = S$; and $N >> S$ (low SNR)

$$(SNR)_{LOOP} = \frac{B_{IF}}{B_L} (SNR)_{IF}^2 \tag{IV.G-33}$$

c) Case for $N_1 = N_2 = N$; $S_1 = S_2 = S$ and $S >> N$ (high SNR)

$$(SNR)_{LOOP} = \frac{1}{2} \frac{B_{IF}}{B_L} (SNR)_{IF} \tag{IV.G-34}$$

For the general case, it is useful to plot the loop SNR vs IF SNR for various bandwidth ratics and for various ratios of S_1/N_1 to S_2/N_2. The loop SNR will be defined as the power of signal #2 divided by the noise power in the loop. The plot is shown in Fig. IV.G-12. The case of $N_1 = 0$ corresponds to the usual phase-lock loop condition.

Several simplifying assumptions were made in arriving at the above results; and in any particular case it may be desirable to perform an analysis using the actual transfer characteristics of the IF filters and the loop, rather than idealized rectangular filters. However, the above results will prove helpful in evaluating the merits of various phase acquisition and tracking schemes.

b. Summary of Phase-Lock Loop Characteristics

The preceding analysis provides results that permit treating a "cross-correlation" phase tracker as a phase-lock loop with characteristics only slightly different from conventional phase-lock loops. In this section, some of the pertinent characteristics of phase-lock loops with various types of filters will be summarized.

The usual representation of a phase-lock loop is shown below:

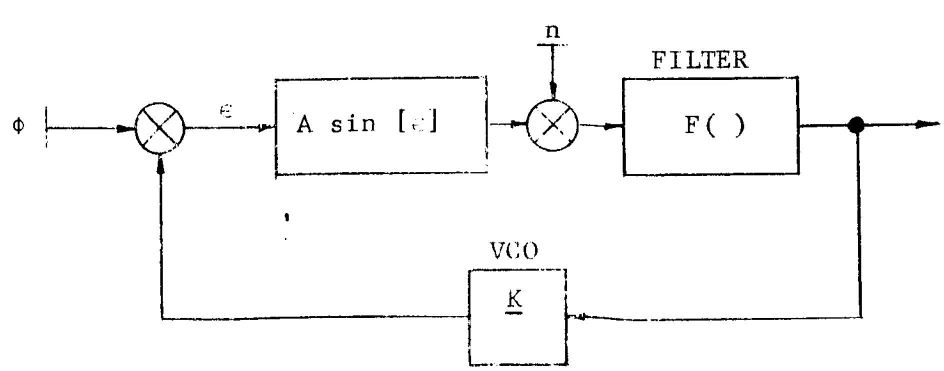

Fig. IV.G-13. Phase-lock loop.

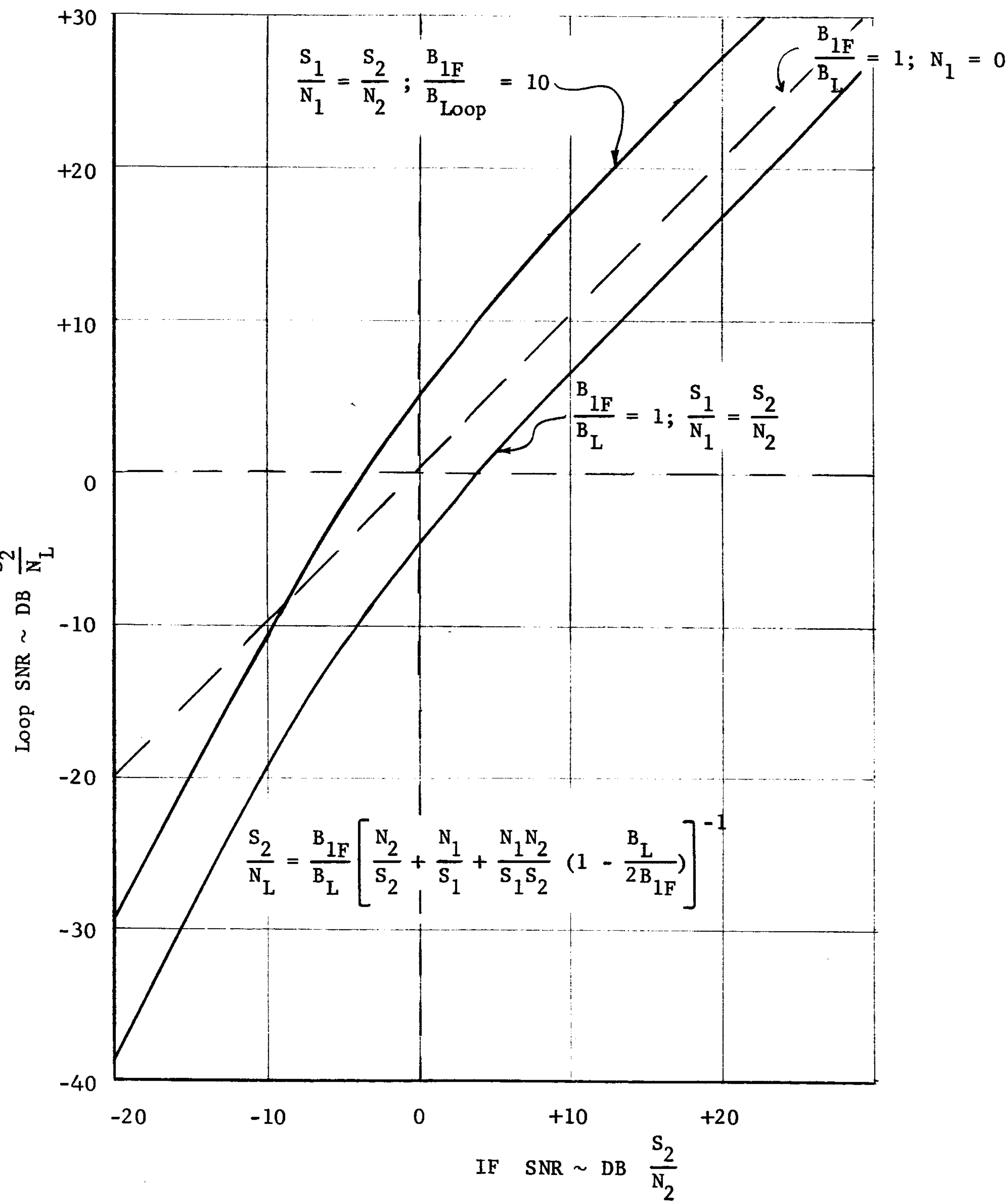

Fig. IV.G-12. SNR in the cross-correlation phase tracking loop.

And when the loop is linearized by assuming a small error $\epsilon(t)$ such that $\sin \epsilon \approx \epsilon$, it is possible to use conventional servo analysis to analyze the behavior of the loop. It is also possible to use a quasilinear approach whereby the sine function is replaced by a function with the same average gain under the assumption that the error $\epsilon(t)$ represents a gaussian process.[28]

Steady-State Errors and Bandwidths

Table G-1 summarizes the steady-state phase errors, the frequency tracking range, and the equivalent noise bandwidths for several forms of open loop transfer functions. In obtaining the tracking range and steady-state errors, the exact differential equation has been used; but the expression for the equivalent noise bandwidth applies only to a linearized loop. The equivalent noise bandwidth is defined as:

$$W_n = \frac{1}{2\pi} \int_o^\infty |H(j\omega)|^2 \, d\omega \text{ cps} \qquad \text{(IV.G-35)}$$

where:

$$H(j\omega) = \frac{G(j\omega)}{1 + G(j\omega)},$$

the closed loop transfer function for the linearized loop.

Mean Square Error

Another characteristic of importance is the mean square value of the loop error when the inputs are stationary random processes. For the linearized loop, the M.S.E. is given by:

$$\sigma_e^2 = \frac{1}{2\pi} \int_o^\infty \left|\frac{1}{1 + G(j\omega)}\right|^2 \Phi_\phi(\omega) \, d\omega + \frac{1}{2\pi} \int_o^\infty \left|\frac{G(j\omega)}{1 + G(j\omega)}\right|^2 \frac{\Phi_n(\omega) d\omega}{A^2} \qquad \text{(IV.G-36)}$$

Transfer Function - Open Loop*	Steady-State Phase Error at $t=\infty$ for: Step Input $\phi=\phi_d$	Ramp Input $\phi=\omega_d t$	Parabolic $\phi=Rt^2/2$	Frequency Tracking Range	Equivalent* Noise Bandwidths
1. $G(s) = G/s$	0	$\sin^{-1}\frac{\omega_d}{G}$	∞	$\lvert\omega_d\rvert < \frac{G}{4}$	$\frac{G}{4}$
2. $G(s) = \frac{G}{\tau s+1}$	$\frac{\phi_d}{1+G}$	∞	∞	0	$\frac{1+G}{4\tau}$
3. $G(s) = \frac{G}{s(\tau s+1)}$	0	$\sin^{-1}\frac{\omega_d}{G}$	∞	$\lvert\omega_d\rvert < \frac{G}{4}$	$\frac{G}{4}$
4. $G(s) = \frac{G(\tau s+1)}{s^2}$	0	0	$\sin^{-1}\frac{R}{G}$	∞	$\frac{G\tau^2+1}{4\tau}$
5. $G(s) = \frac{G(\tau_1 s+1)}{s(\tau_2 s+1)}$	0	$\sin^{-1}\frac{\omega_d}{G}$	∞	$\lvert\omega_d\rvert < \frac{G}{4}$	$\frac{G}{4}\left(\frac{G(\frac{\tau_1}{\tau_2})\tau_1+1}{G\tau_1+1}\right)$
6. $G(s) = \frac{G(\tau_1 s+1)}{s^2(\tau_2 s+1)}$	0	0	$\sin^{-1}\frac{R}{G}$	∞	$\frac{\tau_1^2 G+1}{4(\tau_1-\tau_2)}$ $\tau_1 > \tau_2$

*Applies to linearized system.

TABLE G-1 - SUMMARY OF PHASE-LOCK LOOP CHARACTERISTICS

where:

σ_e^2 is the variance of the process $\epsilon(t)$ (rad^2),

$G(j\omega)$ is the linearized open-loop transfer function of the loop,

$\Phi_n(\omega)$ is the one-sided power spectral density of the noise voltage $n(t)$ $(\frac{\text{volts}^2}{\text{cps}})$,

$\Phi_\phi(\omega)$ is the one-sided power spectral density of the phase process $\phi(t)$ $(\frac{\text{rad}^2}{\text{cps}})$, and

A^2 is the signal power (volts^2).

Thresholds

The tracking threshold of the loop, that is, the point at which the loop will no longer remain in lock for given noise and signal characteristics, is directly related to the M.S.E. of the loop. Other factors affect the threshold, in particular, the higher moments of the statistics of the error process must be considered, as well as the non-stationarity of the input signals. As a conservative engineering approximation, however, a threshold criterion for stationary random inputs may be taken as:

$$\sigma_\epsilon^2 < .25 \text{ rad}^2$$

This value of M.S.E. implies that the probability that the magnitude of the phase error will exceed $\pi/2$ is very small. According to Viterbi,[29] who has considered the exact problem of a first order loop excited by white noise, for this type of loop the above M.S.E. would give an average frequency of skipping cycles of:

$$\frac{\text{Frequency of Skipping Cycles}}{\text{Loop Bandwidth (CPS)}} = 40 \times 10^{-4} \text{ events/sec}$$

And in the first order loop excited by white noise only, this corresponds to a loop SNR of 6 db.

Thus the above bound on the M.S.E., while slightly conservative, should provide a basis for the comparison of various tracking and acquisition schemes and also provide a realistic design criterion.

If the above threshold definition is accepted, it becomes permissable to conduct linear analyses of the loop, because the loop error will, with high probability, remain in the range where $\sin \epsilon = \epsilon$ is a valid approximation.

It should be noted that any steady-state errors will degrade the threshold of a loop since this causes an offset of the error voltage from zero. In an acquisition mode where a frequency search is being conducted, a frequency ramp input is effectively being fed into the loop. In a second order loop this will cause a steady-state phase error. The acquisition threshold will then occur at higher loop SNR for a given input signal than would otherwise be expected. The differences between the tracking threshold and acquisition threshold will depend upon the rate of the frequency search. For values of frequency sweep rate such that;

$$\frac{R}{G} \leq .1$$

where:

G is the gain constant of the second order loop (rad/sec^2) and

R is the rate of frequency search (rad/sec^2).

The acquisition threshold and tracking threshold may be taken as essentially the same value. For example, in reference [26], the results of experiments indicate that for a second order loop, values of R/G = .1 resulted in acquisition 86 times out of 100 trials with a loop SNR of 6 db.

The above thresholds will, of course, depend upon the specific design parameters of the loops; and a statistical description is normally required of the threshold situation. The purpose of the above was to obtain bounds that permit comparison of different tracking and acquisition schemes without unduly complicating the problem.

c. Cross-Correlation Tracker Threshold

Using the results of the previous analyses and the threshold definition given above, an expression may be found that permits determination of the cross-correlation phase tracker threshold in terms of the phase spectrum, IF predetection bandwidth, and the noise spectral densities.

We assume that the additive noise on each individual channel is white over the IF bandwidth. Then the equivalent noise spectral density, for small signal modulation, may be obtained from Fig. IV.G-10:

$$\Phi_{n3}(\omega) = \Phi_{n2} + \frac{S_2}{S_1}\Phi_{n1} + \frac{\Phi_{n1}\Phi_{n2}}{S_1}\left[B_{IF} - |\omega|\right] \quad \text{for } |\omega| \leqq B_{IF/2}$$

$$\Phi_{n3}(\omega) = \frac{\Phi_{n1}\Phi_{n2}}{S_1}\left[B_{IF} - |\omega|\right] \quad \text{for } \frac{B_{IF}}{2} < |\omega| \leqq B_{IF} \qquad \text{(IV.G-37)}$$

$$\Phi_{n3}(\omega) = 0 \quad \text{for } |\omega| > B_{IF}$$

Here the nomenclature is the same as that used in Section G-4a.

Now under the assumption that the non-gaussian nature of the noise does not materially change the threshold, the above expression may be substituted in the expression for the loop M.S.E., equation (IV.G-37), and the bound of $\sigma_\epsilon^2 \leq .25$ used to define the threshold of the cross-correlation tracker.

To simplify the mathematics, it is useful to obtain a form of the noise spectral density that is independent of ω. For loop band-widths much smaller than the bandwidth of the IF, the noise spectral density may be replaced by an equivalent white spectrum of:

$$\Phi'_{n3} = \Phi_{n2} + \frac{S_2}{S_1}\Phi_{n1} + \frac{\Phi_{n1}\Phi_{n2}B_{IF}}{S_1}[1 - k] \qquad \text{(IV.G-38)}$$

where:

k is a constant between 0 and .5.

This artifice should give results essentially the same as would be obtained using the exact spectral density shape for $B_L << B_{IF}$. Using this for the equivalent noise spectral density gives, as an approximate threshold expression for the cross-correlation tracker:

$$.25 \geq \frac{1}{2\pi}\int_o^\infty \left|\frac{1}{1 + G(j\omega)}\right|^2 \Phi_\phi(\omega)d\omega$$
$$+ \frac{1}{2\pi}\int_o^\infty \left|\frac{G(j\omega)}{1 + G(j\omega)}\right|^2 d\omega \left[\left(\frac{1}{S_2}\right)\left(\frac{1}{B_{IF}}\right)\left(N_2 + \frac{S_2}{S_1}N_1 + \frac{N_1N_2}{S_1}[1 - k]\right)\right] \qquad \text{(IV.G-39)}$$

This result may be specialized further by assuming a form for the phase spectral density and the loop transfer function. The power density spectrum of the differential phase fluctuation will be taken as the simple form discussed previously in Section IV.C.

$$\Phi_\phi(\omega) = \frac{2\sigma^2\tau_o}{1+\tau_o^2\omega^2} \qquad \text{(two sided)} \qquad \text{(IV.G-40)}$$

and for the loop transfer function, a simple first order loop will be assumed.

$$G(s) = G/s$$

The first integral in equation (IV.G-39) then becomes:

$$\frac{1}{2\pi}\int_o^\infty \left|\frac{j\omega}{j\omega+G}\right|^2 \left[\frac{4\sigma^2\tau_o}{1+\tau_o^2\omega^2}\right] d\omega$$

$$= \frac{1}{2\pi j}\int_{-\infty}^{\infty} \frac{+j2\,\sigma^2\,\tau_o\,\omega^2\,d\omega}{|-\tau_o\omega^2 + j\,(1+G\tau_o)\omega + G|^2} \qquad \text{(IV.G-41)}$$

$$= \frac{\sigma^2}{1+G\tau_o}$$

And the threshold criterion becomes, from (IV.G-39) and (IV.G-41):

$$.25 \gtrsim \frac{\sigma^2}{1+G\tau_o} + \frac{G}{4B_{IF}}\left[\frac{N_2}{S_2} + \frac{N_1}{S_1} + \frac{N_1N_2}{S_1S_2}\,[1-k]\right] \qquad \text{(IV.G-42)}$$

The loop gain constant G should be chosen to minimize the expression on the right hand side. For values of $G\tau_o >> 1$, the expression may be written as:

$$.25 \geq \frac{\sigma^2}{G\tau_o} + \frac{G}{4B_{IF}}\,[X] \qquad \text{(IV.G-43)}$$

where: $X = \left[\frac{N_2}{S_2} + \frac{N_1}{S_1} + \frac{N_1N_2}{S_1S_2}\,[1-k]\right] \qquad 0 < k < .5$

The value of G that minimizes the right hand side of equation (IV.G-43) is:

$$G \approx 2\sigma\left(\frac{B_{IF}}{X\tau_o}\right)^{1/2} \qquad \text{(IV.G-44)}$$

And for this value of G, the threshold condition becomes:

$$1 > 4\sigma\left(\frac{X}{\tau_o B_{IF}}\right)^{1/2} \qquad \text{(IV.G-45)}$$

For given values of receiver temperature, IF bandwidth, and the parameters of the spectral density of the phase process, the approximate power at which lock will be lost may be determined from the above expression. In terms of the receiver temperature, the threshold condition is:

$$1 > \frac{16\sigma^2}{\tau_o}\left[\frac{KT_2}{S_2} + \frac{KT_1}{S_1} + \frac{K^2 T_1 T_2 B_{IF}}{S_1 S_2}\,[1 - k]\right] \qquad \text{(IV.G-46)}$$

where:

K is Boltzman's constant, (1.38×10^{-23} joules/^{o}K),

T_1, T_2 are the equivalent noise temperatures of the two channels (degrees Kelvin),

τ_o is the correlation time of the differential phase process (sec),

σ^2 is the variance of the differential phase process (rad^2),

S_1, S_2 are the channel signal powers (watts), and

k is a number between 0 - .5.

This threshold criterion is used in Section IV.G-6 for a comparison of this method with other acquisition methods.

5. The Feasibility of Probabilistic Acquisition

The general scheme of probabilistic acquisition is discussed in reference [4]. The incoming signals in each channel of the array are split into two or more symmetrically divided phases and each divided signal is then added in all possible combinations with the other divided signals. The several sum signals are then compared on a SNR basis, and the best signal selected. This method results in a "best" signal with improved SNR. The degree of improvement in SNR and the relative complexity of the scheme may be analyzed as follows. Consider a system as shown in Fig. IV.G-14, using two phase combinations for each signal.

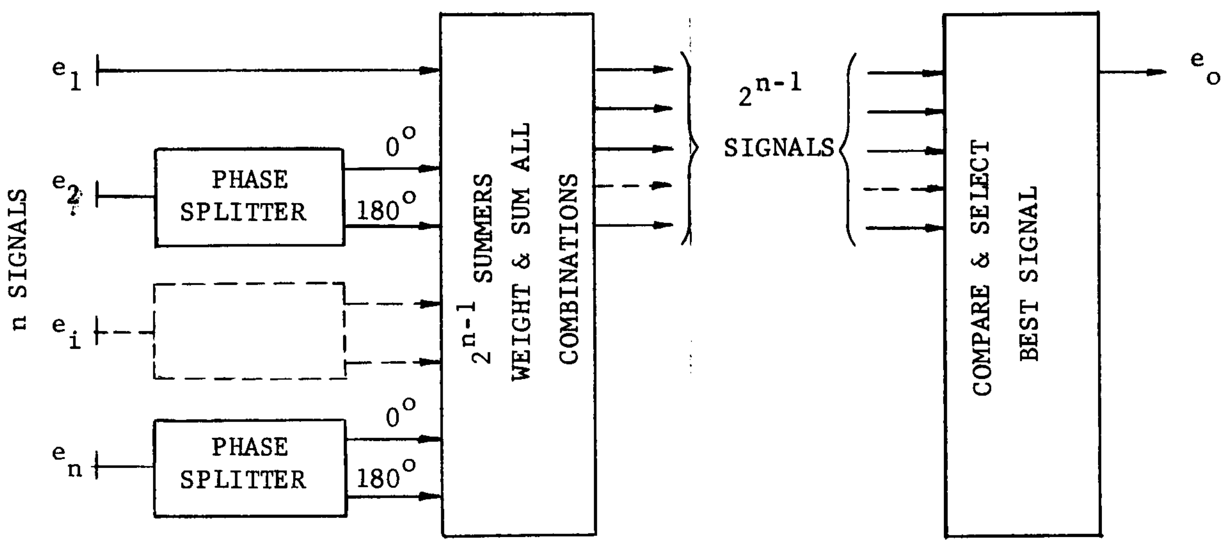

Fig. IV.G-14. Two phase combination-probabilistic acquisition.

Here each individual channel is assumed to have the same signal-to-noise ratio, SNR_1. From the analysis of the effect of random phase errors on the array, a uniform phase distribution among equal amplitude signals in each channel gives

$$SNR_{SUM} = SNR_1 \left[1 + (n - 1) \frac{\sin^2 B}{B^2} \right] \qquad \text{(IV.G-12)}$$

where:

2B is the range of the uniform probability density of the phase ϕ_i. Now if it is assumed that initially, the signal phases are uniformly distributed over the range 0 - 2π, the phase splitting and combining operation will provide one signal combination in which the phases are distributed over a range of $\pi = 2B$. Thus, the best signal from the summer will have, on the average, a SNR of:

$$SNR_0 = SNR_1 \left[1 + (n - 1)\ \frac{4}{\pi^2}\right]$$

Similarly, (IV.G-47)

$$SNR_0 = SNR_1 \left[1 + (n - 1)\ \frac{8}{\pi^2}\right]$$

for a scheme using 4 phase quadrants and 4^{n-1} summers. These results are compiled in Table IV.G-2 and plotted in Fig. IV.G-15, with the gain obtained from a maximal ratio phase tracking system plotted for comparison.

Table IV.G-2

	Two Phase Combinations		Four Phase Combinations	
n	Aver. $\frac{SNR_0}{SNR_1}$	No. Summers	Aver. $\frac{SNR_0}{SNR_1}$	No. Summers
1	0 db	0	0 db	0
2	1.5	2	2.6	4
4	3.5	8	5.4	64
6	4.9	32	7.0	1024
Large	10 log 0.41 n	2^{n-1}	10 log 0.81 n	4^{n-1}

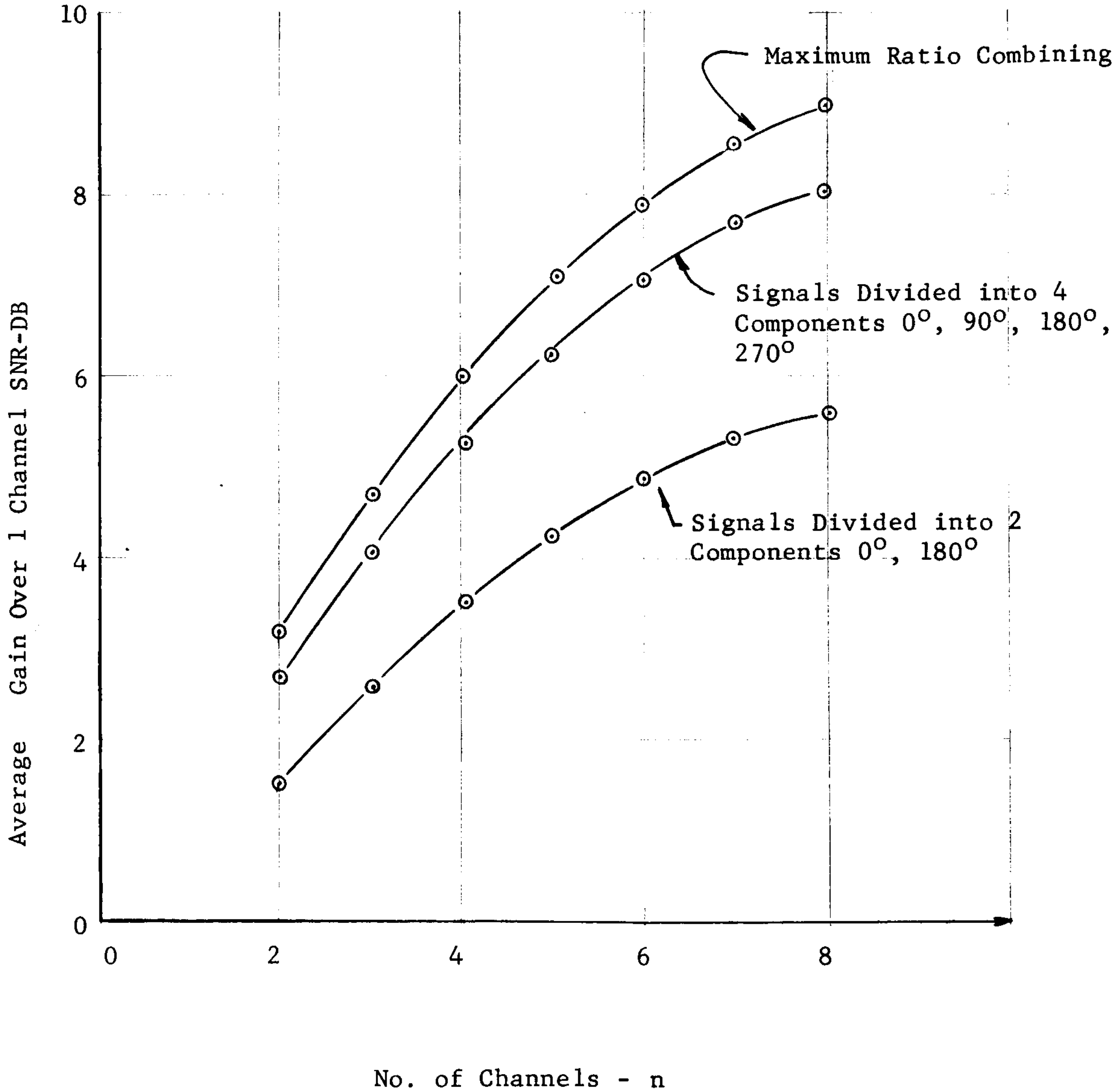

Fig. IV.G-15. Average SNR improvement with "probabilistic" signal processing - uniformly distributed initial phases.

With slowly varying phases and a small number of antennas, the merits of this method look attractive. With a large number of antennas, the complexity of the processing becomes a drawback. In this method, the necessity for phase tracking could be replaced by switching from one signal to another in a manner somewhat similar to a selection diversity system. However, conventional phase tracking would probably be used after acquisition is accomplished.

6. Comparison of Acquisition Techniques

The general results of the several preceding analyses permit a preliminary theoretical comparison to be made among the various acquisition methods. To provide a comparison, three sets of atmospheric conditions will be assumed, and the acquisition threshold of each technique will be estimated for each condition. The atmospheric conditions will be defined in terms of the standard deviation and correlation time of the differential phase fluctuations, as follows:

Condition (1): $\sigma = 100^{o}$; $\tau_o = 5$ sec

Condition (2): $\sigma = 100^{o}$; $\tau_o = 100$ sec

Condition (3): $\sigma = 20^{o}$; $\tau_o = 50$ sec

These conditions are intended to bracket the estimates that have been obtained from various sources. For example, conditions (1) and (2) represent fairly severe conditions such as were encountered in experimental measurements by the Bureau of Standards in Hawaii,[22] at elevation angles of $\approx 7^{o}$ and frequency of 9.4 Gc. Condition (3) represents moderate conditions, such as those that may be encountered at higher elevation angles and/or at frequencies near 2.2 Gc.

The comparison of techniques will be based on the estimated minimum received power for secure phase lock, with a fixed receiver temperature, and with the bandwidth of the common phase fluctuations as a parameter. The comparison is specialized further by assuming a specific number of antennas, 16, and a specific receiver equivalent noise temperature of $50^{\circ}K$. In addition, the assumption is made that the differential phase spectrum appears the same, regardless of which pair of antennas in the array are chosen for examination. Based on data presently available,[4] this would be the case for antenna spacings greater than approximately 500 ft.

For the above situation, the following acquisition techniques are evaluated:

(1) Independent Phase Acquisition, Each Channel

(2) Cross-Correlation Phase Tracker

(3) Acquisition Using Sum Signal (Open-Loop Acquisition)

(4) Array Pre-focused on a Radio Star

Independent Phase Acquisition, Each Channel

For this case, the minimum received power for secure lock will be taken as:

$$S_{min} = 8\ KT_e\ B_L \qquad \text{(IV.G-48)}$$

where:

K = Boltzman's constant (1.38×10^{-23}),

T_e = receiver equivalent temperature ($50^{\circ}K$), and

B_L = equivalent noise bandwidth of the phase detector in the channel.

This expression is obtained by noting from (IV.G-43,44) that the loop gain constant for a phase-lock loop should be adjusted to give approximately equal contributions to the total mean square error from modulation error and from noise error. Since the threshold condition assumed previously in part 4 is:

$$.25 > \sigma^2_{mod} + \sigma^2_{noise} \approx 2\sigma^2_{noise}$$

we have:

$$\sigma^2_{noise} = \frac{.25}{2} = \frac{KT_eB_L}{S_{min}}$$

giving the expression in (IV.G-48) for S_{min}. This approximation is used since the form of the common phase fluctuation spectral density is unknown, and this approximation is consistent with the technique used to estimate the cross-correlation phase tracker threshold. The minimum loop equivalent noise bandwidth B_L is determined by the bandwidth of the common phase fluctuations.

Cross-Correlation Phase Tracker

The theoretical threshold is found from (IV.G-46) by taking k = 0 as a worst case. The minimum received power for the case of equal signal power in each channel may be determined for given values of σ, τ_o, T, and B_{IF}. The predetection bandwidth must be wide enough to pass the common phase fluctuations, hence for comparative purposes the predetection bandwidth (B_{IF}) will be assumed to be set at the same value as the phase detector bandwidth (B_L) for the independent acquisition system in (a).

We assume here that the bandwidth of the cross-correlation loop is determined only by the characteristics of the differential phase spectrum, (IV.G-40), and the noise. The equivalent noise bandwidth of an optimum first order loop may be found from (IV.G-44) and (IV.G-45) as:

$$B_{c.c.} \approx \frac{2\sigma^2}{\tau_o} \quad \text{cps} \tag{IV.G-49}$$

Two forms of cross-correlation phase trackers will be compared: (1) one using adjacent channel reference, Fig. IV.G-3e; and (2) one using the sum channel reference, Fig. IV.G-3d. The latter configuration assumes that open-loop pre-focusing has been used as described in Section IV.D. In this preliminary comparison, the times required for acquisition are not considered; at low bandwidths, this will become an important factor.

Acquisition Using Sum Signal (Open-Loop Acquisition)

In this technique (configuration C in Fig. IV.G-3), the initial phase acquisition is made on the common phase fluctuations, but the enhanced SNR of the sum signal is used. The array is partially pre-focused using the reference signals at the individual antennas as described in Section IV-D. The average SNR of the sum signal may then be calculated from (IV.G-13) for the given atmospheric conditions. It should be pointed out that for a small number of channels, the variance of the sum SNR will be considerable, hence there exists a high probability of acquiring at lower thresholds on the sum than indicated by calculations using the average SNR. With a large number of channels, the variance will be small and the average values are more applicable. In any event, the thresholds calculated in this manner should be interpreted as average thresholds.

Array Pre-focused on a Radio Star

If the array is completely prefocused, the total theoretical array gain is assumed available for acquisition. The minimum received power for secure lock may then be calculated as in (a) above, but S_{min} of

(IV.G-48) will be divided by the number of antennas in the array. This threshold represents the minimum secure lock threshold for phase coherent communications.

The results of the calculations as described above are shown in Figs. IV.G-16, IV.G-17, and IV.G-18--each figure representing a different atmospheric condition. In these curves, the effect of the atmosphere on the various acquisition methods is seen clearly. Under severe atmospheric phase variations as represented by condition (1), the cross-correlation phase tracker does not improve the threshold over single channel acquisition unless the bandwidth required to track the common phase variations is on the order of 2.5 cps. The "open loop" acquisition method provides limited improvement, roughly 2 db over those thresholds obtained in single channel acquisition. The open loop acquisition method in conjunction with the cross-correlation phase tracker provides about 1 db improvement in threshold on the average.

Under less severe atmospheric conditions, as represented in Fig. IV.G-17; condition (2), the benefits obtained by cross-correlation phase tracking become more apparent; but because of the large standard deviation of the phasefront, the improvement obtained by using sum signals is still on the same order as in condition (1). Note that for phase detector bandwidths greater than 3 cps, it is possible to utilize the full array gain for non-coherent communications. That is, the loop which tracks the common phase fluctuations will lose lock before the cross-correlation trackers lose lock.

In Fig. IV.G-18; condition (3), the effect of the atmosphere on the array is almost negligible. Using open loop (sum) acquisition under

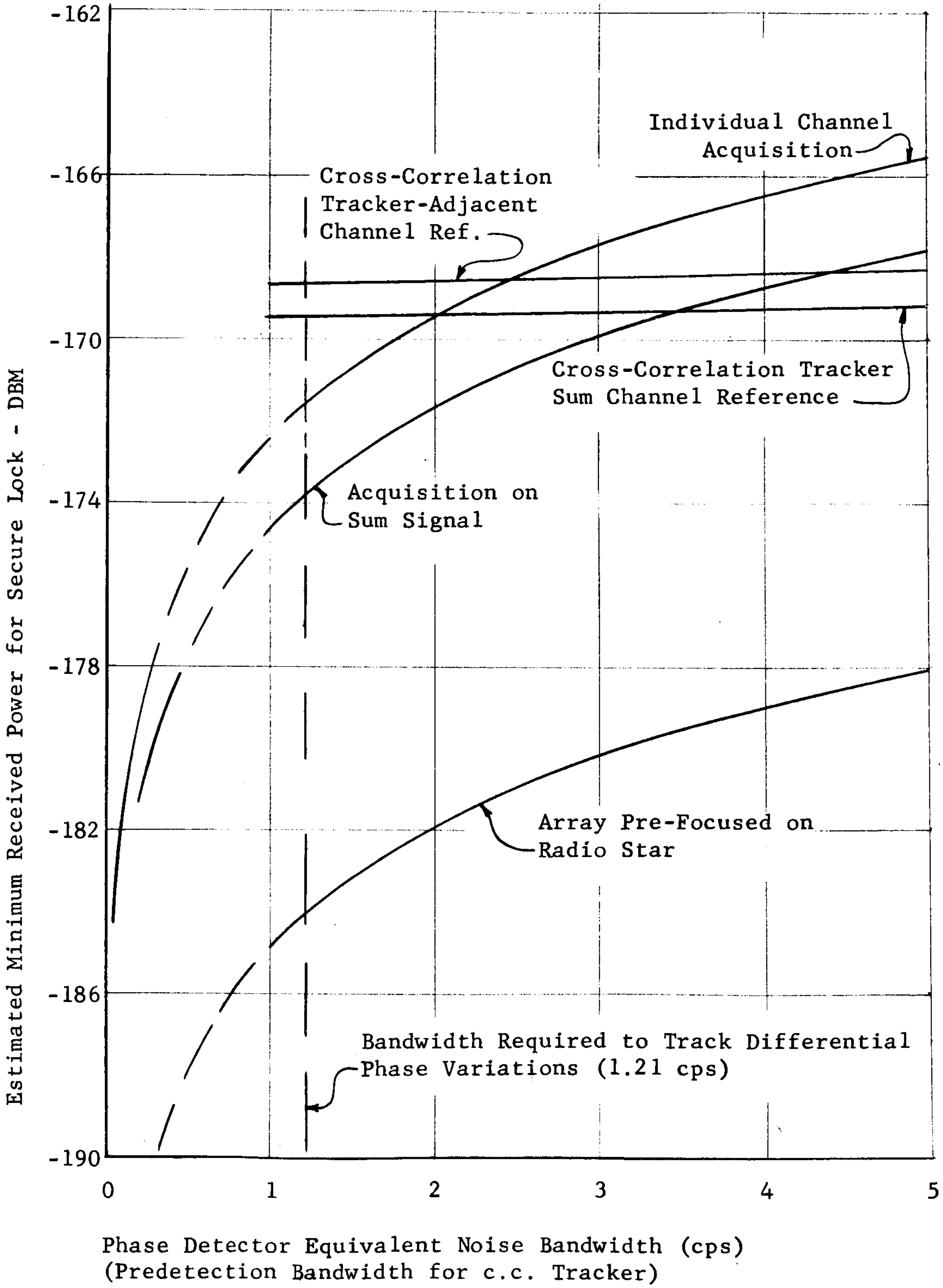

Fig. IV.G-16. Comparison of acquisition techniques - 16 antennas
Equivalent receiver temp. - 50^{o}K.
Atmospheric condition #1 $\sigma = 100^{o}$ $\tau_{o} = 5$ sec.

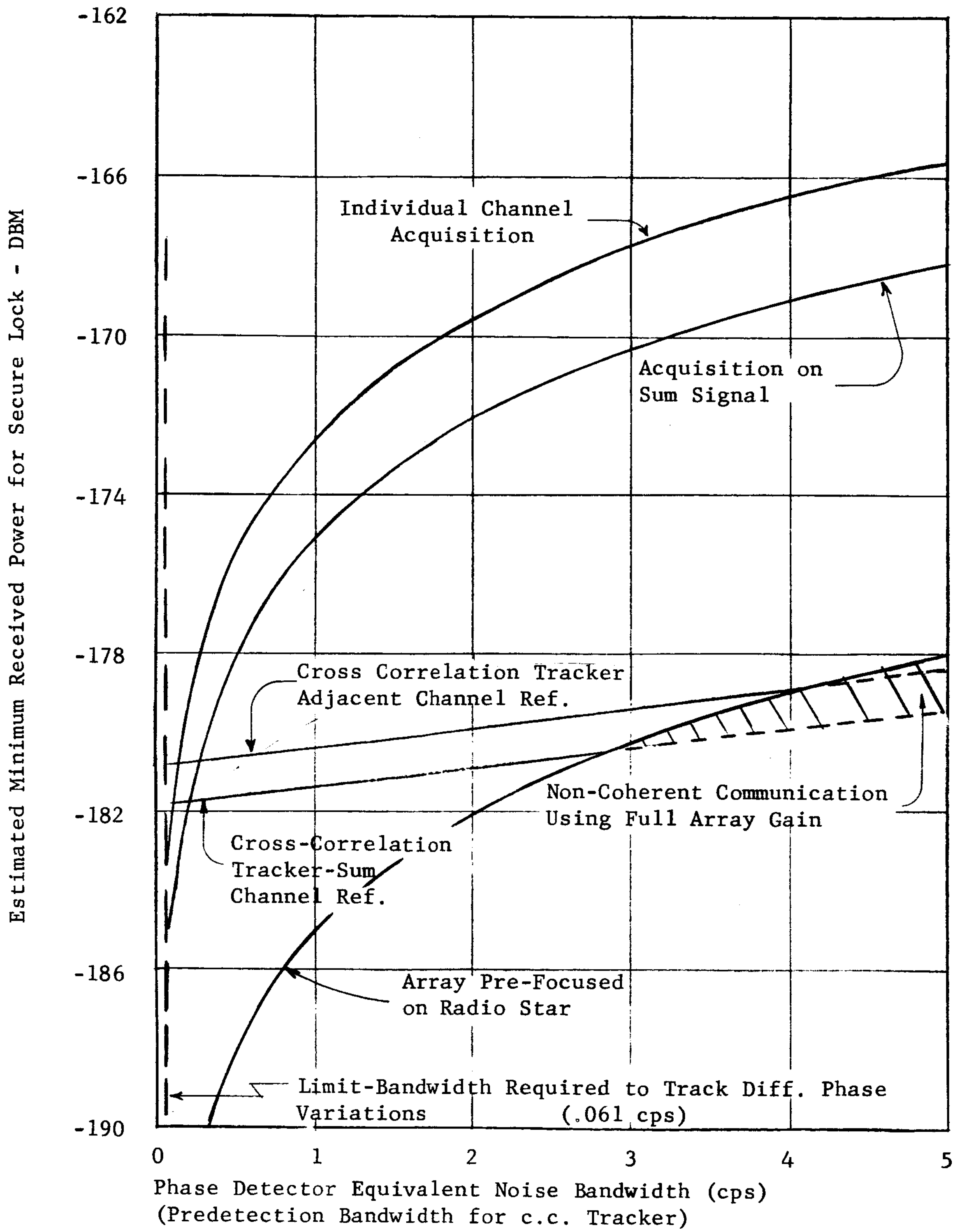

Fig. IV.G-17. Comparison of acquisition techniques - 16 antennas, Equivalent receiver temp. - 50°K. Atmospheric condition #2 $\sigma = 100^{\circ}$; $\tau_o = 100$ sec.

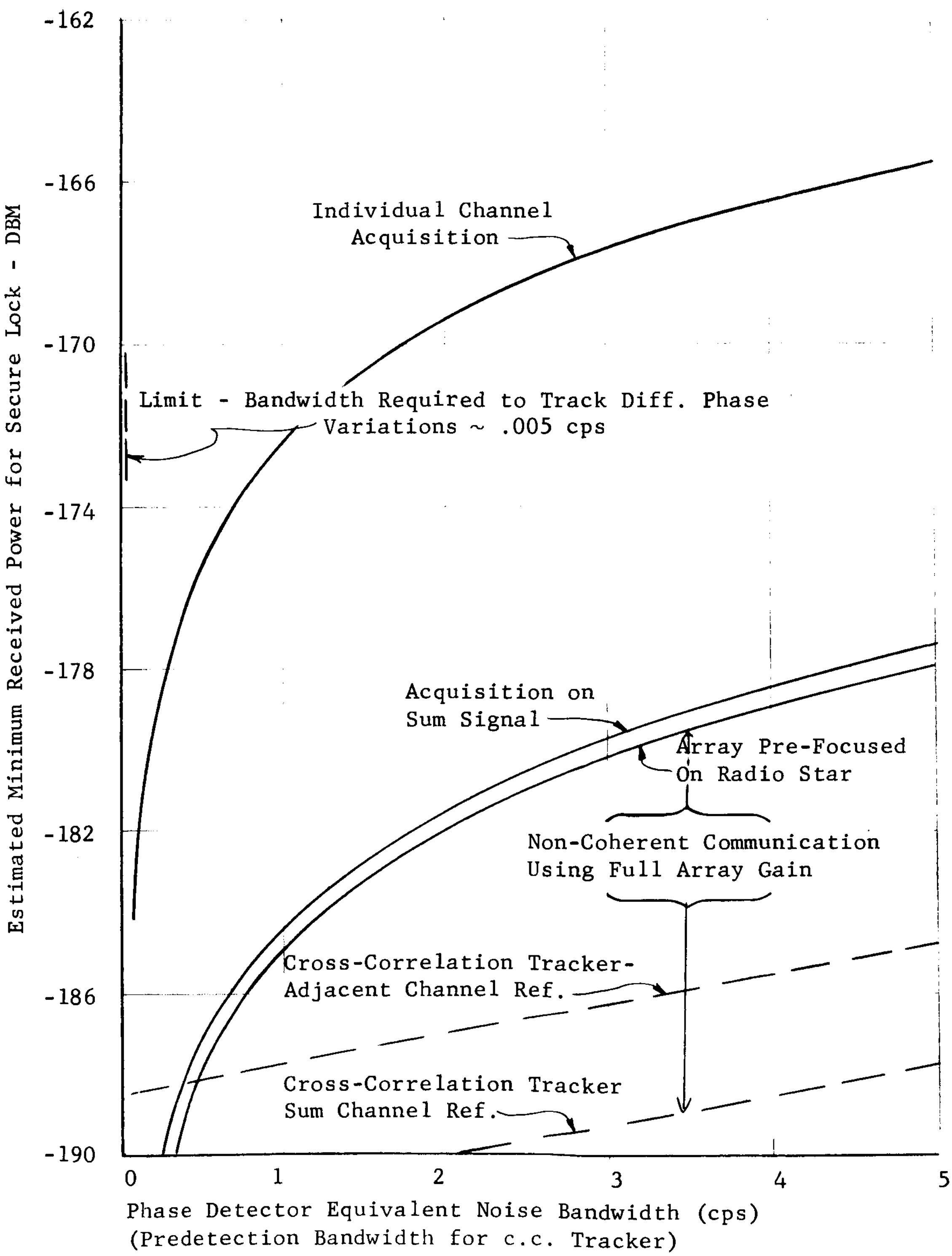

Fig. IV.G-18. Comparison of acquisition techniques - 16 antennas, Equivalent receiver temp. - 50°K. Atmospheric condition #3 $\sigma = 20^{\circ}$ $\tau_o = 50$ sec.

these conditions provides thresholds only .5 db higher than full pre-focusing (on the average). The cross-correlation trackers will acquire at extremely low received powers, and there exists a large region of the plot where non-coherent communication is possible using the full array gain.

It is important to note that in these curves, it has been assumed that the loop bandwidth of the cross-correlation phase trackers is determined solely by the differential phase fluctuations caused by the atmosphere, and thus the curves represent fundamental theoretical comparisons. In practice, the minimum cross-correlator loop bandwidths may be determined by the time available for acquisition or by differential doppler uncertainties. The input bandwidth to the cross-correlation phase trackers is left as a parameter in the curves of Figs. IV.G-16, 17, and 18 because of lack of information on required bandwidth values. This bandwidth will be determined primarily by oscillator instabilities, doppler uncertainties, and atmospheric effects; the latter source is expected to play a minor role relative to the first two sources. In any case, the general conclusions that may be drawn from the curves will be the same. These conclusions are summarized in the following section.

7. Summary and Conclusions

In the above analyses, the several acquisition techniques applicable at long ranges have been investigated and compared. The analyses point out the strong dependency of array capabilities on the atmospheric conditions existing at a particular time. Based on the comparison in part 6, the following tentative conclusions may be drawn:

(a) Open loop acquisition, or partial pre-focusing with coherent reference signals, will permit acquisition using essentially the full array gain for phasefront standard deviations less than 20°.

(b) Open loop acquisition, used in conjunction with cross-correlation trackers or aided individual channel trackers, will always result in an improved acquisition threshold, the degree of improvement depending upon the atmospheric conditions existing at the time of acquisition.

(c) The use of cross-correlation phase trackers will result in improved secure lock acquisition thresholds over individual channel acquisition for bandwidth ratios greater than approximately 2.1 (ratio of common phase tracker to differential phase tracker bandwidth). This result appears to be essentially independent of atmospheric conditions.

(d) Under severe atmospheric conditions (condition #1), an array threshold of -170 dbm will be difficult to achieve if the required common phase tracker bandwidth is greater than 4 cps. The only techniques investigated that will allow lower thresholds under these conditions are those of pre-focusing on a radio star or beacon, or "probabilistic" acquisition.

(e) Communications at power levels below those at which the common phase tracker loses lock, utilizing the full array gain, will be possible at low bandwidths (less than 10 cps) when the atmospheric conditions are not extreme.

(f) A prototype or experimental array should be implemented to confirm the theoretical comparison of acquisition methods. The laboratory tests and experiments that may be performed to confirm the results of this section are discussed in Section V.D.

(g) An attractive acquisition method is one which uses a combination of the open-loop and probabilistic methods. This method would cause the curves labeled "Acquisition on Sum Signal" in Figs. IV.G-16, 17, and 18 to move downward and approach the curves labeled "Array Pre-focused on Radio Star." The improvement in threshold sensitivity is determined by the complexity of the summing method (i.e., the number of summers used).

Further work is needed on the long range acquisition problem, and it is planned to refine some of the analyses during the next report period. In particular, the feasibility of using radio stars for prefocusing operational arrays will be examined in more detail.

A more detailed comparison of the various acquisition methods will be useful when more data becomes available on the characteristics of atmospheric phasefront distortion. This more detailed analysis should take into account the correlations existing between the different antennas of the array, the variations in receiver temperature with elevation angle, the changes in the phasefront distortion with elevation angle, etc. It seems unwarranted to attempt such a fine-grained analysis at this stage, however, because the basic data needed are not available.

V. EXPERIMENTAL PROGRAM

A. Program Requirements

It has been demonstrated that many important questions concerning the performance capabilities and design parameters of antenna arrays remain unanswered. Only a thorough experimental program can supply the necessary data for obtaining the answers to these questions.

Specifically, an experimental program should provide the following data:

(1) measurements of differential phase variations between signals received at two antennas with variable baseline spacing;

(2) measurements of phase variations caused by the component parts in the receiver channels;

(3) tests of the intra-array phase compensation needed to separate (1) and (2), as described in Section IV.D.

(4) correlation of phasefront distortion data with local and regional weather conditions, time of day, season, and sunspot activity;

(5) tests on the feasibility of angle tracking by antenna combinations employing phase-comparison techniques;

(6) comparison of tracking capability of (5) relative to monopulse tracking by a single antenna;

(7) tests on boresighting antennas (for techniques in (5) and (6) by the use of radio stars;

(8) capability for phase acquisition on radio stars; operation of cross-correlation trackers;

(9) capability for pre-focusing on radio stars;

(10) comparison of open-loop pre-focusing (using intra-array phase compensation) with that achieved by phase tracking (i.e., losses in array gain caused by atmospheric effects and equipment phasing errors);

(11) evaluation of methods for providing necessary delays between antenna signals; phase stability of delay devices;

(12) capability for acquiring satellites and space probes with narrow bandwidth phase trackers;

(13) accuracy with which large antennas can be calibrated and maintained in calibration over long periods of time (i.e., absolute pointing accuracies over large angular surface);

(14) system noise temperature (each antenna and prototype array) as dependent upon temperature, weather, time of day, and over long periods of time;

(15) stability of equipment in maintaining bandpass amplitude and phase response;

(16) particular problems associated with operation of arrays of large-aperture antenna (i.e., cooled receivers, control systems for programming antennas to absolute positions with high accuracy, and other problems--some unanticipated);

B. General Description of Program

The optimum experimental program is considered capable of providing measurements with two distinct types of systems:

(1) two antennas with variable baseline separation along E-W and N-S direction; and

(2) a prototype system comprised of at lease three and preferably four large (and fixed) antennas simulating an operational system.

The first system is necessary for making phasefront measurements with variable baseline in order to permit measurements of correlation distances along two orthogonal directions and correlation times over a wide range of elevation angles. This system would be particularly well suited to measurements of the type (1)-(11) in Part A. The second system is necessary for making thorough tests of the type given in (5)-(10), and (12)-(16). Results obtained with this system should be capable of being extrapolated to operational systems. However, the parameters of the prototype system need not be the same as the corresponding optimum parameters of operational systems. The primary purpose of the prototype system is to obtain design information applicable to operational systems, rather than to achieve high receiving area, per se. The prototype system will also play an important role in taking similar data, but more complete, to those taken with the two-antenna system, generally extending a simple interferometer arrangement to an array. This type of information can be extrapolated from one set of parameters to another if the two sets are not greatly different. For example, in order to reduce the cost of a prototype system, the antenna diameters might be appreciably less than the optimum diameter. An extrapolation from 50-60 feet to 100 feet should be possible with a high confidence that no serious, unanticipated problems will be introduced.

As stated in Section III, the operating frequency band is 1-10 Gc with primary frequencies of 2.2 and 8.4 Gc. Therefore, the measurements outlined in Part A above should be made at, or near, these primary frequencies. Because of the frequency sensitivity of propagation effects (Section IV.C.1.), it would also be desirable to include a lower frequency (say 0.8-1.0 Gc) in order to obtain data on ionospheric effects. The value of adding this third frequency can be evaluated only when more specific information is available regarding the likelihood of using the low end of the 1-10 Gc band. The experimental program description includes a discussion of a three frequency system.

Two types of programs are to be studied and both are consistent with the requirements in the above paragraph. The technical outputs of both programs would be very similar. The major differences are in the methods of program planning, the time scale of the overall program, and the manner in which the initial experimental work is meshed into the building of a prototype system. The two types of programs are as follows:

Phase	Program A	Program B
(1) Initial two-antenna system	Two 30 ft. antennas	One 30 ft. and one 60 ft. antenna
(2) Added antennas to make up prototype array	Three 60 ft. antennas	Three 60 ft. antennas

The first phase of each program performs the functions described above for the two antenna system. It is believed that both programs are well suited to this purpose. However, Program A represents less outlay of money at the outset and would probably be preferred if a relatively long delay (say, greater than two years) is anticipated between approvals of the two phases. Many useful measurements can be made with the two-antenna system. The overall cost of the two programs would be comparable because Program A would be expected to last somewhat longer than Program B. Both of these programs are arbitrary in a number of ways and many other useful combinations are possible. After more definitive ground rules are placed on the non-technical factors of the program, a review should be made which takes these factors into account.

Considerable flexibility is permitted in the transition between the two program phases, both in physical configurations and scheduling. It is estimated that approximately two and a half years should be allowed for Phase 1, where one and a half years are required to place the system into operation and one year of measurements can be made. Progress on the prototype system can overlap the latter part of Phase 1; ideally design and manufacture would be a continuous process between the two systems. Approximately three years is expected to be required for placing the prototype system into operation from the time design of this system is started. Once the complete system is placed into operation, it should be treated as a research tool for obtaining useful design information on statistical parameters of the atmosphere, performance information of the type listed in Part A above, and for gaining experience on satellites and deep-space probes. The useful operating life could extend over a period of several years, because a great deal needs to be learned about the characteristics of the atmosphere, interplanetary space, and stellar radiation. The complete experimental system can be a powerful tool for studying these characteristics. Its usefulness could be rather easily extended to operation at several widely spaced frequencies, increasing its capabilities over those for which it is initially designed.

C. System Description

1. Two-Antenna System (Phase 1)

a. Array Configuration

As described earlier in this report, Phase 1 utilizes two 30-foot diameter antennas in Program A and one 30-foot and one 60-foot antenna in Program B. The proposed configuration for these two antenna systems plus support systems is illustrated in Fig. V.C-1. Antenna #1 is a fixed-location antenna, whereas Antenna #2 is so designed that it may be moved to discrete points along either the E-W or N-S baselines. One possible arrangement would be antenna mounting pads located at the 30m, 60m, 120m, 240m, 480m, and 600m points along each of the baselines; distances being measured from the fixed-location antenna out along the respective baselines.

The Central Control and Data Processing building is located as close as practical to the fixed-location antenna, thereby keeping the data links to this system relatively short. The data links for the movable antenna system would be laid along the E-W and N-S baselines. Extension of any data link would then require only the addition of cable from the last position to the next antenna location farther out on the baseline.

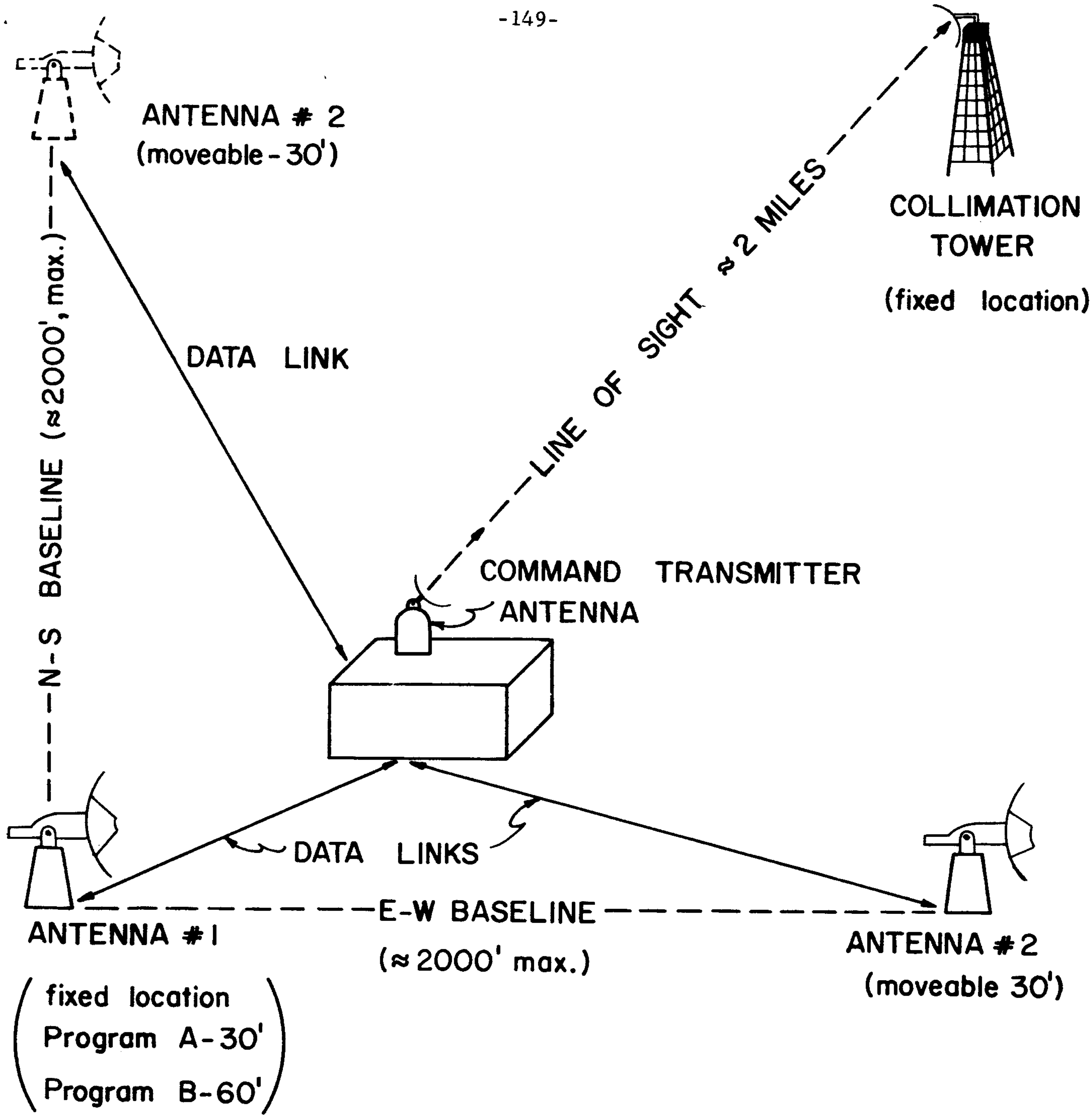

Fig. V.C-1. Experimental array configuration - Phase 1.

In Fig. V.C-1, a collimation or boresight tower is shown located approximately two miles from the fixed antenna site. The particular direction and location of this tower would depend a great deal on local terrain and sources of interference. Beacon transmitters for the frequencies of interest and optical targets would be located on the collimation tower. A command transmitter, which utilizes the small, fixed parabolic reflector shown on top of the Central Control and Data Processing building, is used to supply the coherent reference for the beacon transmitter.

b. Major Systems Parameters

The requirements for the experimental program have been outlined above in Section V.A. The following system parameters or capabilities are required in order to perform the necessary tests:

(1) capability of moving one 30-foot antenna system from one mounting pad to another for the purpose of achieving variable baseline operation;

(2) general capability of operation in the 1-10 Gc band with instrumented capability of single frequency operation in either the 2.29 - 2.30 Gc or 8.4 - 8.5 Gc band with provisions for equipment interchangeability for operation in the other band; a third frequency of the order of 1 Gc is also very desirable in order to observe ionospheric effects;

(3) operation with either vertical or horizontal polarization with capability of change-over to the other polarization;

(4) information bandwidth capability of 5 Mc minimum with a design goal of 10 Mc maximum;

(5) search and automatic acquisition, and angle tracking capability on each antenna;

(6) pointing and tracking accuracy commensurate with the antenna beamwidth and tracking rates which will handle the sidereal rate as well as low altitude satellites;

(7) sufficiently low effective system noise temperature such that certain radio stars may be utilized for testing;

(8) data link phase compensation techniques which will correct for data link phase instabilities, and techniques for separating the equipment phase variations from the atmospheric phase variations;

(9) a variable delay line which compensates for the geometrical path length difference between the two antennas; automatic and continuously variable control of the delay line is desirable but a manual and/or step-variable system may be employed;

(10) conventional and cross-correlation phase trackers for each system;

(11) provision for programming corrections for doppler shifts (common and differential) into the signal channels prior to the phase trackers;

(12) signal summation circuits for optimum combination of the signals from each system; and

(13) data recording and processing equipment for the various experimental data and auxiliary information.

The phase and gain characteristics of the signal channel are of considerable importance in these experiments, therefore each subsystem must be evaluated for its contribution to instabilities in the gain or phase characteristics of the signal.

c. System Description

A block diagram for one complete antenna system for the experimental program is shown in Fig. V.C-2. This diagram also includes equipment common to both antenna systems, as shown inside the dashed lines. The system description at this level applies to both configurations (i.e., Program A which has two 30-foot antennas and Program B which has one 30-foot antenna and one 60-foot antenna).

The equipment to the left side of the data link is located at the antenna site. This includes the low-noise receivers and mixer-preamps, which are located in close proximity to the monopulse feed; the IF amplifiers and phase compensation circuits, the drive system, servo control and tracking receiver. The remainder of the equipment is located in the Central Control and Data Processing building.

As indicated, the path length difference computer, doppler preset, reference oscillator, clock drive and coordinate converter, signal processing circuits, data recording and processing equipment are common to both antenna systems. Thus all equipment shown in Fig. V.C-2, except that just itemized, would be duplicated for the

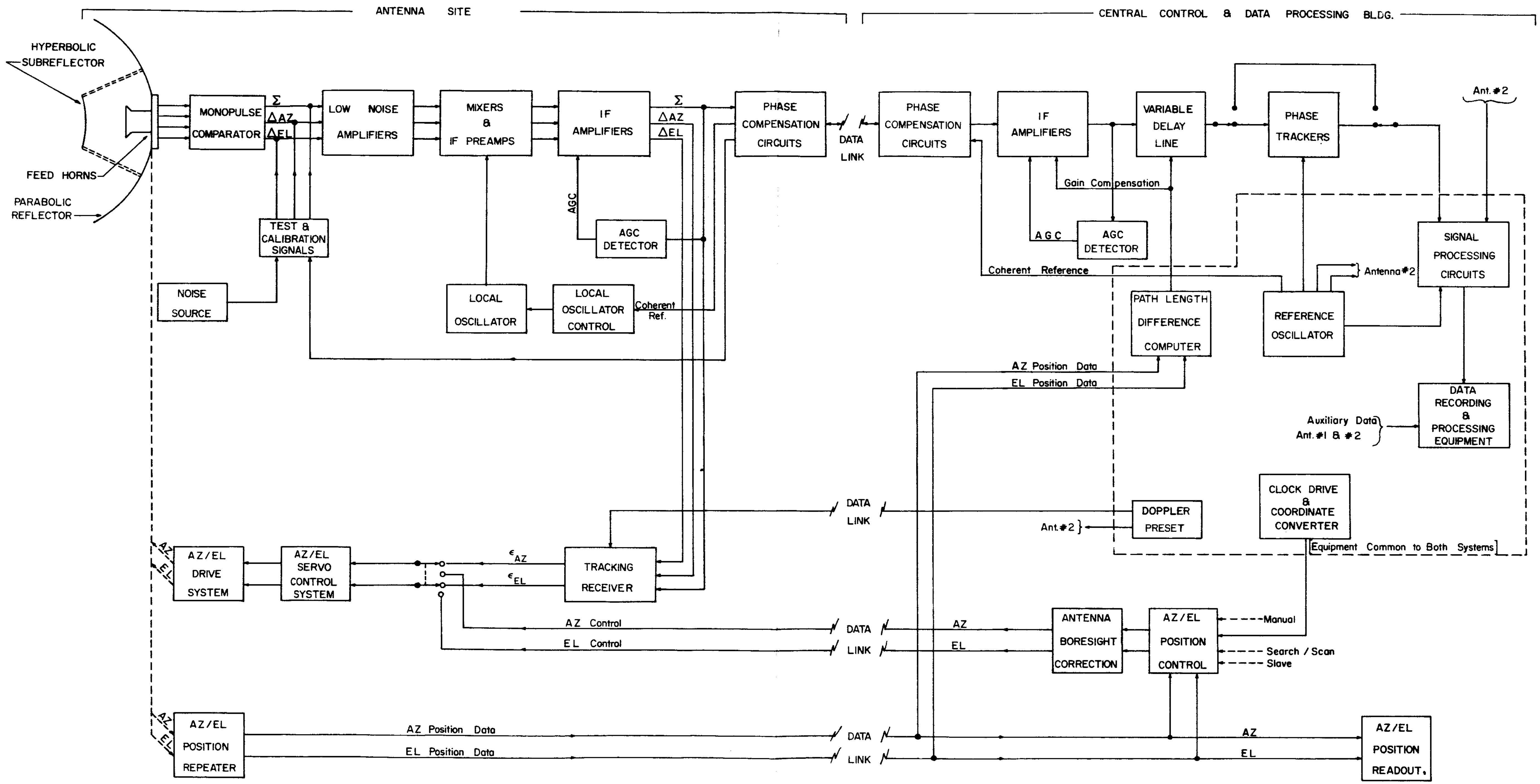

Fig. V. C-2. Block diagram, experimental system, phase I.

1-153

2-153

other antenna system with the possible exception of the variable delay line, which is required in only one or the other signal channel at a time in a two antenna array.

The system is designed for two frequency capability; that is, it may be operated on a single frequency in either the 2.29 - 2.30 Gc band or the 8.4 - 8.5 Gc band where a change of band requires a change of equipment. Such a frequency change-over necessitates the replacement of the monopulse feed system, the low-noise receivers, the mixer-preamp units and the local oscillator. These dual equipments are considered as a part of the system being described. Operation on a third frequency, e.g., in the 0.8 - 1.0 Gc region, would require a third set of these units for the frequency of interest.

2. Subsystems

a. General

A brief description of each antenna system including equipment common to both systems was given above along with a list of the major parameters or system requirements. More detailed descriptions of some of the major subsystems for the experimental array are given below. Complete information on specific equipment required for implementation of each subsystem is not available at this time but general specifications will be given where applicable.

The descriptions will apply, in general, to both the 30-foot and the 60-foot antennas; where significant differences exist, such items will be specifically indicated.

b. Antenna

For purposes of discussion, the antenna subsystem will include the reflector, subreflector, mount, drive, servo and position read-out equipments. A summary of some of the characteristics of the antenna are given below in Table V.C-1.

Table V.C-1

Antenna Characteristics

Group I

Characteristic	Specification
Reflector size	30'/60'
Operating frequency	1-10 Gc
Reflector surface	solid
Surface tolerance	$\leq \lambda/16$
Feed type	Cassegrainian, four-horn, amplitude monopulse
Type mount	Elevation over azimuth
Drive system	Electric or hydraulic
AZ limits	420°
EL limits	-2° to $+90^{\circ}$

One 30-foot antenna has provisions for being moveable over the N-S and E-W baselines; tie down or mounting pads will be provided at discrete points along each baseline. Rotation in azimuth is limited, thereby precluding the need for RF rotary joints. Power, control, and monitoring may be provided above the azimuth axis by use of a standard set of slip rings or cable wind-up. The latter is the least expensive of the two methods.

As described in Section IV.B.4, the Cassegrainian feed system was selected because of its low-noise characteristics relative to a focal-point feed system and because of the convenience in locating the feed, waveguide components, low-noise amplifiers, etc., at the vertex of the main reflector. The resulting accessibility is especially attractive to a research program of this type.

A second set of antenna characteristics, designated as Group II, are presented in Table V.C-2. These are separated for the 30-foot and 60-foot antenna systems. Succeeding paragraphs define some of the criteria used for establishing these specifications.

Table V.C-2
Antenna Characteristics
Group II

Characteristics	Specification	
	30'	60'
Velocity, max. - AZ/EL	5^{o}/sec	5^{o}/sec
Acceleration, max. - AZ/EL	$5^{o}/sec^{2}$	$5^{o}/sec^{2}$
Tracking Rate, min.	0.002^{o}/sec	0.002^{o}/sec
Pointing Accuracy	0.08^{o}	0.04^{o}
Relative Tracking Accuracy - AZ/EL	0.04^{o}	0.02^{o}
Lowest Natural Frequency of Structure, (locked rotor)	3.5 cps	2.5 cps

The beamwidth and gain of large paraboloidal antennas having a 10 db illumination taper may be approximated by

$$\theta^{o}_{3db} = 70 \frac{\lambda}{D} , \qquad G = n \left[\frac{\pi D}{\lambda}\right]^{2} \tag{V.C-1}$$

respectively, where

θ^{o}_{3db} is the half power beamwidth in degrees,

λ is the free-space wavelength of the frequency of interest, D is the diameter of the parabolic reflector, and

n is the efficiency factor (approximately 0.55).

The nominal gain and half-power beamwidth for 30 and 60-foot antennas at the two principal frequencies of interest are given in Table V.C-3.

Table V.C-3

Nominal Gain and Half-Power Beamwidth

	Diameter (ft)	θ_{3db} (degrees)	Gain (db)
f = 2.29Gc	30	1.00	44.3
	60	0.50	50.3
f = 8.45Gc	30	0.27	55.5
	60	0.14	61.5

In order to prevent significant gain reduction, it is desirable to obtain an overall pointing accuracy of approximately one-fourth the 3 db beamwidth (gain reduction approximately 0.7 db). Thus, for 8.4 Gc an overall pointing accuracy of 0.08° and 0.04° would be required for the 30' and 60' antennas, respectively.

The system should be capable of tracking low altitude satellites, which have maximum angular rates of approximately 3°/sec, and also be capable of tracking at the sidereal rate, 0.0042°/sec. Thus, a system tracking capability ranging from a minimum of 0.002°/sec to a maximum of 5°/sec would be satisfactory. This excludes, of course, a direct or near overhead pass for an AZ-EL mount. Maximum acceleration capabilities on both axes of approximately $5^{\circ}/\text{sec}^2$ are satisfactory; this specification may be reduced if it conflicts with other requirements.

The experimental antenna system will have the capability of operating in the following modes: search or scan, automatic acquisition, automatic track and rate memory. In addition, provisions will be included for manual and slave operation. As shown in the system block diagram, a clock drive and coordinate converter unit is provided for open-loop star tracking.

Enviromental conditions for the antenna include temperature range of -10^{o} F to 135^{o} F, and 100% relative humidity. Wind condition requirements are for specified operation to 25 mph, drive to stow to 50 mph, and survival at stow up to 120 mph.

c. RF System

The main RF system components are shown in the block diagram of Fig. V.C-2. These include the monopulse feed and comparator, the low-noise RF amplifiers, the mixer and IF preamplifier units, the main IF amplifiers, the automatic gain control (AGC) detector unit, the local oscillator (LO) and LO control units, and the test and calibration circuits.

The monopulse feed is a four horn amplitude sensing array which is designed to accept a linearly-polarized wave. The output of each horn is fed into the comparator which produces, by means of vectoral additional and substraction of the inputs, an elevation error signal (ΔEL), an azimuth error signal (ΔAZ), and a sum or reference signal. The sum signal amplitude is maximum when the antenna boresight axis is aligned with the target, the difference or error signal amplitudes are a minimum for this condition.

Each of the three signals, sum, ΔAZ, and ΔEL are amplified in the low-noise RF amplifiers, converted to an IF in the range of 60Mc in the mixer circuits and further amplified in the IF preamplifiers and the main IF amplifier units. The signal channel bandwidth is 10 Mc. The local oscillator is locked to the coherent reference signal which has been compensated for phase shifts in the data link. The sum channel signal is split at the output of the main IF amplifier unit into three parts; one part is fed into the tracking receiver along with the ΔAZ and ΔEL signals; a second part is used to derive the automatic gain control signal, which in turn controls the gain of the main IF amplifiers; and the third part is fed into the signal channel through the phase compensation circuits and into the data link.

Test and calibration signals are applied through directional couplers which are located in each channel between the output of the monopulse comparator and the input to each low-noise amplifier. Such signals are used for checking and measuring the noise temperature, gain, and phase characteristics of each channel. A method for separating the equipment phase variations from the external or atmospheric phase variations is discussed in Section IV.D.

The gain and phase characteristics of the RF System are important for two reasons. The differential gain and phase variations between the receiving channels have a direct bearing on the usefulness of the data to be obtained during the experiments. In addition, phase difference and gain unbalances between the three channels, Σ, ΔAZ and ΔEL, in each system have an important effect on the tracking characteristics. This is particularly true for the microwave network which precedes the comparator output. Therefore, the gain and phase characteristics of each unit in the RF System must be carefully evaluated.

The receiver noise temperature depends principally on the low noise RF amplifiers in each channel whereas the system noise temperature includes the noise contributions from the antenna and the wavequide components preceding the low noise amplifiers. Where extremely low noise systems are employed; e.g. when using a maser or cooled parametric amplifier, the noise contributions of the waveguide components have a significant influence on the system noise temperature. The noise introduced by a matched wavequide component may be approximated by

$$T = 66.8\ \alpha\ ,$$

where α is the insertion loss in db for values of $\alpha < 0.5$ db. Thus, a 0.1 db insertion loss effectively increases the system noise temperature approximately 6.7° K.

Due to such factors as cost, complexity and maintenance problems associated with a cooled receiver system, such as a maser or cooled parametric amplifier, it is anticipated that un-cooled parametric or tunnel diode amplifiers will be selected for the experimental system. As an example, specifications for parametric amplifiers which are available from Micromega, Inc. are summarized below.

	X-Band	S-Band
Center frequency	8.5 Gc	2.2 Gc
Nominal Gain	17 db	17 db
Noise Figure	3.5 db	1.6 db
Tuning Range	$\pm$ 150 mc	$\pm$ 20 mc
Bandwidth	100 mc	20 mc

For S-band units, without temperature stabilization and with the temperature varied from 40° to 80° F, gain stability of $\pm$ 1db and phase stability at $\pm\ 4^{\circ}$ over a one hour period may be expected. With temperature stabilization to $\pm\ 2^{\circ}$ F, gain stability of $\pm$ 0.2 db and phase stability of $\pm 1^{\circ}$ are to be expected. For the X-band unit, gain stability is approximately the same as for the S-band unit but because of the wider bandwidth the phase stability will be better by a factor of three or four. Parametric amplifiers for the 0.8 - 1.0 Gc range have characteristics quite similar to the S-band units.

The effective noise temperature, T_e, of each of these units is

$$T_e = T_o(F_r - 1) \quad ,$$

where $T_o = 290^{\circ}$ K, and F_r is the noise factor expressed as a power ratio. Thus, the effective noise temperature of the X-band and S-band units are approximately 360° K and 130° K, respectively. It should be noted that the noise figures given are based on a second-stage noise figure of 10 db.

These receiver noise temperatures indicate that the insertion losses due to the waveguide components located ahead of the low-noise amplifiers become significant contributors when the total insertion loss exceeds 0.5 db, especially in the S-band system. It is anticipated that the total of such insertion losses may be kept below approximately 0.5 db total with proper selection and assembly of waveguide components.

Tunnel diode amplifiers are available for the frequency bands of interest. Units are currently available which have noise figures on the order of 3.3 - 3.8 db for the 0.8 - 2.2 Gc region, and 5.0 db for the 8.4-8.5 Gc band. The gain of such units is typically 15-25 db for bandwidths sufficiently wide for this application. Information on the gain and phase stability of specific tunnel diode amplifiers has not been obtained as yet. If the gain and phase characteristics are satisfactory, then this type unit offers promise for use as the low-noise amplifiers,the question concerning adequacy of the realizable noise temperature with tunnel diode amplifiers remains to be answered.

Integrated mixer-IF preamplifier units are available from LEL, Inc. for both S and X-band. These units have noise figures on the order of 8 db, nominal gains of 35 db and bandwidths of 12 Mc for a 60 Mc center frequency. Amplifiers suitable for the main IF amplifiers are also available from LEL, Inc.; one model, for example, has a 60 Mc center frequency, 10 Mc bandwidth and 80 db gain.

d. Data Link

Data links are provided between the Central Control and Data Processing building and each antenna. For Antenna #1 (see Fig. V.C-1) the data link is a minimum length run and thus poses no problem in using cables for all signal, power and control lines. A microwave relay link between the central site and Antenna #2 was considered but the use of coaxial cables appears more feasible.

The highest frequency to be transmitted over the data link is less than 100 Mc. Some examples of coaxial cables which would be satisfactory for RF links are as follows:

Prodelin 1/2" "Spirofoam," loss-0.83 db/100',

Andrew Type FH4 1/2" Foam "Heliax," loss-0.81 db/100', and

RG - 17/U loss-0.99 db/100',

where the attenuation is that for 100 Mc. Thus, the maximum attenuation over the longest baseline would be less than 20 db, neglecting connection losses. The approximate cost of the second and third cables listed above is 50¢ per foot, therefore this form of RF link is a feasible method from the cost aspect.

Since it is planned that mounting pads will be provided at discrete points along each baseline, it would be feasible to run the data link cables in a direct line between mounting pads and to provide for jumper connections at each mounting pad. Multi-purpose control and signal cables and power cables would be placed along with the RF cables. Direct burial of the cables would improve the stability of the electrical characteristics of the coaxial cables as well as provide a measure of protection for all cables. Duplexers may be used to reduce the number of RF cables required, as shown in the phase compensation systems described in Section IV.D.

e. Delay Lines

Delay lines are required for two reasons: (1) to compensate for the fixed delay due to the difference in length of the data links and (2) to compensate for the geometrical pathlength difference of the received signal. The necessary delay lines for achieving these signal delays in the receiving channels are located between the IF amplifier and the phase trackers, as shown in Fig. V.C-2.

These delays are illustrated by the simple example given below in Fig. V.C-3. The fixed delay due to data-link length difference is shown as d_2. The pathlength difference delay d_1 is shown for the simple case where the elevation angle is zero.

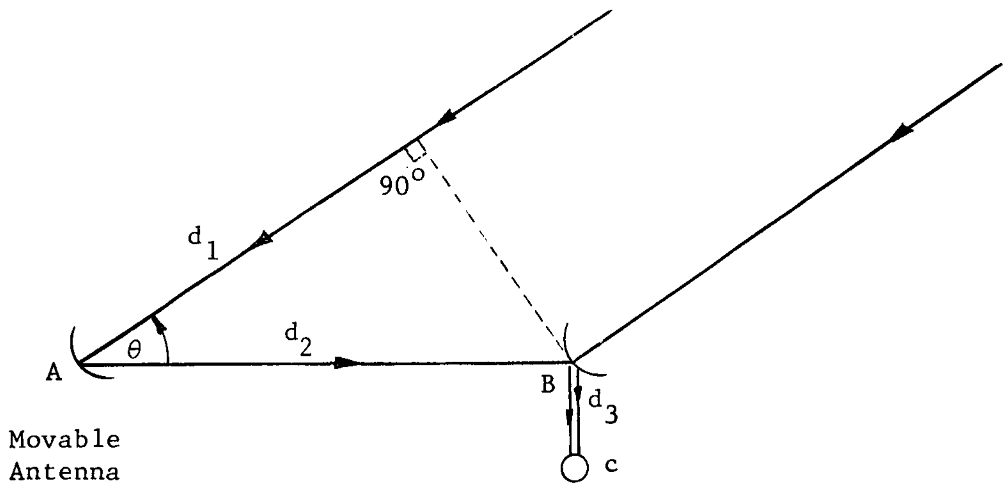

Fig. V.C-3. Illustration of pathlength difference.

For a given azimuth angle θ, the pathlength difference is

$$d_1 = d_2 \cos \theta \quad .$$

Thus the maximum delay which may occur in the geometrical pathlength is equal to d_2, i.e., the effective baseline distance. For a baseline of 600 meters, the maximum geometrical pathlength delay is approximately 3μ sec for the case where the coaxial cable has a nominal velocity of propagation of 70 per cent.

Since the variable delay d_1 is required in only one or the other receiving channels at a time, only one set of variable delay lines will be required for the two-antenna system. The delay lines to compensate for the d_2 delay will be required in the fixed system receiving channel; i.e., Antenna #1 see Fig. V.C-1.

From the geometrical relationships shown in Fig. V.C-4, the delay d_1 required to compensate for the geometrical pathlength difference is

$$d_1 = d_2 \cos\theta \cos\Phi \quad ,$$

where Φ is the elevation angle, θ is the aximuth angle and d_2 is the baseline distance. The type of system used to compute

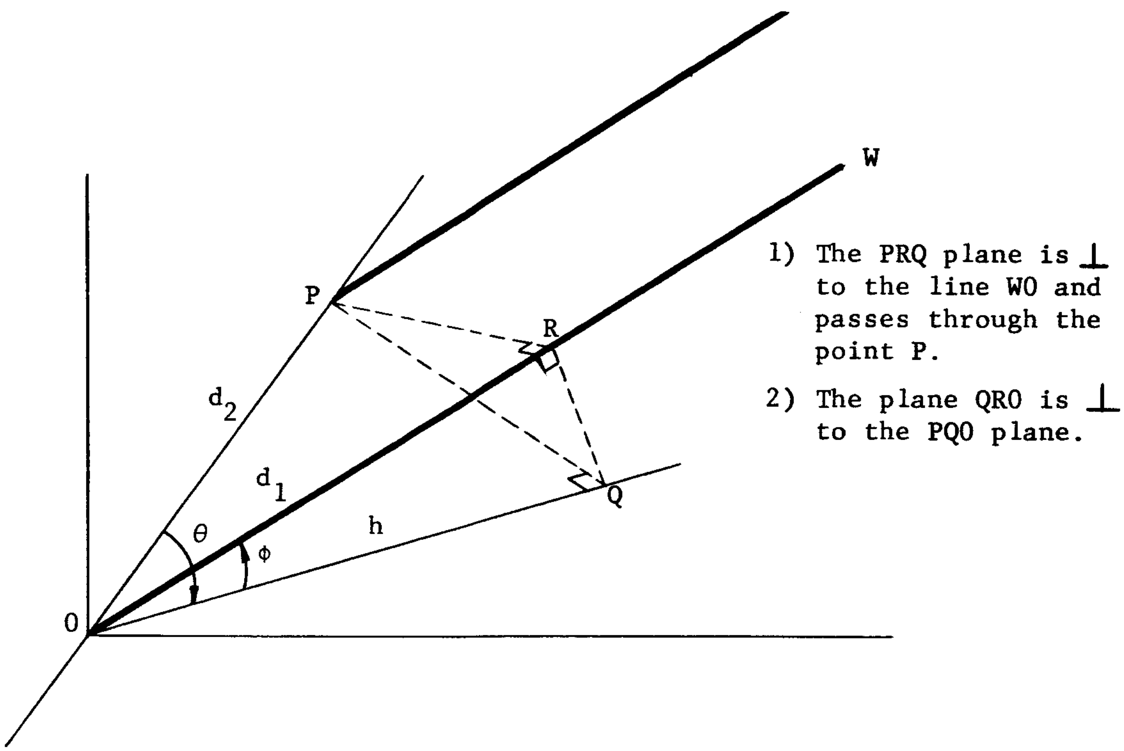

Fig. V.C-4. Geometrical relationship of pathlength difference, d_1.

d_1 will depend to some extent on whether continuously variable or stepped delay lines or a combination of the two types are used to achieve the necessary compensation. If step variable delay lines are used, then the delay steps would desirably be in increments of 2π radians in order to minimize the possibility of phase unlock in the phase trackers. Therefore the minimum incremental delay change for a 60 Mc carrier is 16.7 n sec. Such a step phase shift in the 60 Mc carrier would result in a 60° shift in a 10 Mc carrier envelope.

This would produce a 25% degradation in the vectorally combined signal output for the case of two signals with equal amplitude. For a multiple antenna array, the step delay switching could be arranged such that only a minimum number of the signal channels would be switched simultaneously, thus reducing this effect considerably. The accuracy of each delay step becomes quite important both from the individual incremental delay and the accumulation of such errors.

Another important consideration in determining the applicability of delay lines is that of phase linearity. A plot of phase shift versus frequency on a linear scale should result in a straight line which passes through an integral multiple of π at zero frequency. If the phase versus frequency curve is not linear over the frequency range of interest then the delay time is not constant for the different frequency components and phase distortion results. Phase linearity on the order of $\pm$ 1% is achieveable. Other factors to be considered are the rate of delay variation and the attenuation characteristics. As shown in Fig. V.C-2, gain compensation is provided to compensate for the variation in insertion loss of the stepped or variable delay lines.

One type of variable delay line which has some possibilities is the optically tapped ultrasonic delay cell. These units contain an input transducer which converts the RF signal into ultrasonic waves; these waves travel at a velocity of approximately 0.15 inches/μsec in the delay medium; a movable optical pickoff provides the output signal with the required delay. Such units are feasible up through 30 Mc. The bandwidth, phase, and gain linearity characteristics appear quite suitable. The insertion loss is quite high, on the order of 40-50 db or greater. The main problem associated with this type of device is the optical readout system; the stability, incremental variation, and repeatability is determined mainly by this portion of the device for a given frequency range.

It is obvious that a continuously-variable delay line is to be preferred over the step-variable delay line both for ease of control and the minimization of signal degradation. Further investigations are necessary to determine the best method for delay line variation considering the presently available materials, techniques, and system requirements.

f. Data Recording and Processing

Two basic types of data will be stored during Phase 1 for subsequent processing. One type will be experimental data consisting of differential phase measurements; the other type will be auxiliary data such as air temperature, humidity, barometric pressure, wind velocity and direction, antenna error signals, and antenna azimuth and elevation data.

The experimental data will be machine processed; therefore, for the Phase 1 program, the raw data will be stored in a form adaptable to machine processing and in a form which will permit its re-use. A secondary recording medium providing a visual readout for inspection of the data will also be employed. A magnetic tape recorder such as the Ampex SP-300 with an FM Channel for the experimental data and a direct channel for voice commentary and indexing will be adequate for permanent storage. A recorder such as the Honeywell Visicorder will be adequate for the visual readout.

Auxiliary data will be subjected to visual analysis; therefore, visual recording techniques will be utilized. Since much of the auxiliary data will change at a very slow rate, recording speeds of several inches per hour will suffice. There will be auxiliary data recording requirements incompatible with this slow recording speed, and such data will be recorded on parallel channels of the magnetic tape recorder.

Both digital computer processing (general purpose) and special purpose digital processing are under consideration. Computer processing is the most straight forward approach; however, economic considerations may justify the use of special purpose processing. A study is presently being made of such economic considerations.

3. Transition to Prototype System (Phase 2)

The transition from the two-antenna experimental system to the prototype represents extension of the experimental capabilities to include many tests simulating the performance of operational arrays. The flexibility of the movable 30-foot diameter would be retained, while other large, fixed antennas are brought into operation. It is felt that the configuration shown in Fig. V.C-5 would be very useful, and approximates a portion of an operational array. This configuration applies to both Programs A and B, with the only difference being that one of the fixed antennas has a 30-foot diameter for Program A while it would be a 60-foot diameter for Program B. In both cases, the movable antenna could be used for extending the array in both east-west and north-south directions.

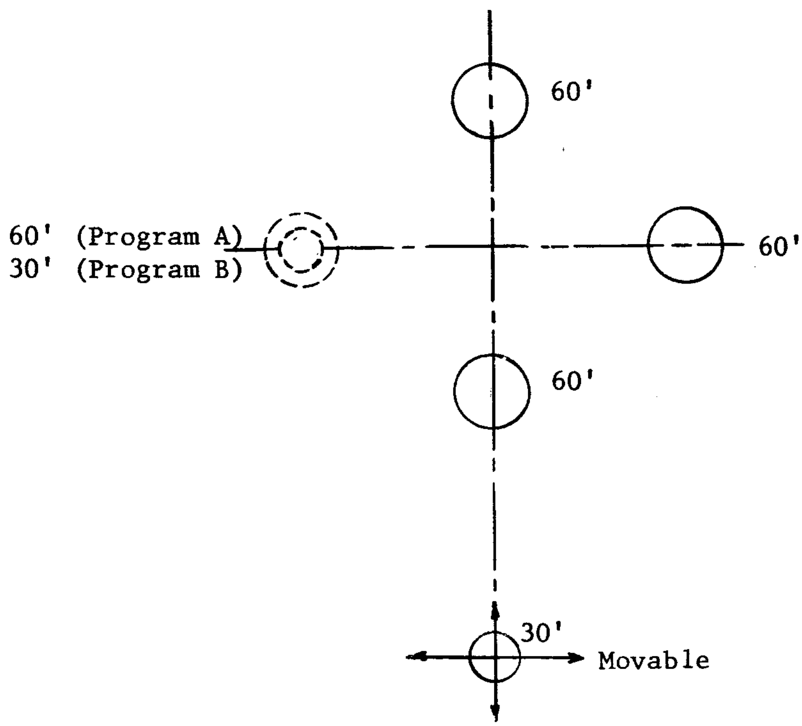

Fig. V.C-5. Configuration of prototype system (Phase 2), incorporating the two-antenna experimental system from Phase 1.

Referring to Fig. V.C-5, the systems for both programs offer a great deal of flexibility to the prototype system. The movable 30-foot antenna can be used in several ways. For example, it can serve as the transmitter for a satellite or spacecraft test program. Alternately, it can be used to extend the receiving array in several directions to a three-antenna system, serving as a good system for testing the acquisition and tracking methods discussed in Sections IV.F and G.

It is important to realize that the experimental phase of the program does not require equipment that will not be useful later to the prototype system; nor does the experimental phase serve merely as an interim system which partially accomplishes the purpose of a prototype system. Actually, the experimental system will supplement the prototype system and enhance the program in the following ways:

(1) it is a flexible research tool in obtaining data on atmospheric characteristics (refractivity variance, scale size, and correlation time), equipment phase variations, and the performance of a data-link stabilization system;

(2) it permits minimization of initial cost (and thus overall cost) by providing the necessary equipment for obtaining the data in (1), while the transition to the prototype system is made more effective by experience gained during the experimental phase; and

(3) it will extend the capabilities of the prototype system, as illustrated in Fig. V.C-5.

Obviously, the major equipment addition required in making the transition from Phase 1 to Phase 2 would be the 60-foot antenna systems with the associated receiving systems, servo and drive systems, data links, and phase trackers. With the configuration shown in Fig. V.C-5 variable delay lines will be required, in general, in each receiving channel. The geometrical pathlength difference computation required for this array will be somewhat more complicated than that for Phase 1.

For the Phase 2 program, data recording and processing techniques required will be essentially the same as for Phase 1. The major difference between the two phases will be in the quantity of the data stored and processed. During the Phase 1 program it will be desirable to store the experimental data in its analog form and then process it. For the Phase 2 program, it may be more expeditious to store the experimental data in digital form thereby saving one step in its processing. Also it may be desirable to have the antenna azimuth and elevation data stored on magnetic tape, thus providing tracking data which can be utilized in a digital computer. Data recording requirements for both phases of the program will be considered further during the second half of this program.

4. Conclusions

A description of the experimental array has been given and the major system parameters outlined. The overall electronic system associated with each antenna in the array has been described and preliminary discussions given on some of the major subsystems. Several of the subsystems, i.e., the tracking receiver, doppler preset unit, servo control and drive system, phase trackers and signal processing circuits, reference oscillator, position readout, and clock drive and coordinate converter unit were not discussed but will be covered in the final report.

The discussions were centered, in general, on the parameters which are the most critical with respect to the program requirements. No one piece of equipment was selected for use in a particular subsystem, only examples of available equipment were given to serve as guidelines in planning the complete experimental system.

Work for the next period will include a more detailed investigation of the important characteristics associated with each major subsystem and the determination of the availability or feasibility of obtaining equipment which will satisfy the system requirements. Particular types and sources of equipment will be recommended, where applicable, for use in the experimental system. Alternate selections will be suggested where trade-offs between cost and specification are deemed feasible.

D. Experiments to be Performed with Phase 1 System (Two-Antenna Experimental System)

1. Laboratory Experiments

Laboratory evaluations and experiments may be conducted prior to, or in conjunction with, the construction of an experimental array. In the laboratory the advanced development work on special hardware requirements should be completed, and those problem areas that do not lend themselves to purely analytical studies evaluated. In these categories, the following experiments are suggested:

(a) Cross-correlation phase tracker performance - A prototype phase tracker using a motor driven phase shifter, operating at 60-100 Mc should be constructed. By simulation of the input signals and noise, the practical thresholds and operating characteristics may be determined. In the experimental set-up, the tracking and acquisition performance of the loop with wideband modulated signals as inputs should be investigated. In addition, the ability of a cross-correlation loop to phase track a noise signal, such as would be obtained from a radio star, can be confirmed. Simulation of extended noise sources could be included in these tests.

The implementation problems connected with operation at extremely low bandwidths, using near perfect integrators, would also be investigated in this experiment.

This prototype phase tracker will be used on the experimental array for further evaluation.

(b) Switched delay line evaluation - Although it appears desirable to use continuous delay lines in the array, discretely switched circuits are more generally available in the delay range and bandwidths required. The technique of switching and the accuracy with which delay compensation can be achieved have a strong bearing on the signal tracking and summation circuits. For example, if switching can be accomplished rapidly and accurately, the phase transient seen by the tracking circuit will be small. At low channel SNR, the phase transients that are introduced by delay switching may adversely affect the array threshold, and may introduce signal distortion. With low bandwidths, such as are anticipated for cross-correlation phase trackers, the recovery time from a phase transient will be appreciable. A prototype switched delay line should be constructed using off-the-shelf components as much as possible, and experimentally evaluated.

(c) Variable delay line evaluation - If variable delay lines with moderate costs are available, tests should be made to determine their adaptability to phase tracking loops. Variation of loop gain and resolution of delay are expected to present the major problems. It is felt at this time that switched delay lines will be adequate and that the advantages of variable delay lines are not sufficient to justify large development costs.

(d) Phase compensation evaluation - A prototype of the phase reference and compensation method as described in Section IV.D should be constructed and evaluated. The accuracy and stability of the system can be evaluated in the laboratory, prior to use on an experimental or prototype array.

The optimum frequencies of operation, multiplying constants, and circuit details must be determined.

(e) Equipment phase and gain stability measurements - As hardware is received for the experimental array, as much as possible should be determined about the phase and gain stability of the RF and IF equipment. The variations of these factors with temperature, humidity, etc., should be determined.

During the remainder of this study, more effort will be concentrated on the definition of the experimental program, and it is expected that the above experiments will be developed in more detail and that the list of the necessary or desirable laboratory work will expand.

2. Field Experiments

The field experiments to be performed with the two-antenna system will satisfy requirements listed in Section V.A, items (1)-(11). Because these items spell out quite clearly what tests are to be made, a similar listing is not given in this section.

3. Signal and Data Processing

a. Signal Processing

The experiments utilizing an experimental array of two antennas will be directed toward:

(1) gathering basic information regarding phasefront distortion due to propagation effects;

(2) evaluation of phase and angle tracking techniques; and

(3) obtaining data pertinent to the operation of an array such as calibration techniques, system noise temperature variations, etc.

Since the primary purpose of the experimental program is to gather data, the initial systems design will be directed toward obtaining a versatile measurement system. The simplified block diagrams of Figs. V.D-1 and V.D-2 represent a tentative arrangement of calibration and signal processing circuits. The remainder of the study period will be directed strongly toward the final design of an experimental system which will result in the recovery of the maximum amount of pertinent data and the evaluation of tracking techniques.

The circuits illustrated in Figs. V.D-1 and V.D-2 incorporate the following features:

(1) a modified Dicke radiometer system[37] which will provide the capability of accurate boresight calibration and system noise temperature calibration;

(2) a cross-correlation tracker which will be used for the measurement of phasefront distortion resulting from atmospheric effects;

(3) correlation radiometers[38] (IF and envelope correlation), which will provide basic measurements supplementary to those of the cross-correlation tracker;

(4) a phase-sensing monopulse angle tracker using both antennas; and

(5) an amplitude-sensing, monopulse, angle tracker for each antenna. (See Fig. V.C-2.)

Each of these features will be discussed with particular reference to their use in recovering data and calibration of the experimental system.

One of the first problems likely to be encountered in the installation of a large antenna is the alignment and calibration of the

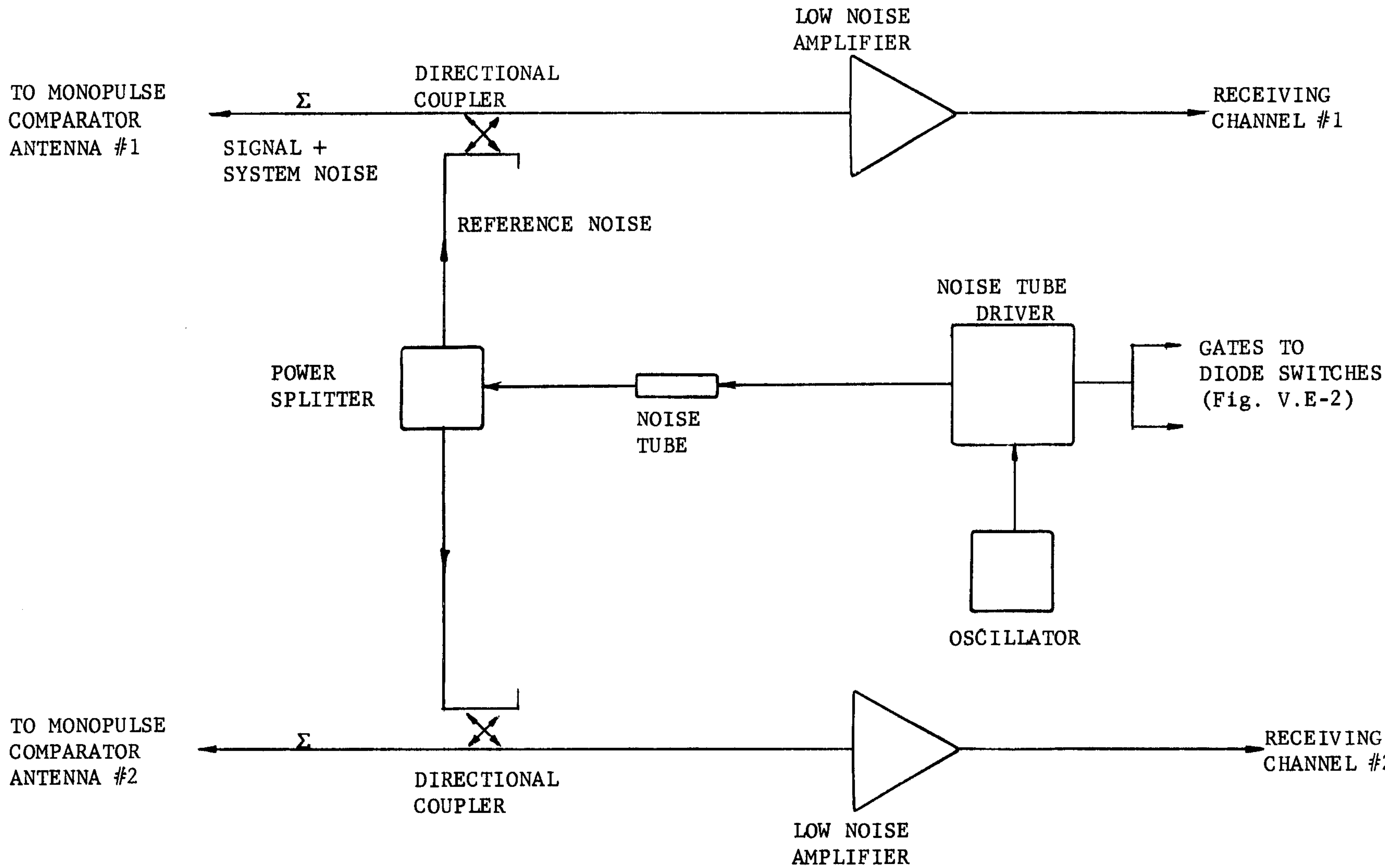

Fig. V.D-1. Test and calibration circuits (partial).

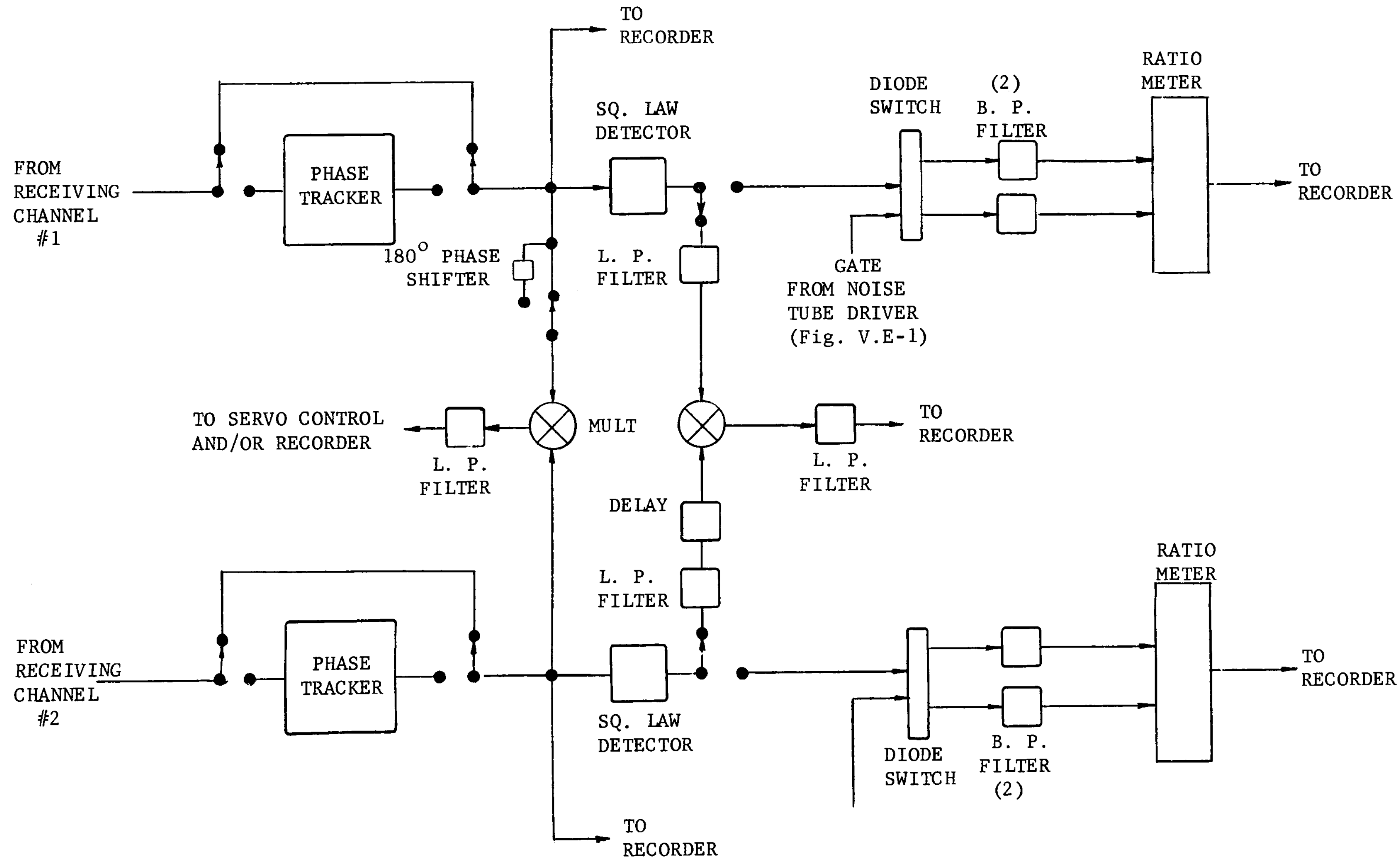

Fig. V.D-2. Signal processing circuits (partial).

electrical boresight axis. This can be accomplished for various azimuth pointing angles by using a test beacon signal located in the far-field region of the antenna. However, in a large antenna structure, it is likely that considerable variation in boresight alignment will occur due to sag in the reflector surface which varies as a function of elevation angle. Thus, a test signal, whose position is accurately known, is required which can be observed at a sufficiently large number of elevation (and azimuth) angles such that the variation in boresight alignment as a function of pointing angle can be formulated. In this manner the effects of variations in boresight alighment can be removed from recovered data.

In a search for discrete signal sources whose positions are accurately known, one is immediately led to consider radio stars. The technique of accomplishing this alignment would then involve directing the antenna toward a selected star and determining the difference in azimuth and elevation between the true star position and the observed position. This procedure can be repeated as stars traverse the celestial sphere. Sufficient data to permit an empirical function to be fitted to boresight alignment variation should be obtainable in this manner. In the application of this technique, the two antennas in a variable baseline system would ideally be calibrated while physically adjacent to eliminate differential variations in the angle of arrival of the received signal due to propagation effects. However, the problems of maintaining calibration of the movable antenna from one location to another may preclude this approach; in this case, propagation effects may be averaged out by tracking a given source over an extended period period of time.

Since the received signal power from radio stars is generally small relative to receiver noise, they are observed by means of a switched receiver which reduces the effects of receiver instability and average noise level (i.e., modified Dicke radiometer). As shown in Fig. V.D-1, the method involves AF switching of a reference noise source into the system ahead of the RF amplifier and observing the ratio: (system noise plus received signal plus reference noise) to (system noise plus received signal). In this manner the effects of the system thermal noise are reduced and a dc signal is obtained whose magnitude is proportional to the power received from the celestial source. An additional advantage is obtained in that receiver gain instabilities lasting longer than one cycle of the switching rate are common to both quantities of the ratio and have no effect on the output.

The following brief analysis of the performance of the modified Dicke radiometer is included to indicate that the results anticipated from its use are realizable. The results of the analysis are somewhat optimistic in that small variations in system performance, such as receiver gain instability, are not included. However, the overall effect of these variations is expected to be small. The use of a cooled RF amplifier in the system would improve overall performance by a factor considerably greater than the degradation due to small variations.

The following symbols and systems characteristics are assumed:

(1) two thirty foot diameter antennas with a 70% aperture efficiency,

(2) a system noise temperature of $300^{\circ}K$,

(3) predetection bandwidth, B_{IF};

(4) equivalent noise bandwidth, B_L, of the correlation loop;

(5) Cygnus A is selected as the radio source and has a flux density of 7.4×10^{-24} watts/m^{-2}/cps at a frequency of 2.2 Gc; and

(6) the criteria used for radiometer performance are the rms value of the output fluctuation in the absence of a source signal (i.e., the minimum detectable system temperature change) and the system angular resolution.

The instantaneous deflection as observed on the output recorder is a randomly varying function about a mean value. The smaller the rms variation about this mean, the smaller the detectable temperature change and thus the higher the system detection sensitivity. This rms variation, ΔT_{rms}, can be expressed as

$$\Delta T_{rms} = T_s \left(1 + \frac{T_s}{T_c}\right) \sqrt{\frac{2}{B_{IF}\tau}} \qquad \text{(V.D-1)}$$

where:

T_s = system noise temperature with the reference noise source off,

T_c = coupled noise temperature from the reference source,

B_{IF} = predetection bandwidth (in cps), and

τ = radiometer time constant (in sec).

The system angular resolution is important in that it determines how accurately the system can measure the position of a celestial source. This resolution will be expressed as an angular uncertainty, ϵ, which decreases with increased source temperature and is directly proportional to the antenna beamwidth,

$$\epsilon \approx \frac{\Theta \, \Delta T_{rms}}{\sqrt{2} \, \Delta T} \tag{V.D-2}$$

where:

Θ = antenna beamwidth, and

ΔT = antenna temperature change due to a received signal.

The change in antenna temperature due to a received signal is:

$$\Delta T = \frac{1}{2} \frac{\Phi_s}{k} \tag{V.D-3}$$

where:

$\Phi_s = A_e S$ = power spectral density of the received signal,

S = received flux density, watts/m^2/cps,

A_e = effective antenna area, m^2, and

K = Boltzman's constant, 1.38×10^{-23} watts/^{o}K/cps.

The coupled noise temperature is:

$$T_c = \frac{1}{\alpha_1} \left[\frac{T_N}{\alpha_2} + T_o \right] \tag{V.D-4}$$

where:

T_N = the noise temperature of the calibrated source,

T_o = room temperature, 290^{o}K,

α_1 = coupling loss of the directional coupler. The overall coupling factor would then be 10 log $(\frac{1}{\alpha_2})$, in db, and

α_2 = coupling loss of the power splitter and associated waveguide losses.

It might be noted that there is an optimum value for α_1 which results in a minimum ΔT_{rms} for a given noise reference temperature. The system noise temperature may be expressed as

$$T_s = T_R + T_A \left(1 - \frac{1}{\alpha_1}\right) + \frac{T_o}{\alpha_1} \qquad \text{(V.D-5)}$$

where T_R is the receiver noise temperature referred to the point where the directional coupler appears in the input, $T_A(1 - \frac{1}{\alpha_1})$ accounts for the antenna temperature loss through the directional coupler and $\frac{T_o}{\alpha_1}$ accounts for the increase in T_s due to coupling through the directional coupler when the noise reference is turned off. Thus by substituting equation (V.D-4) and (V.D-5) into equation (V.D-6) a value for α_1 may be determined which minimizes ΔT_{rms}.

In order to illustrate the computation of ΔT_{rms}, assume a system time constant of $\tau = 1$ sec, and a coupled noise temperature of 500°K. This temperature value was chosen assuming the use of a commercially available noise tube (Bendix TD-30 argon tube, $T_N = 10{,}370^{\circ}$K), a 3 db loss in the power splitter, and a 10 db directional coupler. For the assumed system parameters, the following results are obtained.

$$\Delta T_{rms} = 0.303^{\circ}\text{K}$$

$$\frac{\epsilon}{\theta} = \frac{0.215}{\Delta T} \text{ beamwidths}$$

Using Cygnus A as a source at 2.2 Gc

$$\Delta T = 12.3^{\circ}\text{ K}$$

$$\frac{\epsilon}{\theta} = 0.0175 \text{ beamwidths}$$

Thus, it would certainly appear feasible to accomplish antenna calibration on discrete celestial sources with the system characteristics as assumed.

Another feature of the modified Dicke radiometer which recommends its use in this application is the capability of accurately measuring system noise temperature. The quantity actually measured by the radiometer will be termed the y ratio:

$$y = \frac{T_c + T_s}{T_s} \tag{V.D-6}$$

Then:

$$T_s = \frac{T_c}{y - 1}$$

Since the coupled noise temperature, T_c, is derived from a calibrated source, an extremely accurate measurement of overall system noise temperature can be made.

The cross-correlation phase tracker has been described in detail in Section V.G. The inclusion of this tracker in the experimental system will provide not only an opportunity to evaluate this phase tracking technique but also the capability of convenient and accurate measurement of phasefront distortion resulting from atmospheric effects. The use of correlation phase tracking eliminates the phase variations common to both receiver channels and allows a measurement of the relative phase between the signals received by the two antennas. The use of variable spacing between antennas permits the measurement of relative phase variations as a function of spacing.

In order to demonstrate the feasibility of tracking radio stars using cross-correlation techniques and the system parameters previously described, the sample calculation below is given. From (IV.G-31), the noise power in a two channel cross-correlation loop with equal signal power in each channel is approximately:

$$N_L \approx B_L \left[2\Phi_n + \frac{\Phi_n^2}{P} \; B_{IF} \left(1 - \frac{B_L}{2\,B_{IF}} \right) \right] \tag{V.D-7}$$

where:

B_L = equivalent noise B.W. of loop,

B_{IF} = predetection B.W.,

Φ_n = noise spectral density, and

P = signal power.

The signal power from a radio star will have the approximate form $\Phi_s B_{IF}$, where Φ_s is the power spectral density of the signal from the star. Then the SNR in the loop is:

$$SNR_L = \frac{\Phi_s \, B_{IF}}{B_L} \left[2\Phi_n + \frac{\Phi_n^2}{\Phi_s} \left(1 - \frac{B_L}{2\,B_{IF}} \right) \right]^{-1} \tag{V.D-8}$$

For $B_{IF} \gg B_L$:

$$SNR_L = \frac{B_{IF}}{B_L} \left[2 \left(\frac{\Phi_n}{\Phi_s} \right) + \left(\frac{\Phi_n}{\Phi_s} \right)^2 \right]^{-1} \tag{V.D-9}$$

As an example calculation, an observation of the source Cygnus A at 2.2 Gc with a 30 foot antenna (effective area 46 m^2) gives a receiver power density of

$$\Phi_s = 0.5 \times 46 \times 7.4 \times 10^{-24} = 1.70 \times 10^{-22} \text{ watts/cps}$$

where the 0.5 factor is used because the antenna is not sensitive to both components of polarization. The noise density for 300^{o} temperature is:

$$\Phi_n = 41.4 \times 10^{-22} \text{ watts/cps}$$

giving a ratio $\Phi_n/\Phi_s = 24$. Using this result in (V.D-9) for $B_{IF} = 1$ MC and $B_L = 1$ cps gives a tracker loop SNR of 1600, while $B_{IF} = 1$ Mc and $B_L = 10$ cps gives a SNR of 160. Thus, accurate phase tracking on Cygnus A should be possible with this system. For sidereal tracking rates (.0042 degrees/sec), the time lags corresponding to these loop bandwidths will allow accurate real time phase or angle tracking.

In addition to Cygnus A, it will be possible to track other radio stars, the sun, and available satellites. The sun is a non-discrete source of radiation; however, it will provide a convenient and powerful signal source to test the tracking technique using smaller integration times than can be used with radio stars.

The IF correlation radiometer is included to supplement the measurement capabilities of the cross-correlation phase tracker. The detection performed at IF is the same as the cross-correlation tracker with the tracking loop open.

The envelope correlation detection will provide an output whose magnitude depends on the amplitude correlation between the two channels. This detection will be performed while tracking in either the open or closed loop modes and will provide basic information regarding amplitude variations as a function of antenna spacing.

The envelope correlation radiometer possesses the same order of sensitivity as the Dicke type;[38] thus, an evaluation of its performance will not be made at this point.

An amplitude-sensing angle tracker is included with each antenna in order to accomplish accurate boresighting using a coherent signal source and to provide single antenna acquisition capability. A two antenna phase-sensing angle tracker is included for the purpose of evaluating the feasibility of angle tracking using two separate antennas. It is expected that the results of this evaluation can be extrapolated for purposes of evaluating many of the problems to be expected in the application of angle tracking using multiple antennas.

b. Data Processing

As previously discussed, during the experimental program a requirement will exist for the recording of two basic types of data. One type will be the experimental data such as differential phase measurements; the other type will be auxiliary data such as air temperature, humidity, barometric pressure, wind velocity and direction, antenna angle error signals, and antenna azimuth and elevation data.

The frequencies of interest for the experimental data will range from dc to several cycles per second. To provide a permanent record of the raw data, FM recording on magnetic tape will be utilized. Tape recorders such as the Ampex SP-300 operating at 1 7/8 ips will be adequate for permanent storage requirements. One direct recording channel will be required for voice commentary and indexing. A secondary recording medium providing a visual readout for inspection of the data will also be employed. Recorders such as the Honeywell Visicorder will be adequate for this particular requirement.

This same type visual recorder will be utilized for storing the auxiliary data. Generally speaking, the auxiliary data will change at a very slow rate; therefore, a recording speed of several inches per hour will suffice. Exceptions to the slow recording speed for the auxiliary data will be angle error signals, azimuth and elevation data, and possibly wind velocity. This data can be recorded on parallel channels of the magnetic tape recorder which will be operating at a speed of several inches per second.

Since extremely low frequencies are of interest, data sampling and digital processing techniques are being considered for analysis of the data. In this manner, frequencies down to dc can be conveniently processed. A flow chart for the recording of auxiliary and experimental data and the digital processing of the experimental data appears in Fig. V.D-3.

A method under consideration for estimating the power spectral density of the differential phase measurements has been developed by Blackman and Tukey.[39] Their method consists of computing the autocovariance function of the time series from sampled data and estimating the power spectral density through a Fourier transform of the autocovariance function. A review of this method is presented below.

For the ideal case of continuous data with an indefinite length and zero average, the autocovariance function is defined by

$$C(\tau) = \lim_{T\to\infty} \int_{-T/2}^{T/2} X(t) \cdot X(t+\tau) \cdot dt \qquad \text{(V.D-10)}$$

where:

$X(t)$ is a function of time and

τ is the lag interval

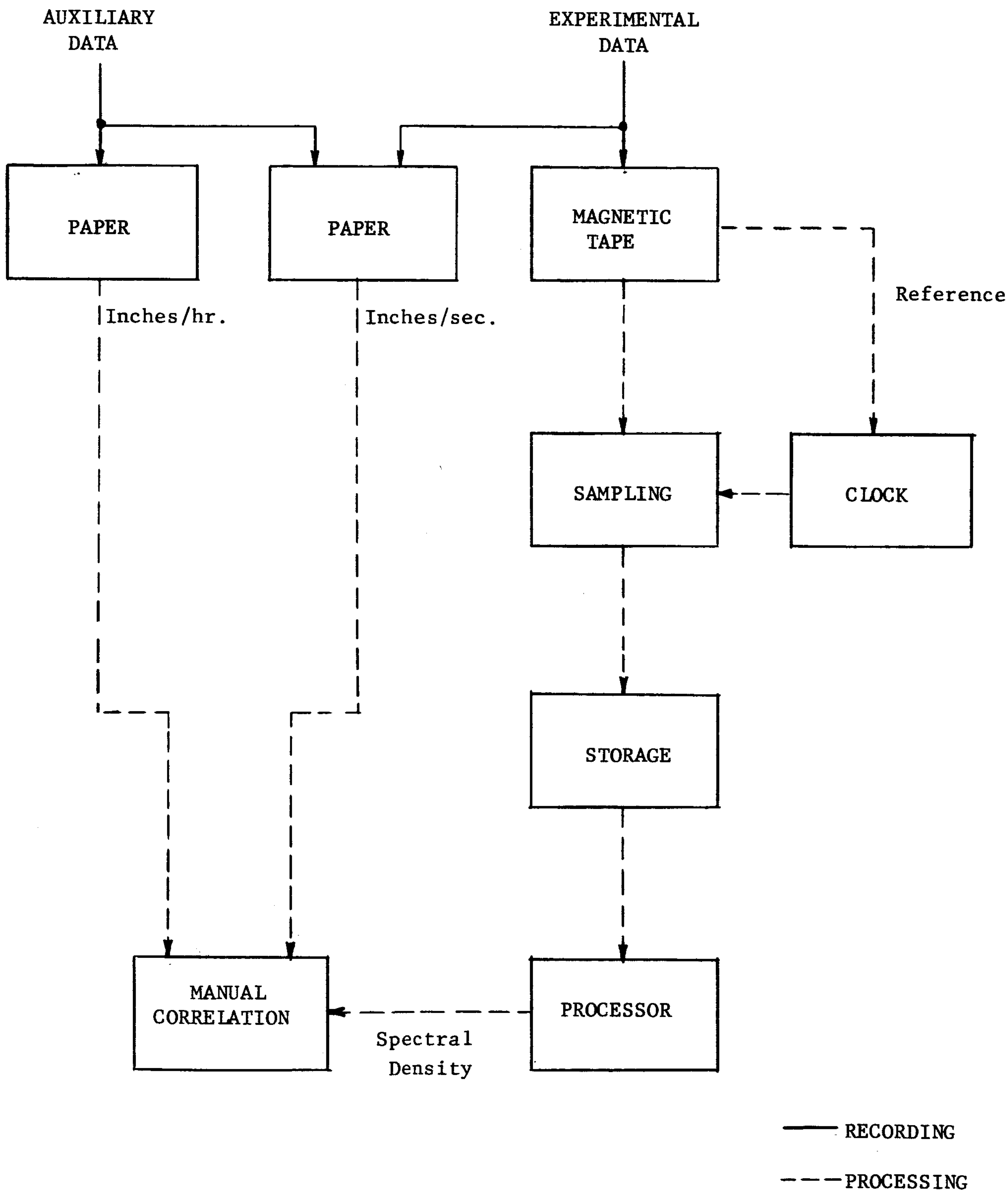

Fig. V.D-3. Recording and processing flow chart.

$C(\tau)$ may be reduced to the form

$$C(\tau) = \int_{-\infty}^{\infty} P(f) \cdot e^{i2\pi f\tau} \cdot df \qquad \text{(V.D-11)}$$

where

$$P(f) = \lim_{T\to\infty} \frac{1}{T} \left| \int_{-T/2}^{T/2} X(t) \cdot e^{-2\pi ft} \cdot dt \right|^2 .$$

The function of frequency P(f) describes the power spectrum of the stationary random process.

Inverting the relation expressing the autocovariance function as the Fourier transform of the power spectrum gives

$$P(f) = \int_{-\infty}^{\infty} C(\tau) \cdot e^{-i2\pi f\tau} \cdot d\tau \qquad \text{(V.D-12)}$$

which is the power spectrum expressed as the Fourier transform of the autocovariance function. The autocovariance function $C(\tau)$ and the power spectrum are even functions of their respective arguments; hence, P(f) can be more simply stated as a one sided cosine transform

$$P(f) = 2\int_{0}^{\infty} C(\tau) \cdot \cos 2\pi f\tau \cdot d\tau \qquad \text{(V.D-13)}$$

Due to practical considerations, analysis must be performed on continuous data of finite length. As Fig. V.D-3 indicates, intervals of continuous data would be sampled and digitized for processing. If X_0, X_1, . . ., X_n are the magnitudes of the data sampled at Δt intervals, the mean lag products (autocovariance) can be computed by

$$C_r = \frac{1}{n - hr} \sum_{q=0}^{q=n-hr} (X_q - \overline{X})\ (X_{q+hr} - \overline{X}) \qquad \text{(V.D-14)}$$

where:

$\Delta\tau = h\Delta t$ = lag interval,

$r = 0, 1, \ldots, m$ and $m \leq \frac{n}{h}$, and

$\bar{X} = \frac{1}{n+1} \sum_{q=0}^{n} X_q.$

Applying a discrete finite cosine series transform to the sequence $C_0, C_1, \ldots, C_m$, the raw spectral density can be computed by

$$V_r = \Delta\tau \left[C_0 + 2 \sum_{q=1}^{q=m-1} C_q \cos \frac{qr\pi}{m} + C_m \cos r\pi \right] \qquad \text{(V.D-15)}$$

for

$$r = 0, 1, \ldots, m$$

V_r arises from replacing $C(\tau)$ in the expression for $P(f)$ as the Fourier integral transform by a finite series of spikes (Dirac delta functions). The result of the above computation is analogous to passing the time varying function through a spectral window with spurious responses, the center frequency of the spectral window being $f = r/2m\tau$. V_r, therefore, may be regarded as an estimate of an average-over-frequency of $P(f)$ in the neighborhood $f = r/2m\tau$. To remove the influence of the spurious responses, a refined spectral density U_r can be computed according to the formula

$$U_r = 0.46\ V_{r-1} + 1.08\ V_r + 0.46\ V_{r+1}$$

when referred to positive frequencies and for frequencies $r/2m\tau$.

When dealing with sampled data, aliasing must be avoided. Aliasing will occur if frequencies higher than twice the reciprocal of the sampling time, Δk, are present in the time function being sampled. Frequencies between 0 and $1/2\Delta t$ will be distinct from one another. Frequencies above $1/2\Delta t$ will be indistinguishable from frequencies less than $1/2\Delta t$, since equally spaced samples from any sine wave about $1/2\Delta t$ will be processed as if it were a frequency less than $1/2\Delta t$.

To prevent aliasing, two cutoff frequencies must be defined prior to processing. There must be a lower cutoff frequency which is the highest frequency for which power spectral density estimates are to be made (this defines the sampling rate) and a higher cutoff frequency at and above which no sampling can occur (these may reasonably be in the ratio of 1 to 2).

The most convenient method for processing the sampled data will be by digital computer. The cost of computer time, however, will be an important factor in choosing this approach for processing. For large amounts of data such as this program could produce, it may be more economical to build (or purchase) a special purpose processor. Before selection of a processing method, a study will be made of the economics of utilizing a general purpose digital computer.

E. Cost and Schedule

Cost estimates are being obtained on the major equipment items required for the implementation of the experimental array. These include such items as the antenna reflector and mount, feed system, servo control and drive system, and parametric amplifiers. Emphasis is being placed on obtaining cost information and technical data on equipment which is commercially available; i.e., equipment that has passed the development stage and to which a fairly high degree of confidence may be attached to the cost and technical data. For some items, such as the continuously variable delay lines described earlier, an effort will be made to determine the most feasible technique or device and the associated cost.

Since insufficient technical information is available on some of the major subsystems, it would be premature to estimate the experimental system costs at this time. In addition, further investigations are required in some specific areas before the applicable equipment may be selected.

A schedule of the estimated time required to obtain the specific equipment, develop special items, assemble and checkout the equipment and systems, and to perform the laboratory and field test programs will be made up during the next period.

VI. PROGRAM FOR NEXT INTERVAL

During the first 3 months of this study, the objective has been to identify and evaluate analytically the major problem areas associated with operational arrays. The program for the remainder of the contract period will have major emphasis on the design of an experimental program and the definition of the experimental measurements. Analytical studies will continue in those areas felt to be of major importance in influencing the design of experiments or the design of a prototype array. Specific areas of effort are listed in three categories below:

Analytical Studies

(1) Optimum antenna diameter - further study will be made by considering the inter-relationships between antenna diameter and noise temperature, theoretical gain capabilities, and beam-pointing problems;

(2) Doppler uncertainties - attempts will be made to obtain information on velocity uncertainties in order to evaluate how they affect the signal acquisition and tracking problems;

(3) Angle acquisition and tracking - a number of possible systems utilizing multiple antennas will be studied to determine their suitability for this function; a selection will be made of specific configurations which will be tested experimentally; and the effects of atmospheric refractivity variations on predicted angular position will be evaluated;

(4) Pre-focusing on radio stars - further study of the number and location of strong sources will be made, with particular attention to their suitability for specific antenna diameters and receiver noise temperatures;

(5) Phasefront distortion measurements - the use of radio stars for this purpose will be studied further to determine the number and location of adequate sources;

(6) Prototype system parameters - overall configuration(s) will be described and recommendations made for the system parameters; and

(7) Operational system model - a program will be described which will permit using experimental data to determine the overall performance of operational systems.

Equipment Study and Selection

(1) System parameters and specifications - specific equipment will be recommended where practical, and the characteristics and specifications of other equipment will be determined;

(2) Signal and data processing techniques - techniques will be evaluated in order to select the parameters of the required systems;

(3) Equipment requiring development - tentative specifications will be determined for equipment not presently available;

(4) Cost estimates - these estimates will be made for the experimental program, within the accuracy permitted by available information from vendors; and

(5) Schedule - an overall program schedule will be recommended.

Experiment Planning

(1) Laboratory experiments - the laboratory tests outlined in Section V.D-1 will be planned and described;

(2) Field tests - the field tests outlined in Section V.D-2 will be planned; the statistical design of experiments required to determine statistical parameters of atmospheric distortion will be made; and

(3) Analysis and use of results - methods of storing and processing the data obtained from the field tests will be described; these data will be put into a form which is suitable for use in the operational system model (item (7) under Analytical Studies).

APPENDIX A

REPORT OF TRIPS

Visits were made to Stanford University, California Institute of Technology, National Bureau of Standards, and Cornell Aeronautical Institute on April 27, 28, 30, and May 13 respectively. RTI personnel were received cordially at each of these places and the following persons were contacted:

Stanford University

Dr. R. S. Colvin, Radio Science Laboratory

Dr. T. Krishnan, Radio Science Laboratory

Dr. P. R. Thompson, Radio Science Laboratory

California Institute of Technology

Dr. T. A. Matthews, Radio Astronomy Department

Dr. R. B. Reid, Radio Astronomy Department

National Bureau of Standards

R. S. Lawrence, Chief, Radio Astronomy Section

R. C. Kirby, Chief, Radio Systems Division

C. C. Watterson, Chief, Modulation Research Section

W. V. Tilston, Antenna Research Section

J. L. Jesperson, Radio Astronomy Section

Martin Decker, Tropospheric and Space Technology Division

K. A. Norton, Consultant, Central Radio Propagation Laboratory

Roy McGavin, Radio Meteorology Section

H. V. Cottony, Chief, Antenna Research Section

Cornell Aeronautical Institute

Dr. W. Flood, Head, Radio Physics Section

J. Doolittle, Department Head, Electronics Systems Section

At each of these facilities the RTI proposed experimental program was described, and criticism of this program was requested. We are particularly interested in the following: use of radio stars as sources for propagation measurements, data on phasefront distortion or related characteristics of the atmosphere, phase instability in equipment and of data links, and accuracy limitations in pointing large antennas as limited by mechanical or atmospheric considerations.

At Stanford University the discussion centered around their activities on a spectroheliograph and two 30 foot diameter antennas used in an interferometer arrangement. The spectroheliograph is composed of 32 equatorially mounted steerable parabolic antennas, each 10 feet in diameter. With this array, the solar emission is mapped daily for the National Bureau of Standards. The method of adjusting the phasing of the array elements consists of observing the standing wave pattern caused by a diode switch which can be inserted near each antenna feed. Phase variations are compensated by adjustment of phase shifters at each antenna in order to cause the standing-wave minimum to fall at the same position from day-to-day. This array does not contain an active phase stabilization system. The instrument is also being used for radio star measurements; however, the signal-to-noise ratios obtained are relatively small, requiring that a long time-constant be used in the output circuit.

Two 30 foot steerable antennas in an interferometer arrangement are in operation at the Stanford site. These units were built at very low cost and use surplus gun mounts for the gear and drive mechanisms. The operating frequency is 3 Gc with approximately 40 megacycles bandwidth, and the integration time at the detector output is 10 seconds. Records of star tracking which were obtained with this system were observed to have high signal-to-noise ratios for several of the more intense radio stars. Although their bandwidth and integration time are somewhat larger than we have proposed using, a large signal-to-noise ratio would be expected even if the product of these two factors is reduced by a factor of 50; therefore, it appears that their system has sufficient sensitivity to be used for the measurement of propagation effects caused by the atmosphere.

The discussions with personnel of California Institute of Technology were somewhat similar to those with Stanford University personnel. Their principal activity is with two 90 foot steerable antennas located at Owens Valley, California. These two antennas operate in the 960 to 3000 Mc range with principal frequencies at 1420 and 2840 Mc. Thus far, the data have been taken primarily with superhetrodyne receivers; however, they have maser amplifiers in operation at 1420 Mc. High signal-to-noise ratios on radio stars have been obtained with the former receivers by using a 20 second integration time. Drs. Matthews and Reid expressed the opinion that there are several radio stars of sufficient intensity to be used as sources for propagation measurements. Unfortunately, it appears that the manner in which their data are being filtered causes phase fluctuations due to propagation effects to be removed from the records. A list of radio sources whose positions are well known was obtained from California Institute of Technology personnel.

Discussions at the National Bureau of Standards were centered primarily around propagation effects. Mr. R. S. Lawrence from the Radio Systems Division expressed interest in the RTI report: "Application of Arrays of Large-Aperture Antennas to Deep-Space Communications." He stated that most of the references with which he was familiar regarding fine-grained characteristics of the ionosphere had been reviewed in this report. He suggested one additional reference on the subject. Although NBS is presently making measurements on tropospheric propagation effects, at this time they have no data to supplement that previously reported in an NBS report. The data now being taken are very similar to that previously reported except that they have added a vertical baseline and a horizontal baseline along the propagation direction. It is not expected that this data will substantially modify the estimates of phase-front distortion in the RTI report mentioned above.

The discussion of most interest at Cornell Aeronautical Laboratories was centered about their wideband interferometer installation. This installation consists of seven 12 foot paraboloids providing baselines of 100 and 1000 meters north-south, 100 and 1000 meters east-west, and 10,000 meters northeast-southwest. The antennas are interconnected with phase-locked loops which compensate for any fluctuations in the electrical transmission path between the receiving antennas and the central site. The system is designed to receive signals from a satellite which transmits a carrier at 2250 Mc and six sidebands spaced at ± 49.5, ± 99, and ± 148.5 Mc from this carrier. This design was intended for studying the limitations of radar resolution in range, angle, and velocity imposed by propagation through the atmosphere. Unfortunately, a satellite has never been orbited for testing the system and the contract is no longer active. Attempts were made to obtain tropospheric data by the use of an aircraft beacon. These tests were not very successful; uncontrollable deviations in the flight path from a straight line places considerably uncertainty in the measured differential phase variations at the ground station. Data analyses of parts of the data were made; the computed phase fluctuations were found to be consistent with those reported by NBS (reference [22])

As a general statement regarding visits to Stanford University and California Institute of Technology, the information of interest to us for propagation studies has not been of primary interest to radio astronomy. This results from the fact that their observations are limited to high elevation angles and their frequencies of operation are selected to minimize propagation effects. Consequently, phase fluctuations caused by atmospheric effects have been treated as a nuisance, but not as a serious problem which has to be corrected. Radio astronomers are concerned with phase instabilities resulting from equipment and from the interconnecting links between antennas. These instabilities have been minimized sufficiently by such techniques as burying interconnecting cables in the ground and by periodic phase adjustments as described for the Stanford University system. No new data on propagation effects of the ionosphere or troposphere were obtained during this trip, nor were quantitative data on equipment phase instabilities obtained.

One major benefit gained from the trips was that our proposal to use radio stars as sources for phasefront measurements appears to be valid. A second benefit was that our tentative conclusion regarding the inavailability of tropospheric and ionospheric data appears to be substantially correct. We feel that a program for the purpose of measuring propagation effects resulting from fine-grain variations in the ionosphere and troposphere is in order.

Trips were also made to the RANTEC Corp. and Rohr Aircraft Company on April 29 and 30 in order to discuss antennas applicable to the planned experimental program. The discussions at RANTEC involved the following persons and were concerned primarily with antenna feeds:

Dr. Seymore Cohn, Director of Research

Alvin Clavin, Director of Marketing

Charles Chandler, Section Head for Antenna Development

Louis A. Kurtz

Possibilities for performing conical-scan tracking as well as monopulse tracking with Cassegrain systems were discussed. There seems to be no inherent difficulty in the design of either system. The complexity of a dual-polarization monopulse system was discussed. We hope to obtain an opinion from RANTEC personnel as to order of complexity in the design of such a feed.

Rohr Corporation personnel included:

Robert D. Hall, Manager

Sal A. Rocci, Chief Engineer

R. A. Peterson, Superintendent of Fabrication

D. L. S. McCoy, Marketing

Primary discussion during this visit was on reflectors, mounts and control systems.

APPENDIX B

1. Amplitude Sensing Monopulse

The amplitude sensing monopulse system utilizes two squinted antenna patterns in each tracking plane, according to well known practice in the radar field. (Tracking in a single plane only is considered here since an analysis of the orthogonal error channel will produce identical results.) A target located on the boresight axis will produce signals of equal amplitude in each of two RF receiver channels, corresponding to the individual antenna patterns. For a target off boresight the signal amplitudes in the two channels will differ. The signals in the two receiver channels are combined in a hybrid network to produce a sum signal, E_s, and a difference signal, E_d.

$$E_s = \frac{1}{\sqrt{2}}(E_a + E_b) \qquad \text{(B-1)}$$

$$E_d = \frac{1}{\sqrt{2}}(E_a - E_b) \qquad \text{(B-2)}$$

where E_a and E_b are the received signals in each channel.

The sum and difference signals are processed by a system as shown in Fig. IV.E-3. An output error voltage is obtained in which the magnitude is proportional to the pointing error and the phase provides information as the the sense of the pointing error. Included in the output, along with the error signal, is a noise component which limits the pointing accuracy of the antenna.

Messrs. R. J. Massa and R. W. Chittenden have derived the output signal-to-noise ratio* of an amplitude-sensing monopulse system.[16] The results of their analysis show:

$$SNR = \frac{\frac{1}{4} P_R^{\,2} (K_1 - K_2)^2}{\left[\frac{B_o}{B}\right]\left\{\frac{P_R}{2}\,\overline{N_R^{\,2}(t)} + \overline{N_A^{\,2}(t)}\;\overline{N_R^{\,2}(t)} + \frac{1}{2}\,\overline{N_R^{\,2}(t)}^{\,2}\right\}} \tag{B-3}$$

where:

P_R = received signal power,

$\overline{N_A^{\,2}(t)}$ = antenna noise power into each channel,

$\overline{N_R^{\,2}(t)}$ = receiver noise power,

B = receiver bandwidth,

B_o = low pass filter bandwidth,

$\sqrt{K_1}$, $\sqrt{K_2}$ are normalized field directivity patterns of the antenna,

$$\sqrt{K_1} = \frac{\sin\left[\frac{\pi D}{\lambda}\sin\left(\gamma + \frac{\gamma_o}{2}\right)\right]}{\frac{\pi D}{\lambda}\sin\left(\gamma + \frac{\gamma_o}{2}\right)}$$

$$\sqrt{K_2} = \frac{\sin\left[\frac{\pi D}{\lambda}\sin\left(\gamma - \frac{\gamma_o}{2}\right)\right]}{\frac{\pi D}{\lambda}\sin\left(\gamma - \frac{\gamma_o}{2}\right)}$$

D = diameter of antenna aperture,

λ = operating wavelength,

*It is to be noted that the SNR as derived are evaluated at the point where the output error signal is maximum; i.e., at the peak of the curve relating output error signal to angle of arrival.

γ = angle of arrival with respect to the boresight, and

$\frac{\gamma_o}{2}$ = squint angle with respect to the boresight.

2. Phase Sensing Monopulse (Interferometer)

The phase sensing monopulse system obtains tracking information by comparing the relative phases of a signal which is received by two or more physically displaced antennas. The signal processing, Fig. IV.E-4, is similar to that for amplitude monopulse.

The signal-to-noise ratio of a phase sensing monopulse system as derived by Massa and Chittenden is given below.

$$SNR = \frac{\frac{1}{4} P_R^2 \left[K_3 - K_4\right]^2}{\left[\frac{B_o}{B}\right]\left[\overline{N_R^2(t)}\, P_R + \overline{N_A^2(t)}\;\overline{N_R^2(t)} + \frac{1}{2}\overline{N_R^2(t)}\right]} \tag{B-4}$$

where:

$\sqrt{K_3} = (\cos\frac{\beta}{2} + \sin\frac{\beta}{2})$,

$\sqrt{K_4} = (\cos\frac{\beta}{2} - \sin\frac{\beta}{2})$,

$\beta = \frac{2\pi}{\lambda} d \sin\gamma$,

γ = angle of arrival with respect to the boresight,

d = antenna baseline (phase center spacing), and

λ = operating wavelength.

3. Conical Scan

The conical scan tracking system utilizes a pencil beam which describes a cone in space as it is rotated about a fixed boresight axis. A target located off the boresight axis will give a signal at the receiver which is sinusoidally modulated at the beam rotation frequency.

Target displacement from the boresight axis is proportional to the amplitude of the modulation and target direction information is contained in the phase of the modulated signal.

This modulated signal has the form

$$S(t) = \left[V + a_1 \cos (\omega_s t + \Psi)\right] \cos \omega_c t + N_A(t) \qquad \text{(B-5)}$$

where:

V = amplitude of the unmodulated carrier,

a_1 = amplitude of the scan modulation,

ω_s = scan frequency,

ω_c = carrier frequency,

Ψ = phase of the scan modulation, and

$N_A(t)$ = antenna noise voltage.

Messrs. Chittenden and Massa have analyzed an idealized conical scan system, Fig. IV.E-5, under conditions of tracking a signal of the form of S(t). The output signal-to-noise ratio which they obtained for such a system is:

$$SNR = \frac{\left[\frac{a_1 V}{2}\right]^2 \cos^2 (\Psi - \alpha)}{B_o R \left[2\ RB_p + 2\ V^2 + \frac{a_1^2}{2} \cos^2 (\Psi - \alpha)\right]} \qquad \text{(B-6)}$$

where:

α = phase of the reference signal,

$$R = \frac{\overline{N_o^2(t)}}{B} = \frac{1}{B}\left[\overline{N_A^2(t)} + \overline{N_R^2(t)}\right]$$

$N_R(t)$ = receiver noise voltage,

B_p = bandpass filter bandwidth, and

B_o = output low pass filter bandwidth.

To provide an expression comparable to those for monopulse systems, the conical scan SNR equation* can be rewritten:

$$SNR = \frac{\frac{1}{8}(\sqrt{K_1} - \sqrt{K_2})^2 P_R^{\,2}}{Q_1} \qquad \text{(B-7)}$$

where:

$$Q_1 = \left[\overline{N_A^{\,2}(t)} + \overline{N_R^{\,2}(t)}\right]\left[\frac{B_o}{B}\right]\left\{2\left(\frac{B_p}{B}\right)\left[\overline{N_A^{\,2}(t)} + \overline{N_R^{\,2}(t)}\right] + 2\,P_R + \frac{(\sqrt{K_1} - \sqrt{K_2})^2}{4}\,P_R\right\},$$

$$a_1 = \frac{\sqrt{2}}{2}\,(\sqrt{K_1} - \sqrt{K_2})\,V,$$

$$P_R = V^2,$$

$\cos^2(\Psi - \alpha)$ assumed unity, and

K_1 and K_2 are defined in equation (B-3).

Since the conical scan receiver operates on the amplitude modulation of the received signal, it is susceptible to interference from any low frequency extraneous modulation of the spacecraft beacon. Though it is not likely that the communications content of the received beacon will be in the form of low frequency amplitude modulation, it is quite likely that the requirement of positioning a directive spacecraft antenna will

*This form of the conical scan SNR equation assumes 100% modulation of the received carrier by the scan frequency.

impose low frequency amplitude variation of the received beacon signal. The purpose of this analysis is to investigate the power density spectrum of the derived error signal from a conical scan receiver under the conditions of an extraneous interfering sinusoidal modulation of the received beacon.

The assumed form of the received signal* at the output of the mixer (Fig. IV.E-5) is:

$$W(t) = \left[V + a_1 \cos\ (\omega_s t + \Psi) + a_2 \cos\ (\omega_e t + \theta)\right] \cos\ \omega_i t + N_o(t) \quad \text{(B-8)}$$

where:

a_2 = amplitude of the extraneous modulation,

ω_i = receiver intermediate frequency,

ω_e = frequency of the extraneous modulation,

θ = phase of the extraneous modulation, and

$N_o(t)$ = total system noise voltage.

It is assumed that the system noise has a gaussian distribution and a uniform power spectrum over the receiver bandwidth B, with zero mean and variance, $\sigma_N^2 = \Phi_{No}(0)$.

$$\overline{N_o^2(t)} = B\left[kT_A + k(F - 1)T_o\right] = \left[\overline{N_A^2(t)} + \overline{N_R^2(t)}\right] \quad \text{(B-9)}$$

*This form of the received signal is based on the assumption that a_1 and a_2 are small quantities; i.e., the cross product term between the scan modulation and interfering modulation is small enough to be neglected. This assumption is not entirely compatible with the assumed 100% modulation produced by the scan frequency. Both assumptions tend to produce an optimistic SNR for the conical scan system.

where:

T_A = antenna noise temperature,

$T_o = 290^{\circ}K$,

k = Boltzman constant,

F = receiver noise figure, and

$\Phi_{No}(0)$ = autocorrelation function evaluated at $\tau = 0$.

Assume the envelope detector to be an ideal square law detector with a low pass filter at the output.

$$y(t) = b\left[W(t)\right]^2$$

where b = constant

$$y(t) = b\left\{\left[V + a_1 \cos(\omega_s t + \Psi) + a_2 \cos(\omega_e t + \theta)\right] \cos \omega_i t + N_o(t)\right\}^2 \quad \text{(B-10)}$$

$$\begin{aligned} y(t) = {} & \frac{b}{2}\left[V^2 + \frac{a_1^2}{2} + \frac{a_2^2}{2}\right] + a_1 bV \cos(\omega_s t + \Psi) \\ & + a_2 bV \cos(\omega_e t + \theta) + \frac{a_1^2 b}{4} \cos 2(\omega_s t + \Psi) \\ & + \frac{a_2^2 b}{4} \cos 2(\omega_e t + \theta) + bN_o^2(t) + 2bVN_o(t) \cos \omega_i t \\ & + 2ba_2 N_o(t) \cos(\omega_e t + \theta) \cos \omega_i t + 2ba_1 N_o(t) \cos(\omega_s t + \Psi) \cos \omega_i t \\ & + \frac{bV^2}{2} \cos 2\omega_i t + \frac{a_1^2 b}{4} \cos 2(\omega_s t + \Psi) \cos 2\omega_i t \\ & + \frac{a_2^2 b}{4} \cos 2(\omega_e t + \theta) \cos 2\omega_i t + a_1 bV \cos(\omega_s t + \Psi) \cos 2\omega_i t \end{aligned} \quad \text{(B-11)}$$

$$+ a_2 bV \cos(\omega_e t + \theta) \cos 2\omega_i t + \frac{a_1^2 b}{4} \cos 2\omega_i t$$

(B-11 Continued)

$$+ \frac{a_2^2 b}{4} \cos 2\omega_i t + a_1 a_2 b \cos(\omega_s t + \Psi) \cos(\omega_e t + \theta)$$

$$+ a_1 a_2 b \cos(\omega_s t + \Psi) \cos(\omega_e t + \theta) \cos 2\omega_i t$$

Assume the low pass filter has a cutoff frequency, ω_c, such that:

$$\left[2\omega_e \text{ or } 2\omega_s\right] < \omega_c \ll \left[\omega_i - (2\omega_s + 2\omega_e)\right]$$

Then the output of the low pass filter is:

$$Z(t) = \frac{b}{2}\left[V^2 + \frac{a_1^2}{2} + \frac{a_2^2}{2}\right] + a_1 bV \cos(\omega_s t + \Psi)$$

$$+ a_2 bV \cos(\omega_e t + \theta) + \frac{a_1^2 b}{4} \cos 2(\omega_s t + \Psi)$$

$$+ \frac{a_2^2 b}{4} \cos 2(\omega_e t + \theta) + bN_o^2(t)$$

$$+ 2bVN_o(t) \cos \omega_i t + 2ba_1 N_o(t) \cos(\omega_s t + \Psi) \cos \omega_i t \qquad \text{(B-12)}$$

$$+ 2ba_2 N_o(t) \cos(\omega_e t + \theta) \cos \omega_i t$$

$$+ \frac{a_1 a_2 b}{2} \cos\left[(\omega_s t + \Psi) - (\omega_e t + \theta)\right]$$

$$+ \frac{a_1 a_2 b}{2} \cos\left[(\omega_s t + \Psi) + (\omega_e t + \theta)\right]$$

In order to obtain the power density, $\Phi_Z(\omega)$, of Z(t) first calculate the autocorrelation function, $\phi_Z(\tau)$ which is defined as:

$$\phi_Z(\tau) = \lim_{T \to \infty} \frac{1}{T}\int_o^T Z(t)Z(t+\tau)dt \tag{B-13}$$

Then $\Phi_Z(\omega)$ is the Fourier Transform of the autocorrelation function.[17]

$$\Phi_Z(\omega) = \int_{-\infty}^{\infty} \phi_Z(\tau)e^{-i\omega\tau}d\tau \tag{B-14}$$

$$\begin{aligned}
\phi_Z(\tau) = {} & \left(\frac{b}{2}\right)^2\left[V^2 + \frac{a_1^2}{2} + \frac{a_2^2}{2}\right]^2 + \frac{1}{2}(a_1bV)^2 \cos\omega_s\tau \\
& + \frac{1}{2}(a_2bV)^2 \cos\omega_e\tau + \frac{1}{2}\left[\frac{a_1^2b}{4}\right]^2 \cos 2\omega_s\tau \\
& + \frac{1}{2}\left[\frac{a_2^2b}{4}\right]^2 \cos 2\omega_e\tau + b^2\sigma_N^2 + 2b^2\phi_{N_o}^2(\tau) \\
& + \frac{1}{2}(2bV)^2\phi_{N_o}(\tau)\cos\omega_i\tau + (a_1b)^2\phi_{N_o}(\tau)\cos\omega_i\tau\cos\omega_s\tau \\
& + (a_2b)^2\phi_{N_o}(\tau)\cos\omega_i\tau\cos\omega_e\tau \\
& + \left[\frac{a_1a_2b}{2}\right]^2 \cos\omega_s\tau\cos\omega_e\tau + b^2\left[V^2 + \frac{a_1^2}{2} + \frac{a_2^2}{2}\right]\overline{N_o^2(\tau)}
\end{aligned} \tag{B-15}$$

Since the purpose of determining the power spectrum, $\Phi_Z(\omega)$, is to set requirements on and determine the resulting effects of the band pass filter, it is believed that a direct pictorial representation of the power spectrum is more meaningful than the analytical expression.

The dc and periodic components of Z(t) give line spectra as shown in Fig. B-1. It can be noted that a bandpass filter of bandwidth

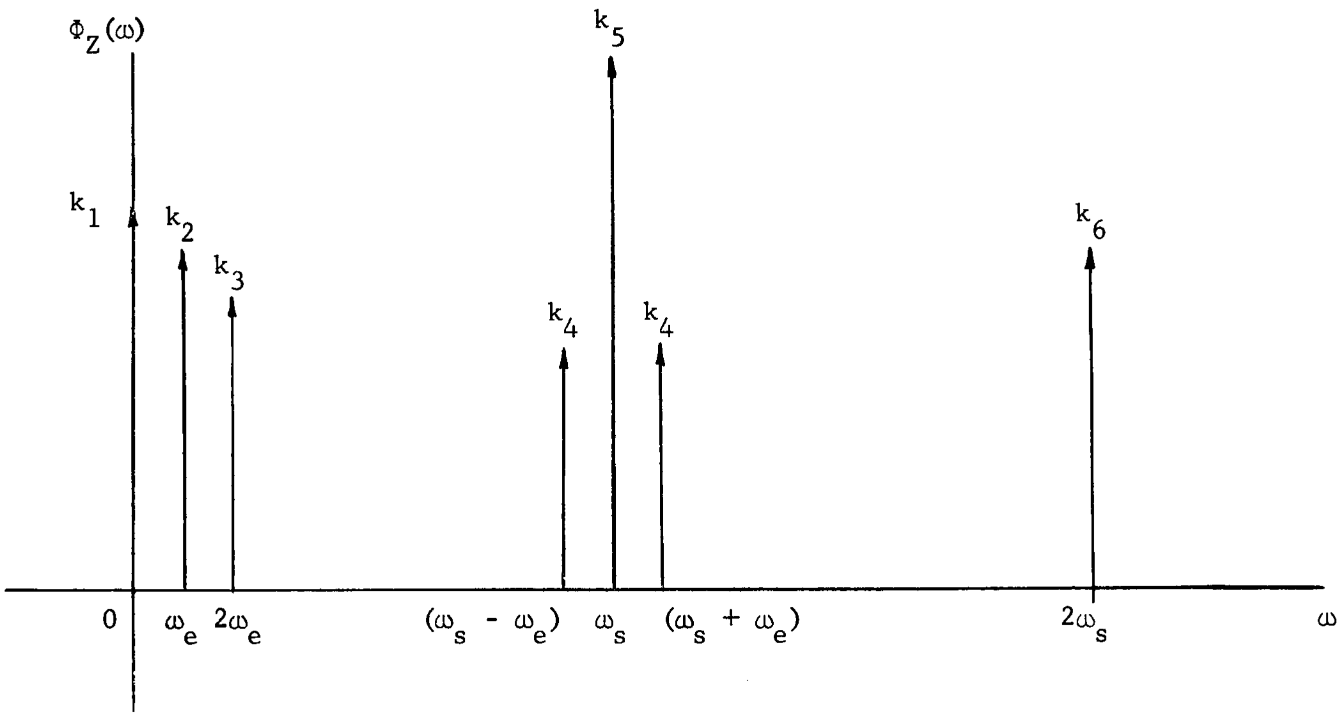

$$k_1 = \left(\frac{b}{2}\right)^2 \left[V^2 + \frac{a_1^2}{2} + \frac{a_2^2}{2}\right]^2 + b^2 \phi_{N_o}^{\;2}(0) + b^2 \left[V^2 + \frac{a_1^2}{2} + \frac{a_2^2}{2}\right] \overline{N_o^{\;2}(t)}$$

$$k_2 = \frac{1}{2} \left[a_2 bV\right]^2$$

$$k_3 = \frac{1}{2} \left[\frac{a_2^{\;2} b}{4}\right]^2$$

$$k_4 = \frac{1}{2} \left[\frac{a_1 a_2 b}{2}\right]^2$$

$$k_5 = \frac{1}{2} \left[a_1 bV\right]^2$$

$$k_6 = \frac{1}{2} \left[\frac{a_1^{\;2} b}{4}\right]^2$$

Fig. B-1. Power spectrum-line components in Z(t).

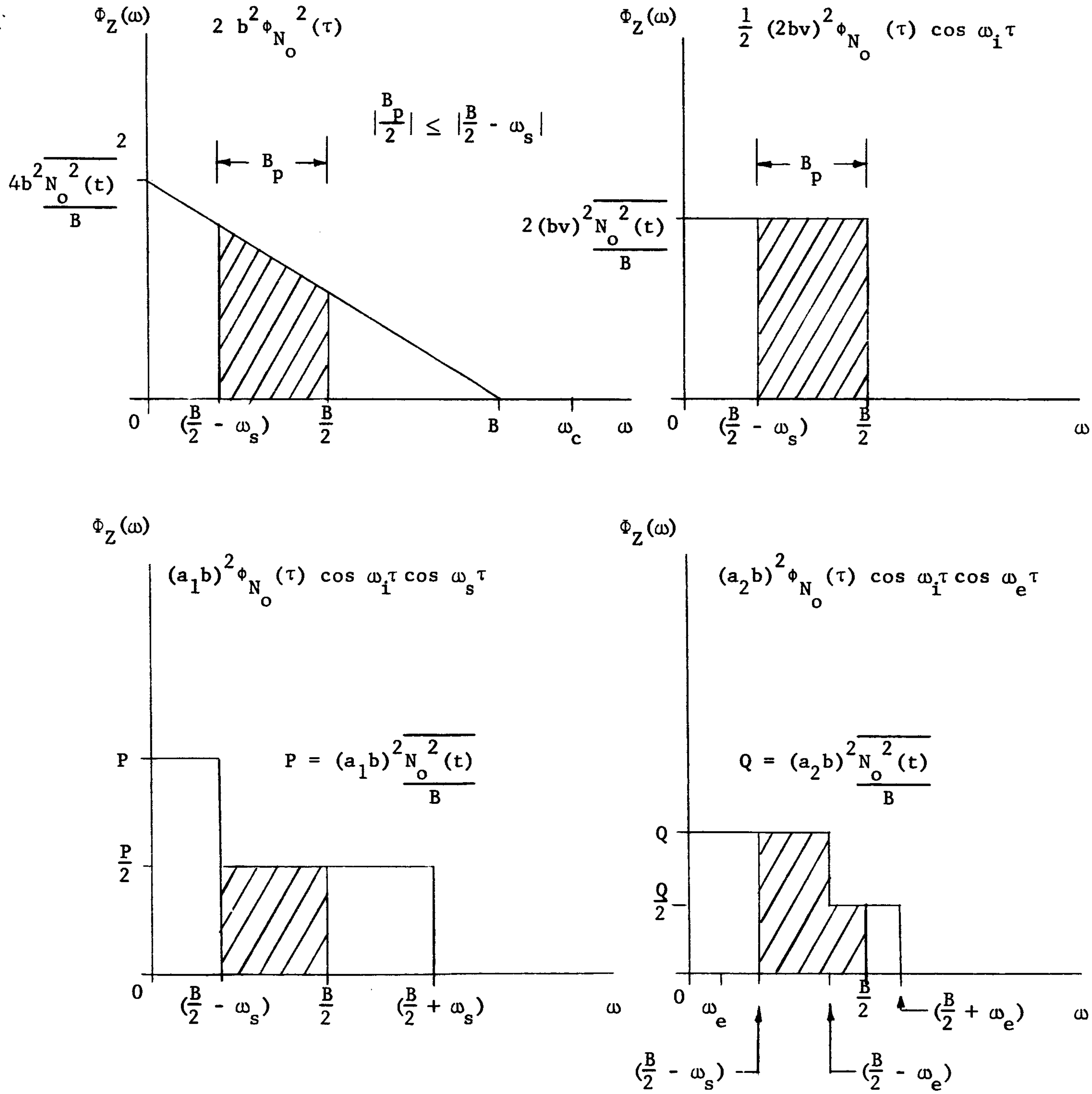

B = Receiver IF Bandwidth

$|B| < |\omega_c|$

Fig. B-2. Power spectrum-continuous components of Z(t).

B_p such that

$$\left|\frac{B_p}{2}\right| \leq |\omega_s - 2\omega_e|$$

centered at ω_s will reject the line components at dc, ω_e, $2\omega_e$, and $2\omega_s$. Ideally, one could filter out the components at ω_e radians away from ω_s; however, it is here assumed that the extraneous interference is of such low frequency that this filter is unrealizable.

An examination of the continuous power spectrum components of Z(t), Fig. B-2, indicates the desirability of a restriction on the bandpass filter such that

$$\left|\frac{B_p}{2}\right| \leq \left|\frac{B}{2} - \omega_s\right|$$

with the band edges located at $\frac{B}{2} - \omega_s$ and $\frac{B}{2}$. (It is to be noted that the requirement on the receiver IF bandwidth B is such that $\frac{B}{2} > \omega_s$ in order that the scan modulation be received.) Since the actual radian frequency of the extraneous modulation is not likely to be known, it is this bandwidth which will be assumed for the bandpass filter. The crosshatched areas of Fig. B-2 indicate the portions of the spectrum passed by such a filter.

The signal, X(t), at the output of the bandpass filter is:

$$X(t) = a_1 bV \cos(\omega_s t + \Psi) + \Big[bN_o^2(t)\Big]_{B-P}$$

$$+ 2bV \Big[N_o(t) \cos \omega_i t\Big]_{B-P} \qquad \text{(B-16)}$$

$$+ 2ba_1 \Big[N_o(t) \cos \omega_i t \cos(\omega_s t + \Psi)\Big]_{B-P}$$

$$+ 2ba_2 \left[N_o(t) \cos \omega_i t \cos (\omega_e t + \theta)\right]_{B-P}$$

$$+ \frac{a_1 a_2 b}{2} \cos \left[(\omega_s t + \Psi) - (\omega_e t + \theta)\right]$$

$$+ \frac{a_1 a_2 b}{2} \cos \left[(\omega_s t + \Psi) + (\omega_e t + \theta)\right]$$

Where B-P indicates that only the portion of the spectrum of $X(t)$ passed by the bandpass filter is to be included in the output.

The next stage of the system is the product angle error detector. (Errors in a single plane only are considered since an analysis of the orthogonal error channel would be identical.) The output, $E(t)$, for an error in a single plane is formed from the product of $X(t)$ and a reference signal, $A \cos (\omega_s t + \alpha)$, from the servo system. The output is of the form:

$$E(t) = E_{dc} + \text{NOISE}$$

$$E(t) = \frac{a_1 bVA}{2} \cos (\Psi - \alpha) + \frac{a_1 bVA}{2} \cos (2\omega_s t + \Psi + \alpha)$$

$$+ \left\{\left[bN_o^{\,2}(t)\right] A \cos (\omega_s t + \alpha)\right\}$$

$$+ \left\{2bVA \left[N_o(t) \cos \omega_i t\right] \cos (\omega_s t + \alpha)\right\}_{B-P} \qquad \text{(B-17)}$$

$$+ \left\{2ba_1 A \left[N_o(t) \cos \omega_i t\right] \cos (\omega_s t + \Psi) \quad \cos \quad \omega_s t + \alpha)\right\}_{B-P}$$

$$+ \frac{a_1 a_2}{2} bA \cos (\Psi - \alpha) \cos (\omega_e t + \theta)$$

$$+ \frac{a_1 a_2}{2} bA \cos (2\omega_s t + \Psi + \alpha) \cos (\omega_e t + \theta)$$

(B-17 Continued)

$$+ \left\{ 2ba_2 A \left[N_o(t) \cos \omega_i t \cos (\omega_e t + \theta) \right] \cos (\omega_s t + \alpha) \right\}_{B-P}$$

The autocorrelation function for E(t) may be shown to be:

$$\phi_E(\tau) = \left[\frac{a_1 bVA}{2}\right]^2 \cos^2 (\Psi - \alpha) + \frac{1}{2} \left[\frac{a_1 bVA}{2}\right]^2 \cos 2\omega_s \tau$$

$$+ \frac{1}{2} \left[Ab\right]^2 \sigma_{N_o}{}^4 \cos \omega_s \tau + \frac{1}{2} \left[Ab\right]^2 \phi_{N_o}{}^2 (\tau) \cos \omega_s \tau$$

$$+ \frac{1}{2} \left[2bVA\right]^2 \left[\phi_{N_o}(\tau) \cos \omega_i \tau \cos \omega_s \tau\right]$$

$$+ \frac{1}{2} \left[ba_1 A\right]^2 \cos^2 (\Psi - \alpha) \phi_{N_o}(\tau) \cos \omega_i \tau$$

$$+ \frac{1}{2} \left[ba_1 A\right]^2 \phi_{N_o}(\tau) \cos \omega_i \tau \cos 2\omega_s \tau \qquad \text{(B-18)}$$

$$+ \frac{1}{2} \left[\frac{a_1 a_2 bA}{2}\right]^2 \cos^2 (\Psi - \alpha) \cos \omega_e \tau$$

$$+ \frac{1}{2} \left[\frac{a_1 a_2 bA}{4}\right]^2 \cos (2\omega_s + \omega_e)\tau$$

$$+ \frac{1}{2} \left[\frac{a_1 a_2 bA}{4}\right]^2 \cos (2\omega_s - \omega_e)\tau$$

$$+ \frac{1}{2} \left[ba_2 A\right]^2 \phi_{N_o}(\tau) \cos \omega_i \tau \cos (\omega_s - \omega_e)\tau$$

$$+ \frac{1}{2} \left[ba_2 A\right]^2 \phi_{N_o}(\tau) \cos \omega_i \tau \cos (\omega_s + \omega_e)\tau$$

The output spectrum, $\Phi_E(\omega)$, of E(t) is shown in Fig. B-3a. The effects of a low pass filter of bandwidth B_o will now be examined. In order to maintain general results, two cases will be considered. Case I, $B_o > \omega_e$, thus the line component due to the extraneous interfering modulation will not be removed. This case will be applicable under the condition that the interfering modulation is of low enough frequency such that a low pass filter which would remove the line component is incompatible with the servo response time requirements. Case II, $B_o < \omega_e$, in this case the line component of the interfering frequency is removed. In any case the cutoff frequency, B_o, can be chosen such that all components of the power spectrum equal to or greater than ω_s will be removed.

Case I, $B_o > \omega_e$.

The signal-to-noise ratio for this case is:

$$\text{SNR} = \frac{\text{desired error component}}{\text{noise + extraneous modulation component}}$$

$$\text{SNR} = \frac{\left[\frac{a_1 V}{2}\right]^2 \cos^2 (\Psi - \alpha)}{Q_2} \tag{B-19}$$

where:

$$Q_2 = RB_o \left[2RB_p + 2V^2 + \frac{1}{2} a_1^{\,2} \cos^2 (\Psi + \alpha) + \frac{1}{2} a_2^{\,2}\right] + \frac{1}{2} \left[\frac{a_1 a_2}{2}\right]^2 \cos^2 (\Psi - \alpha)$$

$$R = \frac{\overline{N_o^{\,2}(t)}}{B}$$

Equation (B-19) can be rewritten:

$$\text{SNR} = \frac{\frac{1}{8} (\sqrt{K_1} - \sqrt{K_2})^2 \, P_R^{\,2}}{Q_3} \tag{B-20}$$

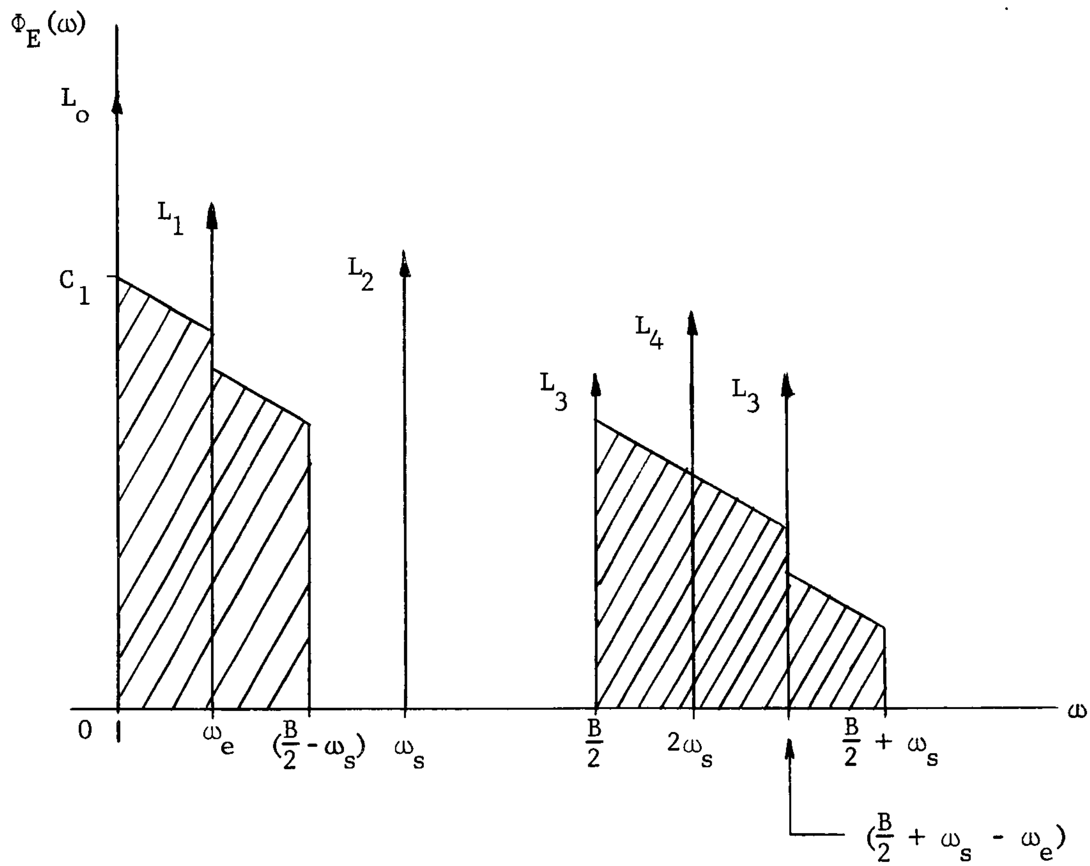

Desired error component, L_o, is at dc. See page following for component values.

Fig. B-3a . Error signal, E(t), power spectrum before low pass filtering.

Line:

$$L_o = \left[\frac{a_1 bVA}{2}\right]^2 \cos^2 (\Psi - \alpha)$$

$$L_1 = \frac{1}{2}\left[\frac{a_1 a_2 bA}{2}\right]^2 \cos^2 (\Psi - \alpha)$$

$$L_2 = \frac{1}{2}\left[Ab\right]^2 \sigma_N^{\ 4}$$

$$L_3 = \frac{1}{2}\left[\frac{a_1 a_2 bA}{4}\right]^2$$

$$L_4 = \frac{1}{2}\left[\frac{a_1 AbV}{2}\right]^2$$

Continuous around $\omega = 0$:

$$C_1 = \left[Ab\right]^2 \left[2R^2 B_p + 2V^2 R + \frac{1}{2} a_1^{\ 2} \cos^2 (\Psi - \alpha) R + \frac{1}{2} a_2^{\ 2} R\right]$$

$$\text{where } R = \frac{\overline{N_o^{\ 2}(t)}}{B}$$

Fig. B-3b. Components of power spectrum shown in Fig. B-3a.

where:

$$Q_3 = \left[\overline{N_A^{\ 2}(t)} + \overline{N_R^{\ 2}(t)}\right]\left[\frac{B_o}{B}\right]\left\{2\left(\frac{B_p}{B}\right)\left[\overline{N_A^{\ 2}(t)} + \overline{N_R^{\ 2}(t)}\right]\right.$$

$$\left. + 2P_R + \frac{(\sqrt{K_1} - \sqrt{K_2})^2}{4} P_R + \frac{1}{2} a_2^{\ 2}\right\} + \frac{1}{16} a_2^{\ 2} (\sqrt{K_1} - \sqrt{K_2})^2 P_R^{\ 2}$$

Case II, $B_o < \omega_e$.

$$SNR = \frac{\left[\frac{a_1 V}{2}\right]^2 \cos^2 (\Psi - \alpha)}{RB_o\left[RB_p + 2V^2 + \frac{1}{2} a_1^{\ 2} \cos^2 (\Psi - \alpha) + \frac{1}{2} a_2^{\ 2}\right]} \tag{B-21}$$

which can be rewritten:

$$SNR = \frac{\frac{1}{8} (\sqrt{K_1} - \sqrt{K_2})^2 P_R^{\ 2}}{Q_3} \tag{B-22}$$

where:

$$Q_3 = \left[\overline{N_A^{\ 2}(t)} + \overline{N_R^{\ 2}(t)}\right]\left[\frac{B_o}{B}\right]\left\{2\left(\frac{B_p}{B}\right)\left[\overline{N_A^{\ 2}(t)} + \overline{N_R^{\ 2}(t)}\right]\right.$$

$$\left. + 2P_R + \frac{(\sqrt{K_1} - \sqrt{K_2})^2}{4} P_R + \frac{1}{2} a_2^{\ 2}\right\}$$

REFERENCES

[1] RTI Proposal G-63-11, "Analytical and Experimental Study Program for Arrays of Independently-Steerable Antennas"; June 11, 1963.

[2] Addendum to RTI Proposal G-63-11, July 18, 1963.

[3] RTI Proposal R-64-2, "Analytical Study to Define an Experimental Program for the Evaluation and Optimization of Multi-Element Large-Aperture Arrays," Submitted in response to NASA Request for Proposal L-4062, December, 1963.

[4] P. G. Smith, "Application of Arrays of Large-Aperture Antennas to Deep-Space Communications," RTI Report RSL 1; February 25, 1964.

[5] M. Breese, R. Colbert, W. Rubin, and P. Sferrazza, "Phase-Locked Loops for Electronically Scanned Antenna Arrays," IRE Transactions on Space Electronics and Telemetry, Vol. SET-7, pp. 95-100; December, 1961.

[6] J. H. Schrader, "Receiving System Design for the Arraying of Independently Steerable Antennas," IRE Transactions on Space Electronics and Telemetry, Vol. SET-8, pp. 148-153; June, 1962.

[7] R. B. Battelle, "Feasibility Analysis of a Deep-Space Receiving Terminal Array of Large Equivalent Aperture," SRI Interim Report; January, 1964.

[8] R. C. Hansen, "Gain Limitations on Large Antennas," IRE Transactions on Antennas and Propagation, Vol. AP-8, No. 5, pp. 490-495; September, 1960.

[9] R. S. Lawrence, C. G. Little, and H. J. A. Chivers, "A Survey of Ionospheric Effects Upon Earth-Space Radio Propagation," Proc. IEEE, Vo. 52, No. 1, pp. 4-27; January, 1964.

[10] R. C. Hansen and L. L. Barlin, "A New Method of Near Field Analysis," IRE Transactions on Antennas and Propagation, Vol. AP-7, Special Supplement; December, 1959.

[11] P. W. Hannan, "Microwave Antennas Derived from the Cassegranian Telescope," IRE Transactions on Antennas and Propagation, Vol. AP-9; March, 1961.

[12] S. Silver, "Microwave Antenna Theory and Design," Vol. 12, Radiation Laboratory Series, McGraw-Hill Book Company.

[13] Staff Report, "Shaft Angle Encoders, Computer Design;" December, 1963.

[14] Hewlett-Packard Journal, Vol. 15, No. 5, January, 1964, and Vol. 15, No. 2, October, 1963.

[15] E. L. Kaplan, "Signal Detection Studies, With Applications," Bell System Technical Journal; March, 1955.

[16] R. J. Massa and R. W. Chittenden, "Technical Note on Satellite Tracking Techniques and an Evaluation of Interference Phenomena," ASTIA publication AD-244264.

[17] Mischa Schwartz, "Information Transmission Modulation and Noise," McGraw-Hill; 1959.

[18] M. I. Skolnik, "Introduction to Radar Systems," McGraw-Hill; 1962.

[19] D. R. Rhodes, "Introduction to Monopulse," McGraw-Hill; 1959.

[20] A. P. Deam and B. M. Fannin, "Phase-Difference Variations in 9.35 KMc Radio Signals Arriving at Spaced Antennas," Proc. IRE, Vol. 43, No. 11, pp. 1402-1404; October, 1955.

[21] D. G. Brennan, J. C. James, J. Max, and T. F. Rogers, "Some Aspects of Space Communication," MIT Final Report on NASA contract NASw-161; March 21, 1962.

[22] K. A. Norton, et al, "An Experimental Study of Phase Variations in Line-of-Sight Microwave Transmissions," National Bureau of Standards Monograph 33; November, 1961.

[23] D. G. Brennan, "Linear Diversity Combining Techniques," Proc. of the IRE, pp. 1075-1101; June, 1959.

[24] R. T. Adams and B. M. Mindes, "Evaluation of IF and Baseband Diversity Combining Receivers," IRE Transactions on Communication Systems, pp. 8-13; June, 1958.

[25] C. S. Weaver, "Thresholds and Tracking Ranges in Phase-Locked Loops," IRE Transactions on Space Electronics and Telemetry, pp. 60-85; September, 1961.

[26] J. P. Frazier and J. Page, "Phase Lock Loop Frequency Acquisition Study," IRE Transactions on Space Electronics and Telemetry, pp. 210-227, September, 1962.

[27] J. H. Schrader, "A Phase-Lock Receiver for the Arraying of Independently Directed Antennas," IEEE Transactions on Antennas and Propagation, pp. 155-161; March, 1963.

[28] J. A. Develet, Jr., "A Threshold Criterion for Phase-Lock Demodulation," Proc. of the IEEE, pp. 349-356; February, 1963.

[29] A. J. Viterbi, "Phase-Locked Loop Dynamics in the Presence of Noise by Fokker-Plank Techniques," Proc. of the IEEE, pp. 1737-1753; December, 1963.

[30] L. R. Malling, "Phase Stable Oscillators for Space Communications Including the Relationship Between the Phase Noise, the Spectrum, the Short Term Stability, and the Q of the Oscillator," Proc. of the IRE, pp. 1656-1664; July, 1962.

[31] W. K. Victor, R. Titsworth and E. Rechtin, "Telecommunication Aspects of a Manned Mars Mission," Technical Report No. 32-501, JPL; August, 1963.

[32] W. J. Gruen, "Theory of AFC Synchronization," Proc. of the IRE, pp. 1043-1048; August, 1953.

[33] R. M. Jaffe and E. Rechtin, "Design and Performance of Phase Lock Circuits Capable of Near Optimum Performance Over a Wide Range of Input Signal and Noise Levels," IRE Transactions on Information Theory, pp. 66-76; March, 1955.

[34] S. G. Margolis, "The Response of a Phase-Locked Loop to a Sinusoid Plus Noise," IRE Transactions on Information Theory, pp. 135-144; March, 1957.

[35] W. L. Nelson, "Phase-Lock Loop Design for Coherent Angle-Error Detection in the Telstar Satellite Tracking Systems," Bell System Technical Journal; September, 1963.

[36] H. C. Ko, "Amplitude Scintillation of Radio Stars at Ultra-High Frequency," Proc. IRE, Vol. 48, No. 11, pp. 1871-1880; November, 1960.

[37] R. H. Dicke, "The Measurement of Thermal Radiation at Microwave Frequencies," Rev. Sci. Instru., Vol. 17; July, 1946.

[38] K. Fujimoto, "On the Correlation Radiometer Technique," IEEE Transactions on Microwave Theory and Techniques, Vol. MIT-12, No. 2; March, 1964.

[39] R. B. Blackman and J. W. Tukey, "The Measurement of Power Spectra," Dover Publications, Inc., New York, N. Y.; 1959.